İSTANBUL TECHNICAL UNIVERSITY ★ INSTITUTE OF SCIENCE AND TECHNOLOGY

SYNTHESIS AND ELECTROPOLYMERIZATION OF BIS(N-METHYL PYRROLE 4,4´-DIETHYL,2,2´ BITHIAZOLE)

Ms.C. Thesis by

Şebnem Şaziye TAYYAR

Department : Polymer Science and Technology

Programme: Polymer Science and Technology

JUNE 2008

İSTANBUL TECHNICAL UNIVERSITY ★ INSTITUTE OF SCIENCE AND TECHNOLOGY

SYNTHESIS AND ELECTROPOLYMERIZATION OF BIS(N-METHYL PYRROLE 4,4´-DIETHYL,2,2´ BITHIAZOLE)

Ms.C. Thesis by
Şebnem Şaziye TAYYAR
(515061024)

Date of submission : 5 May 2008

Date of defence examination: 11 June 2008

Supervisor (Chairman): Prof. Dr. Belkıs USTAMEHMETOĞLU

Members of the Examining Committee Assoc.Prof.Dr. Esma SEZER(İTU)

Assoc.Prof.Dr. Cemal ÖZEROĞLU (İÜ)

JUNE 2008

İSTANBUL TEKNİK ÜNİVERSİTESİ ★ FEN BİLİMLERİ ENSTİTÜSÜ

BİS (N-METiL PİROL 4,4′-DİETİL,2,2′ BİTİYAZOL) KOMONOMERİNİN SENTEZİ ve ELEKTROPOLİMERİZASYONU

YÜKSEK LİSANS TEZİ
Şebnem Şaziye TAYYAR
(515061024)

Tezin Enstitüye Verildiği Tarih : 5 Mayis 2008
Tezin Savunulduğu Tarih : 11 Haziran 2008

Tez Danışmanı : Prof. Dr. Belkıs USTAMEHMETOĞLU
Diğer Jüri Üyeleri: Doç. Dr. Esma SEZER (İTU)
Doç. Dr. Cemal ÖZEROĞLU (İU)

HAZİRAN 2008

ACKNOWLEDGEMENT

I would like to thank my advisor, Professor Belkıs USTAMEHMETOĞLU, for her guidance, continuous encouragement throughout this work, and also being more than a supervisor.

I am grateful to Associate Prof. Dr. Esma SEZER, for her invaluable help, supports during this study and also, giving inspiration throughout my development.

I would also like to express my grateful thanks to my friend Gamze BAKKALCI and also Çağdaş KAYA, for their help during my late time works.

I like to thank to my friends Pelin YAZICI, Esin ATEŞ, Koray YILMAZ, Deniz TOPUZ and Ayşegül YÖRÜR for their support, encouragement and friendship.

Finally, I would like to thank to my parents to being always with me and whatever supporting me. Especially to Taha Mert TAYYAR.

June, 2008 Şebnem Şaziye TAYYAR

TABLE OF CONTENTS

LIST OF ABBREVIATIONS

ATR-FTIR : Attenuated Total Reflactance Fourier Transform Infrared
ACN : Acetonitrile
CP : Conducting Polymer
C_1 : Capacitance
C_{dl} : Double Layer Capacitance
CA : Chronoamperometry
CV : Cyclic Voltametry
DC : Direct Current
DCM : Dichloromethane
EIS : Electrochemical Impedance Spectroscopy
E_g : Band Gap
E_o : Half Wave Potential
F : Faraday Constant
IHP : Inner Helmholtz Plane
PA : Polyacetylene
P(N-MePyEBTN-MePy) : Poly(N-methyl pyrrole 4,4´-dıethyl,2,2´ bıthıazole)
N-MePyEBTN-MePy : Bıs(N-methyl pyrrole 4,4´-dıethyl,2,2´ bıthıazole)

LIST OF TABLES

LIST OF FIGURES

Page No

SYNTHESIS AND ELECTROPOLYMERIZATION OF BIS(N-METHYL PYRROLE 4,4´-DIETHYL,2,2´ BITHIAZOLE)

SUMMARY

The Synthesis and characterization of a novel donor acceptor donor type N-MePyEBTN-MePy comonomer and its electrochemically prepared polymer on platin botton electrode reported in this study. Comonomer was synthesised via stille coupling reaction. NMePyEBTNMePy was characterize with H-NMR and ATR-FTIR spectroscopies. NMePyEBTNMePy comonomer was electropolymerize in different conditions with different methods. Comonomer had been polymerized in $TBAPF_6$/DCM and $TBAClO_4$/DCM with CV and CA methods. Obtained polymers redox behaviour was investigated with CV and also capacitive properties were determined with EIS. n-doping properties of comonomer had also studied. Electrochemical Impedance Spectroscopy is a powerful tool for the analysis of electrochemical system. This technique was used to explained electrochemical characteristics of the polymer electrodes like resistance, capacitance and impedance.

The cyclic voltammetry is a dynamic electrochemical method in which the potential applied to an electrochemical cell is scanned and any resulting changes in cell current are monitored to yield a cyclic voltammogram (CV) of the redox (reduction and oxidation) properties of the material under study. CV was used to synthesise the comonomer and also investigate synthesised copolymer. The choronoamperometry (CA) is an electrochemical method in which a constant potential applied to an electrochemical cell and resulting changes in current versus time are monitored. We have also used CA measuremnts to electropolymerize our copolymer.

Due to N atom in the bithiazole ring oxidation potential is higher than P(N-MePy) but added to p-doping properties of P(NMePyEBTNMePy) displays n-doping in the -1,5V-1,5V region. The polymers band gap was found to be 0,417 eV. It was found out that PF_6^- dopant is a beter dopant for electropolymerization of NMePyEBTNMePy also cyclic voltametry is beter method.

BİS (N-METiL PİROL 4,4´-DİETİL,2,2´ BİTİYAZOL) KOMONOMERİNİN SENTEZİ ve ELEKTROPOLİMERİZASYONU

ÖZET

Bu çalışmada, N-Metil Pirol Etilbitiyazol N-Metil Pirol komonomeri sentezlenmiş ve platin elektot üzerine elektrokimyasal polimerizasyonu gerçekleştirilmiştir. Komonomer Stil kenetlenme reaksiyonu ile sentezlenmiş. Sentezlenen komonomer H-NMR ve ATR-FTIR spektrometreleri ile karakterize edilmiştir. N-Metil Pirol Etilbitiyazol N-Metil Pirol komonomeri değişik şartlarda değişik metotlar ile polimerleştirilmiştir. TBAPF$_6$/DCM ve TBAClO$_4$/DCM destek elektrolitleri ile siklik voltametri ve kronoamperometri metotları ile polimerizasyon gerçekleştirilmiştir. Elde edilen polimerlerin redoks davranıları siklik voltametry ile kapasitif davranıları ise elektrokimyasal impedans spektroskopisi ile incelenmiştir. Polimerin negatif doplanma özellikleri de araştırılmıştır. Elektrokimyasal impedans spektroskopisi elektrokimyasal sistemlerin analizi için güçlü bir yöntemdir. Polimerin elektrotların direnç, kapasitans, impedans gibi elektrokimyasal karakteristiklerini açıklamak için kullanılmıştır. Siklik voltametri elektrokimyasal hücreye uygulanan potansiyelin hücre akımındaki değişiminin siklik voltamogram alınarak redoks özelliklerinin incelendiği dinamik elektrokimyasal bir yöntemdir. Siklik voltametry elektrokimyasal polimerizasyon ve oluşan kopolimerlerin incelenmesi için kullanılmıştır. Kronoamperometry ise sabit potansiyelde akımın değişiminin zamana karşı izlendiği bir elektrokimyasal yöntemdir. Komonomerinin polimerizasyonu kronoamperometre yöntemi kullanılarakta gerçekleştirilmiştir.

Bitiyazol halkasındaki N atomuna bağlı olarak N-metil pirol ile karılaştırıldığında komonomerin oksidasyon potansiyelinin yükseldiği görülmüştür. Ama buna rağmen, Bitiyazol halkasındaki N atomu N-metil pirol monomerinin artı doplanma ek olarak eksi doplanma özelliği vermiştir. Elde edilen polimerin band aralığı 0,417 eV olarak çok düşük bir değerde bulunmuştur. PF_6^- dopantının ve CV yönteminin NmetilpiroletilbitiyazolNmetil pirol komonomeri için daha uygun olduğu saptanmıştır.

1. INTRODUCTION

The exciting applications envisaged for semiconducting polymers, such as light-emitting diodes (LEDs), field- effect transistors (FETs), and photovoltaic cells [1] have stimulated the search for novel conjugated polymers with tailor-made properties [2]. In recent years considerable attention has been given to the preparation and properties od alternating conjugated copolymers in which the nature of comonomers affords a novel means to design materials with improved funcitonal properties that cannot be attained by the corresponding homopolymers [3,4]. As an example, copolymers consisting of alternating electron-rich and electron deficient rings may exhibit a significantly red-shifted absorption and result in extremely low band gap materials [5].

Although polypyrrole (PPy) has received considerable attention as a conducting material in its oxidized form[6], its semiconducting properties and the incorporation of PPy in in LEDs or FETs have not been considered in great detail, mainly because PPy has a low oxidation potential (-0,2V vs SCE [7]) and is diffucult to obtain and maintain in the undoped form. With a proper choice of a second monomer unit, however, the electron rich character of pyrrole (Py) and its alkyl-substituted derivatives can be utilized to generate alternating copolymers with novel and fine-tunable semiconducting electronic and optical properties [8-10]. Nevertless, such polymers have recieved only limited attention and have not been exploited as semiconductors in electrooptical devices.

Well-defined alternating heterocyclic copolymers are in general prepared using organometallic cross-coupling reactions such as the Stille [11,12] or Suzuki [8,13,14] reaction. Transition metal-catalyzed polymerizations toward oligo and PPys have been described in recent years [15-17], but only a limited number of alternating pyrrole-containing copolymers have been prepared, either via Suzuki [8] or Stille cross coupling reaction [9,10] or via alternative routes such as the conversion of precursor polymers using the Setter reaction [18].

The Poly(alkylbithiazoles) has received considerable attention because of its n-doping capability and usage in light emitting diodes construction, this new class of conjugated polymer exhibit interesting thermochromic andelectrochemical behavior[19-26].

The cyclic voltammetry is a dynamic electrochemical method in which the potential applied to an electrochemical cell is scanned and any resulting changes in cell current are monitored to yield a cyclic voltammogram (CV) of the redox (reduction and oxidation) properties of the material under study. CV was used to synthesise the comonomer and also investigate synthesised copolymer.

The choronoamperometry (CA) is an electrochemical method in which a constant potential applied to an electrochemical cell and resulting changes in current versus time are monitored. We have also used CA measuremnts to electropolymerize our copolymer.

The electrochemical impedance spectroscopy (EIS) is one of the most effective and the reliable method to extract information about electrochemical characteristics of the electrochemical system for instance double layer capacitance (C_{dl}), diffusion impedance, determination of the rate of the charge transfer and charge transport processes, solution resistance etc. [27,28].

Here we report the synthesis and electropolymerization of a new conjugated alternating copolymer consisting of N-Methly Pyrrole (NMePy) and ethlybithiazole via the Stille coupling rection. Resulting comonomer N-methyl Pyrrole Ethlybithiazole N-methly Pyrrole (NMePyEBTNMePy) structure is given in Figure 1.1.

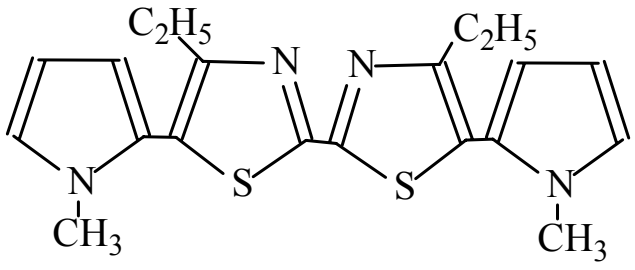

Figure 1.1. Structure of N-methyl Pyrrole Ethlybithiazole N-methly Pyrrole (NMePyEBTNMePy)

2. THEORETICAL PART

2.1. Conducting Polymers

Electrically conducting polymers (ECPs) are materials with an extended system of C=C conjugated bonds. They are obtained by reduction or oxidation reactions (called doping), giving materials with electrical conductivities up to 10^5 S/cm. These materials differ from polymers filled with carbon black or metals because the latter are only conductive if the individual conductive particles are mutually in contact and form a coherent phase.

This review concerns the synthesis routes, polymerization techniques, doping, orientation, and development of well-defined, highly conducting polymeric materials. Their wide range of potential uses from electrodes in rechargeable batteries to organic transistors is limited by their vulnerability to air and moisture due to their highly conjugated structures and the doping agents. Electrically conducting materials are compiled, their specific properties and potential applications are described.

Numerous attempts have been made to synthesize "conductive organic materials". The first was the synthesis of polyaniline by F. GOPPELSROEDER in 1891 [29]. After decades interest grew in organic polymers as insulators, but not as electrical conductors.

In the late 1950s organic semiconductors became the focus of investigations. Preliminary studies in this field up until the mid 1960s are reviewed in [30]. The semiconducting polymers were termed "covalent organic polymers", "charge-transfer complexes", "organometallic polymers", "hydrogen-bonded polymers", and "mixed polymers". Highest conductivity values reached about 10^{-3} S/cm. In 1964 LITTLE theoretically evaluated the possibility of superconductivity in polymers and suggested a model, consisting of a polyene chain with cyanine, dyelike substituents [31]. In the same year systematic studies were presented based on aromatic and heterocyclic compounds exhibiting electrical conductivities of 0.5 S/cm [32],

followed by studies correlating doping, pressure, irradiation, and chain length to conductivity, with values up to 100 S/cm [33].

Interest heightened and became acute from 1975 when IBM scientists showed that poly(sulfur nitride), $(SN)_n$, was superconductive [34] and MACDIARMID'S group reported [38] the doping of polyacetylene films prepared by SHIRAKAVA [39] reaching conductivity values of 38 S/cm. Since then many expectations have been raised, but scientific progress and practical applications have been limited; they depend on the reproducible production of well-defined specimens, the determination of synthesis conditions, and the laws relating these conditions to product properties. Synthetic methods are improving; more easily processible, soluble, flexible materials are now being produced.

2.1.1. Theory of Band Gap and Electrical Conductivity

The polyacetylene (PA) produced by Shirakawa [29] in the late 1970s exhibited a 12 order of magnitude increase in electrical conductivity when exposed to oxidizing agents. Since that discovery, vast arrays of other conducting polymers (CP) have been synthesized. The most common of these, in addition to PA, are shown below in Figure 2.1.

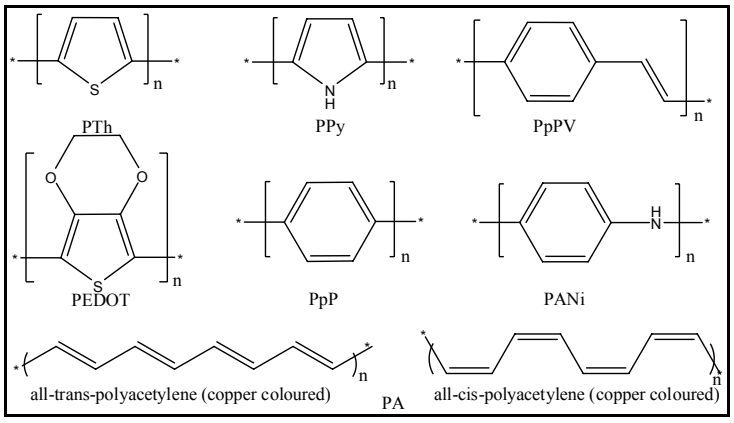

Figure 2.1. Some conducting polymers.

A large number of conjugated polymers have been synthesized and studied in the last two decades. Their structures, electronic structures, and numerous properties have been reviewed extensively [37]. A few representative structural formulas are shown in Figure 2.1.

In addition to bond length alternation (BLA), defined as the difference between the long and short carbon-carbon bonds in a conjugated molecule, several other factors influence the band gaps of these complex systems.

Most of the factors involved are normally interdependent; no general formula can be given. For instance, as in the case of poly(thiophene), PTh, and poly(pyrrole), PPy, heteroatoms affect the gap by both influencing the degree of BLA and mixing of the heteroatom orbital. The latter can be viewed as a direct heteroatomic effect. For purely interpretative purposes, based on the perturbation approach of qualitative molecular orbital theory, the following qualitative formula expresses the main contributions affecting the band gap [38]:

$$Eg \cong E_g^{topol} + E_g^{\Delta r} + E_g^{\theta} + E_g^{arom} + E_g^{sub} + E_g^{error} \qquad \textbf{(2.1)}$$

where E_g^{topol} is the topological band gap, $E_g^{\Delta r}$ is the contribution from BLA or geometry relaxation along the main chain (including a large exchange contribution), E_g^{θ} is a contribution arising from the effect of ring torsion (non-planarity), E_g^{arom} is owing to the presence of an aromatic ring along the chain, which limits π-electron delocalization outside the ring, E_g^{sub} comes from substitution effects, and E_g^{error} normally includes geometry defects, disorder, and inter-chain interactions. Bond distances play a key role in those cases, when the topological band gap is zero, e.g., PA or polyacetylene. However, the strong coupling of the frontier orbital(s) remains important even if the topological band gap is not zero, as is the case for all polymers in Figure 2.1, except PA. Therefore, the geometry influences the band gap directly [39].

2.1.1.1. The Extended π-system

Since that discovery of conducting polymers, vast arrays of other (Conducting Polymers) CPs have been synthesized. Apart from polyaniline, all of these systems share one common structural feature, namely a rigid nature brought about by the sp^2 carbon-based backbone. The utilization of the conjugated construction affords polymer chains possessing extended π-systems, and it is this feature alone that separates CPs from their other polymeric counterparts.

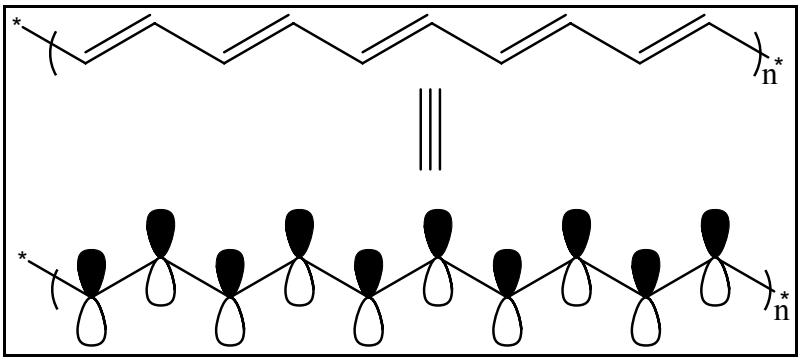

Figure 2.2. The π-system model.

Using this generic, lowest energy (fully bonding) molecular orbital (MO) representation as shown by the π-system model, the picture of primary concern that is generated by these networks consists of a number of π and π* levels (Figure 2.2).

The electrical properties of any material are a result of the material's electronic structure. The presumption that CP's form bands through extensive molecular orbital overlap leads to the assumption that their electronic properties can be explained by band theory. With such an approach, the bands and their electronic population are the chief determinants of whether or not a material is conductive. Here, materials are classified as one of three types shown in Figure 2.4, being metals, semiconductors, or insulators.

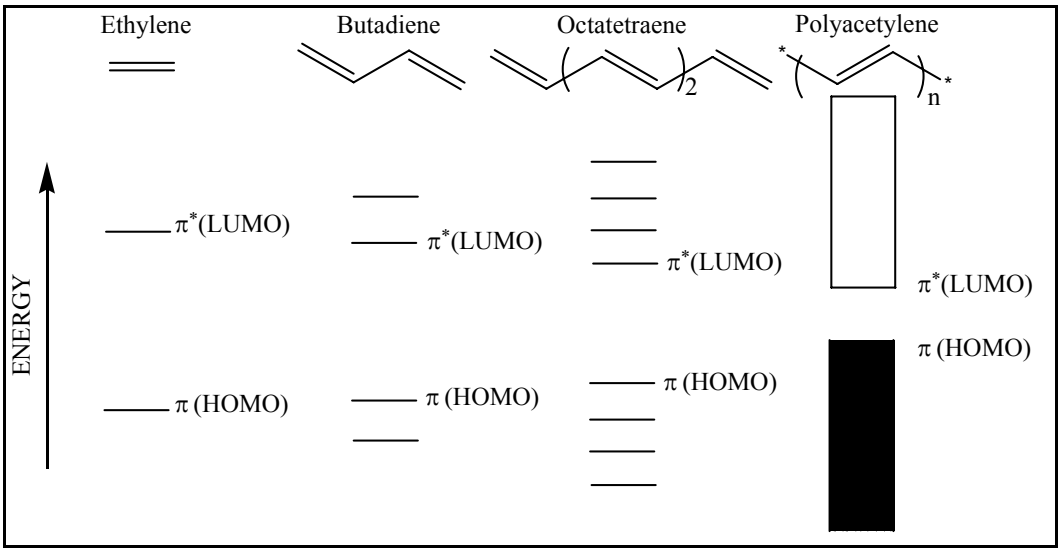

Figure 2.3. Molecular orbital (MO) diagram.

Metals are materials that possess partially filled bands, and this characteristic is the key factor leading to the conductive nature of this class of materials.

Semiconductors, on the other hand, have filled (valence bands) and unfilled (conduction bands) bands that are separated by a range of forbidden energies (known as the "band gap"). The conduction band can be populated, at the expense of the valence band, by exciting electrons (thermally and/or photochemically).

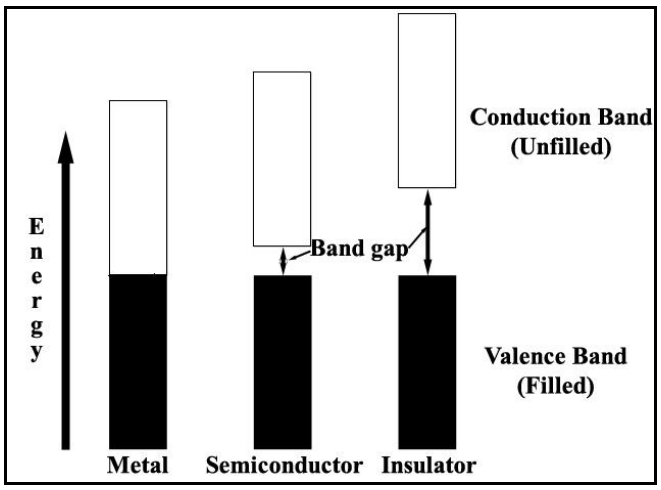

Figure 2.4: Classification of materials, and schematic of valence and conduction

Insulators possess a band structure similar to semiconductors except here the band gap is much larger and inaccessible under the environmental conditions employed.

At first glance one might necessarily expect that the p electrons of polyacetylene would produce a half-filled band and result in the polymer being metallic in nature. However, the one-dimensional nature of the polyacetylene chain leaves it susceptible to an instability that forces the polymer to retain its strict, alternating series of long and short bonds. This instability, analogous to a "Peierl's distortion", is very common among molecular solids and is the result of the coupling of electrons with phonons (lattice vibrations) [40]. Given the relatively soft nature of the lattice in such low dimensional solids, the total energy of the system can be decreased through a doubling of the unit cell, concomitantly opening a gap in the conduction band at the Brillouin zone boundary. In fact, structural studies of polyacetylene have shown the polymer to possess a localized backbone consisting of alternating long and short bonds [41]. This is in stark contrast to aromatic molecules, such as benzene, where the bonds are completely delocalized.

It is the Peierl's instability that is believed to be responsible for the fact that most CPs in their neutral state are insulators or, at best, weak semiconductors. Hence, there is enough of an energy separation between the conduction and valence bands that thermal energy alone is insufficient to excite electrons across the band gap. To explain the

conductive properties of these polymers, several concepts from band theory and solid state physics have been adopted. For electrical conductivity to occur, an electron must have a vacant place (a hole) to move to and occupy. When bands are completely filled or empty, conduction can not occur. Metals are highly conductive because they possess unfilled bands. Semiconductors possess an energy gap small enough that thermal excitation of electrons from the valence to the conduction bands is sufficient for conductivity; however, the band gap in insulators is too large for thermal excitation of an electron across the band gap.

2.1.1.2. Doping and Electrical Conductivity

In the late 1970s Heeger and MacDiarmid found that polyacetylene produced by Shirikawa's method exhibited a 12 order of magnitude increase in electrical conductivity when exposed to oxidizing agents. So how does this 12 order of magnitude increase in electrical conductivity for polyacetylene occur? The diffuse nature of the extended π-system readily allows electron removal from, or injection, into the polymer. The term "doping" has been borrowed from semiconductor physics with "p-doping" and "n-doping" being used to describe polymer oxidation and reduction, respectively. Doping in regards to semiconductors is quite different as it is a very distinct process carried out at low levels (< 1 %) as compared to CP doping (usually 20-40%). However, the manner by which doping transforms a neutral CP into a conductor remained a mystery for many years.

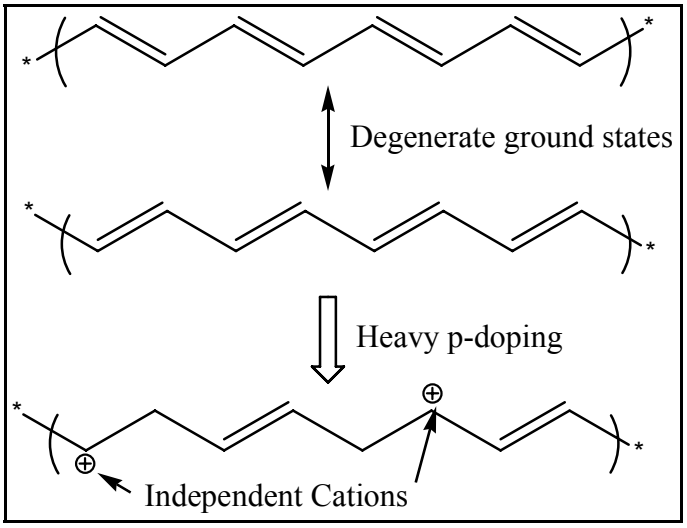

Figure 2.5. p-doping of polyacetylene.

Electron Paramagnetic Resonance (EPR) studies have shown that both the neutral and heavily doped CPs possess no net spin, interpreted as no unpaired electrons, while

moderately doped materials were discovered to be paramagnetic in nature. Conductivity experiments showed that it was the "spin-less", heavily-doped form that is the most conductive for a given CP. Such behavior marks an abrupt departure from simple band theory, which centers around spin-containing charge carriers.

Polyacetylene turns out to be a special case when considering its neutral and doped forms. Comparison of the two neutral forms, shown in Figure 2.5, reveals them to be structurally identical, and thus, their ground states are degenerate in energy. Two successive oxidations on one chain could yield radical cations that, upon radical coupling, become non-associated charges termed positive "solitons".

In contrast to polyacetylene, the other CPs shown in Figure 2.1, have non-degenerate ground states (i.e. they do not possess two equivalent resonance forms), and thus, do not show evidence of soliton formation. In this instance, the oxidation of the CP is believed to result in the destabilization (rising of the energy) of the orbital from which the electron is removed. This orbital's energy is increased and can be found in the energy region of the band gap as shown in Figure 2.6a. Initially, if only one electron per level is removed a radical cation is formed and is known as a "polaron" (Figure 2.6b). Further oxidation removes this unpaired electron yielding a dicationic species termed a "bipolaron" (Figure 2.6c). High dopant concentrations create bipolaron-"rich" materials and eventually lead to band formation of bipolaron levels. Such a theoretical treatment, thereby, explains the appearance, and subsequent disappearance, of the EPR signal of a CP with increased doping as the neutral polymer transitions to the polaronic form and subsequently to the spinless bipolaronic state.

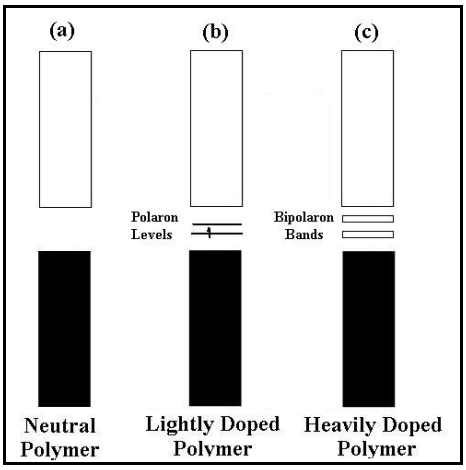

Figure 2.6: The energy region of the band gap.

Contrary to polyacetylene's independent charges, the bipolaron unit remains intact and the entire entity propagates along the polymer chain. Figure 2.7 shows this behavior using polythiophene as an example. In the case of unsubstituted polythiophene, the bipolaronic unit is believed to be spread over six to eight rings. This "bipolaron length" is by no means an absolute number as different polymer backbone and substituent types yield various lengths.

While this general model for charge carrier generation has developed over the years, it is not without conjecture. As one alternate possibility, the presence of diamagnetic π-dimers, resulting from the combination of cation radicals, has been proposed [42, 43]. Much of the basis for these theories comes from investigations into the structural and electronic properties of small conjugated molecules.

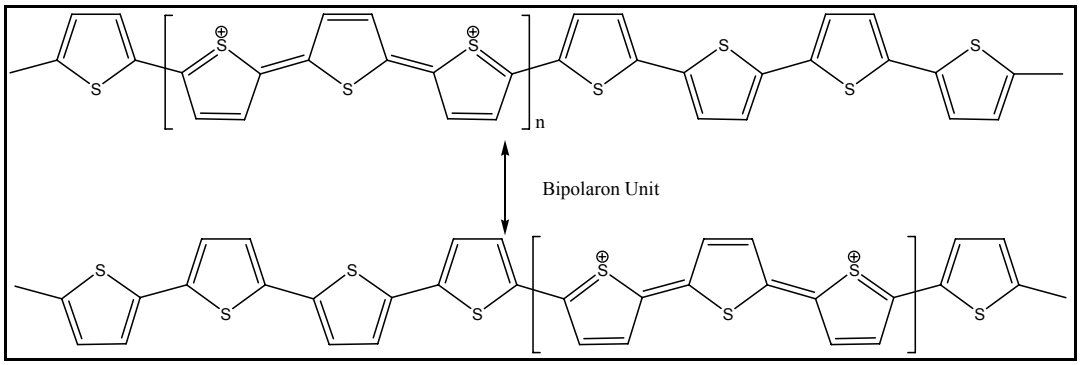

Figure 2.7: Bipolaron unit on polythiophene.

One early explanation of conducting polymers used band theory as a method of conduction. This said that a half filled valence band would be formed from a continuous delocalized π-system. This would be an ideal condition for conduction of electricity. However, it turns out that the polymer can more efficiently lower its energy by bond alteration (alternating short and long bonds), which, introduces a band width of 1.5 eV making it a high energy gap semiconductor. The polymer is transformed into a conductor by doping it with either an electron donator or an electron acceptor. This is reminiscent of doping of silicon based semiconductors where silicon is doped with either arsenic or boron. However, while the doping of silicon produces a donor energy level close to the conduction band or a acceptor level close to the valence band, this is not the case with conducting polymers. The evidence for this is that the resulting polymers do not have a high enough concentration of free spins, as determined by electron spin spectroscopy. Initially the free spins concentration increases with concentration of dopant. At larger concentrations, however, the concentration of free

spins levels of at a maximum. To understand this it is necessary to examine the way in which charge is stored along the polymer chain and its effect.

The polymer may store charge in two ways. In an oxidation process it could either lose an electron from one of the bands or it could localize the charge over a small section of the chain. Localizing the charge causes a local distortion due a change in geometry, which costs the polymer some energy. However, the generation of this local geometry decreases the ionization energy of the polymer chain and increases its electron affinity making it more able to accommodate the newly formed charges. This method increases the energy of the polymer less than it would if the charge was delocalized and, hence, takes place in preference of charge delocalization. This is consistent with an increase in disorder detected after doping by Raman spectroscopy. A similar scenario occurs for a reductive process.

Typical oxidizing dopants used include iodine, arsenic pentachloride, iron (III) and chloride. A typical reductive dopant is sodium naphthalide. The main criteria is its ability to oxidize or reduce the polymer without lowering its stability or whether or not they are capable of initiating side reactions that inhibit the polymers ability to conduct electricity. An example of the latter is the doping of a conjugated polymer with bromine. Bromine it too powerful an oxidant and adds across the double bonds to form sp^3 carbons.

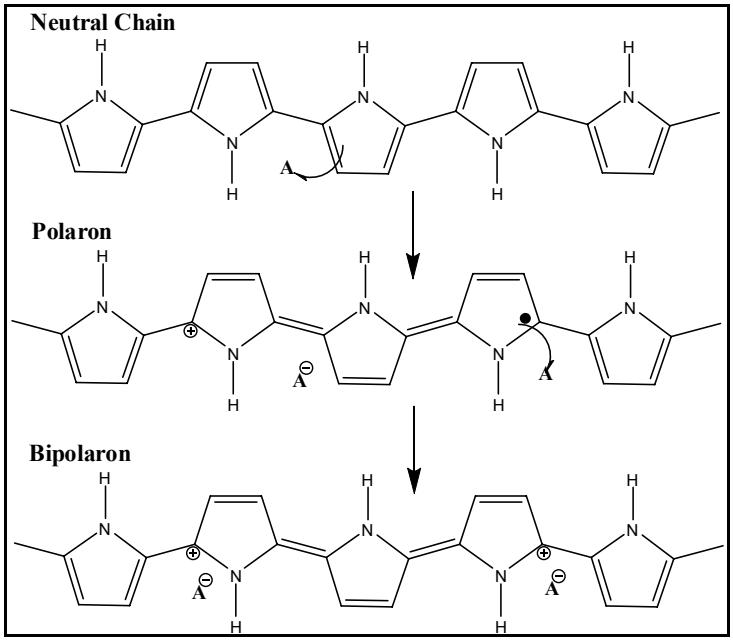

Figure 2.8: Oxidative doping of pyrrole. ($A^{\ominus}$: dopant).

The oxidative doping of polypyrrole proceeds in the following way (Figure 2.8). An electron is removed from the π-system of the backbone producing free radical and a spinless positive charge. The radical and cation are coupled to each other via local resonance of the charge and the radical. In this case, a sequence of quinoid-like rings is used. The distortion produced by this is of higher energy than the remaining portion of the chain. The creation and separation of these defects costs a considerable amount of energy. This limits the number of quinoid-like rings that can link these two bound species together. In the case of polypyrrole it is believed that the lattice distortion extends over four pyrrole rings. This combination of a charge site and a radical is called a polaron. This could be either a radical cation or radical anion. This creates a new localized electronic state in the gap, with the lower energy states being occupied by a single unpaired electron. The polaron state of polypyrrole is symmetrically located about 0.5 eV from the band edges.

Upon further oxidation the free radical of the polaron is removed, creating a new spinless defect called a bipolaron. This is of lower energy than the creation of two distinct polarons. At higher doping levels it becomes possible that two polarons combine to form a bipolaron. Thus at higher doping levels the polarons are replaced with bipolarons. The bipolarons are located symmetrically with a band gap of 0.75 eV for polypyrrole. This eventually, with continued doping, forms into a continuous bipolaron bands. Their band gap also increases as newly formed bipolarons are made at the expense of the band edges. For a very heavily dope polymer it is conceivable that the upper and the lower bipolaron bands will merge with the conduction and the valence bands respectively to produce partially filled bands and metallic like conductivity.

2.1.1.3. Charge Transport

Although solitons and bipolarons are known to be the main source of charge carriers, the precise mechanism is not yet fully understood. The problem lies in attempting to trace the path of the charge carriers through the polymer. All of these polymers are highly disordered, containing a mixture of crystalline and amorphous regions. It is necessary to consider the transport along and between the polymer chains and also the complex boundaries established by the multiple numbers of phases. This has been studied by examining the effect of doping, of temperature, of magnetism and the frequency of the current used. These test show that a variety of conduction mechanisms

are used. The main mechanism used is by movement of charge carriers between localized sites or between solitons, polaron or bipolaron states. Alternatively, where inhomogeneous doping produces metallic island dispersed in an insulating matrix, conduction is by movement of charge carriers between highly conducting domains. Charge transfer between these conducting domains also occurs by thermally activated hopping or tunneling. This is consistent with conductivity being proportional to temperature

2.1.2. Stability and Processability

There are two distinct types of stability. Extrinsic stability is related to vulnerability to external environmental agent such as oxygen, water, peroxides. This is determined by the polymers susceptibility of charged sites to attack by nucleophiles, electrophiles and free radicals. If a conducting polymer is Extrinsic unstable then it must be protected by a stable coating.

Many conducting polymers, however, degrade over time even in dry, oxygen free environment. This intrinsic instability is thermodynamic in origin. It is likely to be cause by irreversible chemical reaction between charged sites of polymer and either the dopant counter ion or the π-system of an adjacent neutral chain, which produces an sp^3 carbon, breaking the conjugation. Intrinsic instability can also come from a thermally driven mechanism which causes the polymer to lose its dopant. This happens when the charge sites become unstable due to conformational changes in the polymer backbone. This has been observed in alkyl substituted polythiophenes.

Conjugated polymers may be made by a variety of techniques, including cationic, anionic, radical chain growth, co-ordination polymerization, step growth polymerization or electrochemical polymerization. Electrochemical polymerization occurs by suitable monomers which are electrochemically oxidized to create an active monomeric and dimeric species which react to form a conjugated polymer backbone. The main problem with electrically conductive plastics stems from the very property that gives it its conductivity, namely the conjugated backbone. This causes many such polymers to be intractable, insoluble films or powders that cannot melt. There are two main strategies to overcoming these problems. There are to either modify the polymer so that it may be more easily processed, or to manufacture the polymer in its desired shape and form. There are, at this time, four main methods used to achieve these aims.

The first method is to manufacture a malleable polymer that can be easily converted into a conjugated polymer. This is done when the initial polymer is in the desired form and then, after conversion, is treated so that it becomes a conductor. The treatment used is most often thermal treatment. The precursor polymer used is often made to produce highly aligned polymer chain which is retained upon conversion. These are used for highly orientated thin films and fibers. Such films and fibers are highly anisotropic, with maximum conductivity along the stretch direction.

The second method is the synthesis of copolymers or derivatives of a parent conjugated polymer with more desirable properties. This method is the more traditional one for making improvements to a polymer. What is done is to try to modify the structure of the polymer to increase its processability without compromising its conductivity or its optical properties. All attempts to do this on polyacetylene have failed as they always significantly reduced its conductivity. However, such attempts on polythiophenes and polypyrroles proved more fruitful. The hydrogen on carbon 3 on the thiophene or the pyrrole ring was replaced with an alkyl group with at least four carbon atoms in it. The resulting polymer, when doped, has a comparable conductivity to its parent polymer whilst be able to melt and it is soluble. A water soluble version of these polymers has been produced by placing carboxylic acid group or sulphonic acid group on the alkyl chains. If sulphonic acid groups are used along with built-in ionizable groups then such system can maintain charge neutrality in its oxidized state and so they effectively dope themselves. Such polymers are referred to as "self-doped" polymers. One of the most highly conductive derivatives of polythiophene is made by replacing the hydrogen on carbon three with a $-CH_2-O-CH_2CH_2-O-CH_2CH_2-O-CH_3$. This is soluble and reaches a conductivity of about 1000 S cm^{-1} upon doping.

The third method is to grow the polymer into its desired shape and form. An insulating polymer impregnated with a catalyst system is fabricated into its desired form. This is then exposed to the monomer, usually a gas or a vapor. The monomer then polymerizes on the surface of the insulating plastic producing a thin film or a fibre. This is then doped in the usual manner. A variation of this technique is electrochemical polymerization with the conducting polymer being deposited on an electrode either the polymerization stage or before the electrochemical polymerization. This cast may be used for further processing of the conducting polymer. For instance, by stretching

aligned bends of polyacetylene/polybutadiene the conductivity increase 10 fold, due to the higher state of order produced by this deformation.

The final method is the use of Langmuir-Blodgett trough to manipulate the surface active molecules into a highly ordered thin films whose structure and thickness which are controllable at the molecular layer. Amphiphilic molecules with hydrophilic and hydrophobic groups produces monolayers at the air-water surface interface of a Langmuir-Blodgett trough. This is then transferred to a substrate creating a multilayer structure comprised of molecular stacks which are normal about 2.5 nm thick. This is a development from the creation of insulating films by the same technique. The main advantage of this technique is its unique ability to allow control over the molecular architecture of the conducting films produced. It can be used to create complex multilayer structures of functionally different molecular layers as determined by the chemist. By producing alternating layers of conductor and insulator it is possible to produce highly anisotropic film which is conducting within the plane of the film, but insulating across it

Table 2.1: Stability and Processing Attributes of Some Conducting Polymers.

POLYMER	Conductivity (Ω^{-1} cm^{-1})	Stability (doped state)	Processing Possibilities
Polyacetylene	10^3 - 10^5	poor	limited
Polyphenylene	1000	poor	limited
PPS	100	poor	excellent
PPV	1000	poor	limited
Polypyrroles	100	good	good
Polythiophenes	100	good	excellent
Polyaniline	10	good	good

2.1.3. Thiazoles

There has been some interest recently in thiazole-based conjugated polymers. [44] Bredas and co-workers [45 have used valence effective Hamiltonian (VEH) calculations, a method known to give very good band structures for sulfur and nitrogen-containing polymers, [46] to investigate the effect of placing nitrogen atoms in the

conduction pathway of a poly(a-thiophene) structure. They conclude that doped polythiazoles should be good conductors.

The electronic, optical, and electric properties of π-conjugated poly(arylene)s have been the subject of many papers [37]. Among the poly(arylene)s, those made up of recurring five-membered rings (Figure 2.11) have received much attention because of their interesting chemical and physical properties. They are considered to take coplanar structures and to form highly extended π-conjugated systems owing to their less sterically hindered structures compared with those of poly(arylene)s constituted of six-membered rings [e.g., poly(*p*-phenylene), PPP].

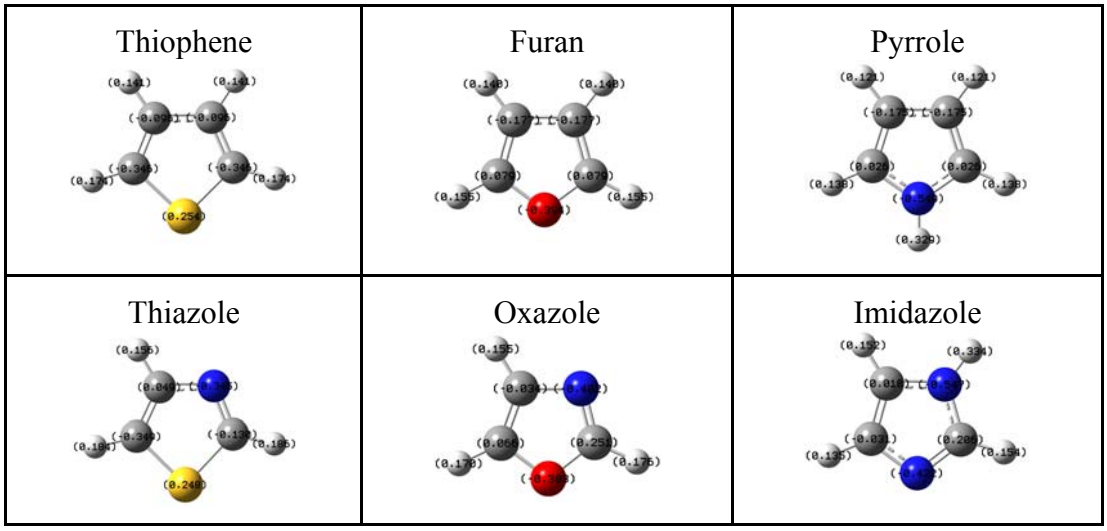

Figure 2.9: The most studied five-membered rings with Mulliken atomic charges.

Table 2.2: Mulliken atomic charges calculated using Gaussian 98 with Hartree Fock using the b3lyp/6-31g basis set.

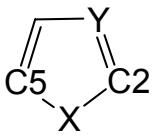

X	Y	ρ (C2)	ρ (C5)
S	CH	-0.346	-0.346
O	CH	0.079	0.079
NH	CH	0.026	0.026
S	N	-0.130	-0.349
O	N	0.251	0.066
NH	N	-0.031	0.206

PTh and PPy are made up of "electron-excessive" heterocyclic units and are susceptible to chemical and electrochemical oxidation (or p-doping). On the other hand, it has been recently reported that π-conjugated polyheterocycles containing electron-withdrawing imine nitrogen(s) (e.g., poly(pyridine-2,5-diyl) PPyb and poly-(quinoxaline-5,8-diyl) derivatives P[5,8-Qx(R1R2)]) show electron-accepting properties and are susceptible to reduction (or n-doping).

However, despite many examples of six-membered ring poly(arylene)s with imine nitrogen(s), analogous π-conjugated polymers composed of recurring five-membered heterocyclic units have received much less attention. Here we report the preparation of new π-conjugated five-membered-ring poly(arylene)s containing the imine nitrogen and their redox and optical properties in comparison with those of other π-conjugated polyheterocycles described above.

2.1.4. Polypyrroles

Among the conducting polyheterocycles, the most intensively studied polymers are polypyrrole, polythiophene, and their derivatives as well as polyphenylene and polyphenylene chalcogenides. Polypyrrole was shown to be a conducting polymer in 1968. Dall'Olio et al [47] prepared it by oxidation of pyrrole in sulfuric acid as a black powder with room temperature conductivity of 8 S cm^{-1}. This work was then extended by workers at IBM who showed that films of this polymer can be obtained by electrochemical polymerization. These films could be cycled electrochemically between a conducting (doped) state and an insulating state, with conductivities varying from [48] 100 to 10^{-10} S cm^{-1}. Unlike the morphology of the Shirakawa's polyacetylene, which is fibrillar, polypyrrole films are dense. Thus, physically impermeable films of polypyrrole could be prepared.

A fairly long period elapsed before this organic π-system attracted general interest and was found to be electrically conductive. Conductive polypyrrole films are obtained directly by anodic polymerization of pyrrole in aqueous or organic electrolytes (acetonitrile) [48]. They are black and, under suitable reaction conditions, can be detached from the anode in the form of self-supporting films (minimum thickness ca. 30 μm). Some of the conducting salt used in the electrolyte solution is incorporated in the film as a counterion. In contrast to polyacetylene, polypyrrole has a high mechanical and chemical stability and can be produced continuously as flexible film (thickness 80 μm; trade name: Lutamer, BASF) by electrochemical techniques. The

quality of the polymers is greatly influenced by many factors, e.g., impurities, electrode material, pressure, concentrations, temperature, and comonomers. The most decisive, however, are the current density and the electrolyte, particularly the conducting anion X^- [49] because it is incorporated into the polymer as a counterion. The properties of the counterion (e.g., its size, geometry, charge) influence the properties of the polymer. The amount of counterion (anion) incorporated depends on the reaction conditions. In general, one anion is incorporated for every three pyrrole units. Exceptions are pyrrole or thiophenesulfonic acids where the counterion is coupled directly to the monomer (self doping) [50]. Some typical conducting anions are fluoroborate, perchlorate, aromatic sulphonic acids, penicillin, n-dodecyl sulfate [49], phthalocyanine sulphonic acid, poly(styrene sulphonic acid), camphor sulphonic acid, styrene sulphonic acid, and heparin.

By changing reaction conditions, polymers with different surface morphologies, (e.g., an open porous structure) can be obtained.

The anion X^- can also be released, e.g., by applying a negative potential. Release can be specifically controlled, offering interesting possibilities for active counterions of medical interest (e.g., heparin and monobactam) that are incorporated into polypyrrole. Variation of the monomers and their substituents yields polymers with conductivities between 10^2 and 10^{-4} S/cm. Alkyl substituents also increase the solubility of the polymers with the result that electrically conducting polymers can be applied as coatings from solutions. This also applies to polymers derived from bridged pyrroles. An interesting variant is the chemical oxidation of heterocycles (e.g., thiophene or pyrrole [51] dissolved in an organic solvent (e.g., ethanol) on the surface of various materials. Conductive coatings (thickness 0.01 μm) can be produced on films of poly(phenylene sulfone), block copolymers of butadiene and styrene (Ultrason, Styrolux), poly(vinyl chloride), or other polymer films to give transparent, antistatic films with conductivities of about 0.001 S/cm. Ceramics and glass can also be coated in this way. Porous material (e.g., wood, fabrics, and open celled foams) or fibers (e.g., polyamide, glass, or carbon fibers) can also be modified and rendered antistatic by this method. Conductive powders (e.g., polypyrrole) with particle sizes of about 0.1 μm and conductivities of up to 10 S/cm can also be produced by chemical oxidation and can be incorporated as fillers in thermoplastics. These materials can be used for chip carriers.

2.1.5. Application Areas of Conducting Polymers

The commercialization exemplified by the following list of materials illustrates the effects of Heeger's, McDiarmid's and Shirakawa's work on the later development of conductive polymers. The principal interest in the use of polymers is in low-cost manufacturing using solution-processing of film-forming polymers. Light displays and integrated circuits, for example, could theoretically be manufactured using simple inkjet printer techniques [52-55]. Doped polyaniline is used as a conductor and for electromagnetic shielding of electronic circuits. Polyaniline is also manufactured as a corrosion inhibitor.

Polythiophenes have been studied extensively for use in light-emitting diodes, among other applications, due to the chemical variability offered by substitution at the 3- and 4- positions. The regularity of the side-chain incorporation strongly affects the electronic band gap of the conjugated main chain and is critical to device performance [56].

Polypyrrole has been tested as microwave-absorbing "stealth" (radar-invisible) screen coatings and also as the active thin layer of various sensing devices. The conductivity of polypyrrole film suggests applications such as flexible conductive paths in printed circuits, heating films, and film keyboards. Polypyrrole films show good electromagnetic shielding effects of about 40 dB over a wide range of frequencies (0 – 1500 MHz).

Other possible applications of conductive polymers include supercapacitors and electrolytic-type capacitors. Some conductive polymers such as polyaniline show a whole range of colors as a result of their many protonation and oxidation forms. Their electrochromic properties can be used to produce, e.g. "smart windows" that absorb sunlight in summer. An advantage over liquid crystals is that polymers can be fabricated in large sheets and unlimited visual angles. They do not generally respond as fast as in electron-gun displays, because the dopant needs time to migrate into or out from the polymer - but still fast enough for many applications.

2.2. Electropolymerization and Characterization Techniques

In an electrochemical polymerization, the monomer, dissolved in an appropriate solvent containing the desired anionic doping salt, is oxidized at the surface of an

electrode by application of an anodic potential (oxidation). The choice of the solvent and electrolyte is of particular importance in electrochemistry since both solvent and electrolyte should be stable at the oxidation potential of the monomer and provide an ionically conductive medium. Organic solvents like acetonitrile or propylene carbonate have very large potential windows [27], and a high dielectric constant which allows a good dissociation of the electrolyte and thus a good ionic conductivity. As a result of the initial oxidation, the radical cation of the monomer is formed and reacts with other monomers present in solution to form oligomeric products and then the polymer. The extended conjugation in the polymer results in a lowering of the oxidation potential compared to the monomer. Therefore, the synthesis and doping of the polymer are generally done simultaneously. The anion is incorporated into the polymer to ensure the electrical neutrality of the film and, at the end of the reaction, a polymeric film of controllable thickness is formed at the anode. The anode can be made of a variety of materials including platinum, carbon fiber, gold, glassy carbon, and tin or indium-tin oxide (ITO) coated glass [57]. The electropolymerization is generally achieved by potentiostatic (constant-potential) or galvanostatic (constant-current) methods. These techniques are easier to describe quantitatively and have been therefore commonly utilized to investigate the nucleation mechanism and the macroscopic growth. Potentiodynamic techniques such as cyclic voltammetry corresponds to a repetitive triangular potential waveform applied at the surface of the electrode. The latter method has been mainly used to obtain qualitative information about the redox processes involved in the early stages of the polymerization reaction, and to examine the electrochemical behavior of the polymer film after electrodeposition [57].

Cyclic voltammetry (CV) is very often used to characterize conducting polymer films. This is the method of choice for studying the reversibility of electron transfer because the oxidation and reduction can be monitored in the form of a current-potential diagram [58]. Intermediate species of very short lifetimes can be observed with microelectrodes using high scanning speeds [59]. These intermediate species (radical cations) are extremely important for the understanding of the polymerization mechanism. Another electrochemical technique, coulometry, and measures the amount of electricity involved in the oxidation process. The knowledge of the initial charge used to polymerize the monomer, and the charge involved in the doping process allows the estimation of the doping level in the conducting polymer

Chronoamperometry, *i.e.* measuring the current as a function of time, is a method of choice to study the kinetic of polymerization and especially the first steps [57]. As a potential step is large enough to cause an electrochemical reaction is applied to an electrode, the current changes with time. The study of this current response as a function of time is called chronoamperometry (CA). CA is a useful tool for determining diffusion coefficients and for investigating kinetics and mechanisms. Unlike CV, CA can yield this information in a single experiment.

2.3. Characterization Techniques

2.3.1. Electrochemical Impedance Spectroscopy (EIS)

With impedance data a complete description of an electrochemical system is possible [60]. Representations of the electrified interface have gradually evolved from repeated modifications (see Figure 2.12.) of the model first proposed by Helmholtz [61]. In a simple case, the interface can be modeled by an equivalent circuit (see Figure 2.13.), also called a Randles circuit [62], made of a double-layer capacitor in parallel with a polarization resistor (also known as a charge transfer resistor with certain constraints) and a Warburg impedance, connected in series with a resistor that measures the resistance of the electrolyte solution. Depending on the types of electrochemical reactions involved at the interface, the equivalent circuit can be much more complicated.

The model given in the Figure 2.13 predicts that a faradic current, which is due to the redox reactions, is always coupled with a capacitive component. Capacitance is regarded as noise, and considerable efforts have been made to eliminate or minimize it, resulting in tast (sampling), normal pulse, and differential pulse voltammetry [27]. However, reducing or minimizing the effects of non-faradic currents is considered a passive way to solve the problem. A more active and direct approach would be to determine and separate the faradic currents from the non-faradic signals [63], which is possible with Electrochemical Impedance Spectroscopy (EIS) because it provides all the information about the interface and the electrolyte solution.

Impedance is a totally complex resistance encountered when a current flows through a circuit made of resistors, capacitors, or inductors, or any combination of these. Depending on how the electronic components are configured, both the magnitude and the phase shift of an ac can be determined. Because an inductive effect is not usually

encountered in electrochemistry, we consider only the simple equivalent circuit shown in Figure 2.13 in which no inductor is present.

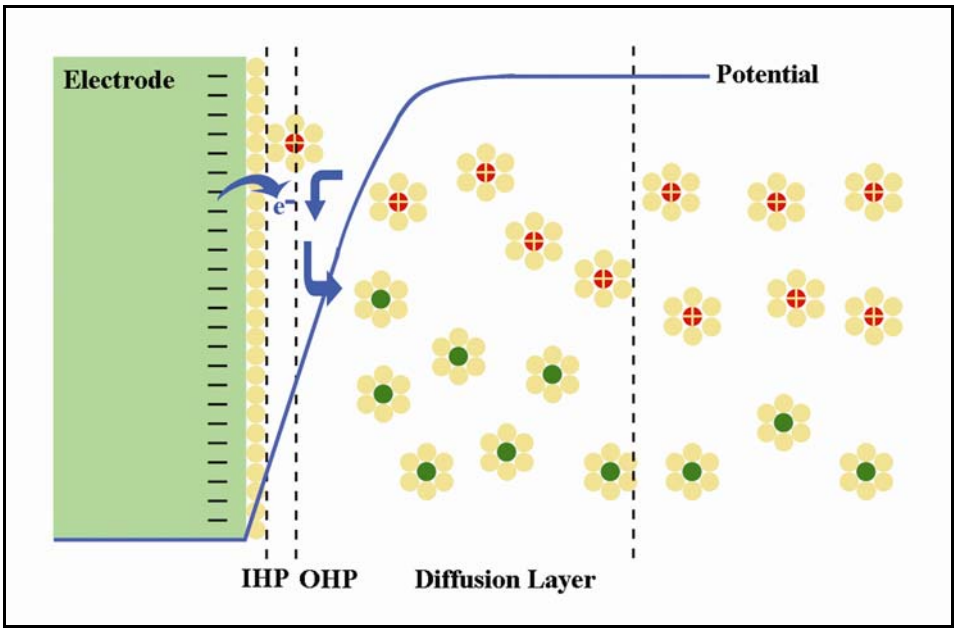

Figure 2.10: The oxidants (red) with a positive charge diffuse toward the negatively charged electrode, accept electrons from the electrode at the interface, become the reductants (green), and diffuse to the bulk of the solution. The oxidant is also a counterion to the electrode. No specific adsorption is considered at the interface. IHP and OHP are the inner and outer Helmholtz planes, respectively.

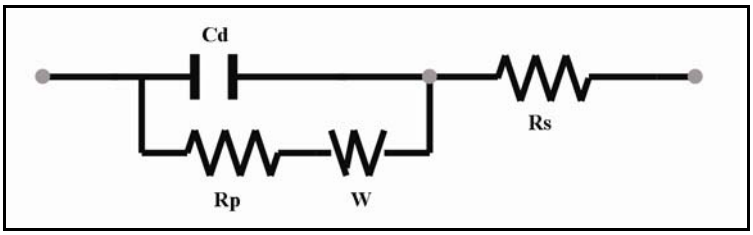

Figure 2.11: An equivalent circuit representing each component at the interface and in the solution during an electrochemical reaction is shown for comparison with the physical components. Cd, double layer capacitor; Rp, polarization resistor; W, Warburg resistor; Rs, solution resistor.

However, first consider an experiment in which a series of increasing dc potentials (a ramp) are applied to a working electrode in an electrochemical cell containing an electroactive species. A current–potential curve (Figure 2.14) is obtained, which is described by the Butler–Volmer equation (solid line)

$$i = i_0 \left[e^{\frac{-\alpha nF}{RT}\eta} - e^{\frac{(1-\alpha)nF}{RT}\eta} \right] \qquad \textbf{(2.2)}$$

in which η is the overpotential defined as $E - E_{eq}$, with E and E_{eq} representing the applied and equilibrium potentials, respectively; i_0 is the exchange current at $\eta = 0$; n is the number of electrons transferred; F is the Faraday constant; R is the gas constant; T is the absolute temperature; and α is the transfer coefficient for electron transfer. The faradic current i is limited by the mass transport (dashed line curving to the right) when the rate of electron transfer becomes large enough. At a given overpotential η_{bias}, the slope of the curves, $d_i/d\eta_{bias}$, is $1/R_p$, in which R_p is the polarization resistance. When a small ac voltage wave of frequency ω at η_{bias} (Figure 2.14.) is superimposed, the ac of the same frequency will be flowing on top of the dc. Because the interface has resistors and a capacitor (Figure 2.13), the flowing ac will experience a phase shift, expressed as i_{bias}, caused by the ac wave perturbation. For an equivalent circuit (Figure 2.13), a straightforward impedance expression can be derived by applying Ohm's law to two components connected in parallel. One of these is R_p, and the other is $1/(j\omega C_d)$, in which C_d is the double-layer capacitance.

$$Z(\omega) = R_s + \frac{R_p}{1 + j\omega R_p C_d} = R_s + \frac{R_p}{1 + \omega^2 R_p^2 C_d^2} - \frac{j\omega R_p^2 C_d}{1 + \omega^2 R_p^2 C_d^2} = Z' + jZ'' \qquad \textbf{(2.3)}$$

To make the derivation of the equation and its interpretation straightforward, we neglected the contribution of the Warburg component. Thus, the impedance of the interface consists of two parts, a real number Z' and an imaginary number Z'' with a complex representation, $Z(\omega) = Z'(\omega) + jZ''(\omega)$ with phaseangle $\phi = \tan^{-1}[Z''(\omega) + Z'(\omega)]$. Although the capacitance is relatively constant over the potential at a given electrode, the R_p varies as a function of η_{bias} applied to the electrode.

At a given dc bias potential, a series of $Z(\omega)$ data are obtained in a range of frequencies, typically 100 kHz to 10^{-4} Hz. The impedance varies, depending on frequencies, and is often plotted in different ways as a function of frequency (making it a spectroscopic technique), hence, the name EIS [27, 28].

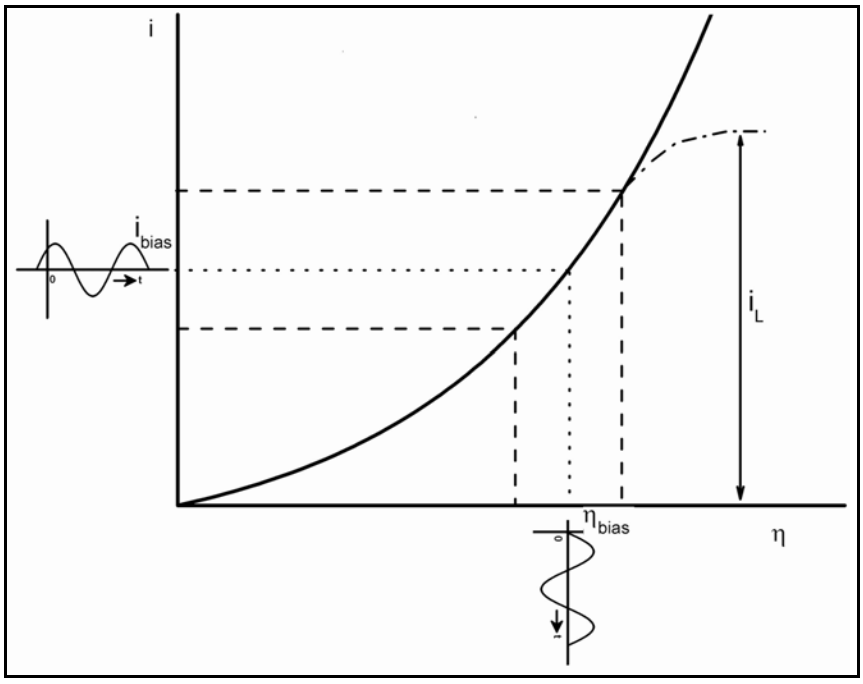

Figure 2.12: The dc plotted as a function of overpotential according to the Butler–Volmer equation (solid line), which is limited by mass transport at large overpotentials (dashed line curving to the right), an ac voltage (broken line) superimposed on the dc bias potential, η_{bias} (dot-dashed line), shown on the i axis $[\eta_{bias} + \Delta\eta \sin(\omega t)]$, and the resulting ac superimposed on the dc on the i axis $[i_{bias} + \Delta i \sin(\omega t + \phi)]$. Rp is obtained by taking $\Delta\eta/\Delta i$, in which I is obtained after applying the ac voltage wave at a given η.

By treating the impedance data in such a frequency range, system characteristics for an electrochemical reaction (i.e., R_s, R_p, and C_d) can be obtained. R_p is a function of potential; however, at $\eta = 0$, it becomes the charge-transfer resistance R_{CT}. Two convenient ways of treating the impedance data are the Nyquist plot, in which imaginary numbers $Z''(\omega)$ are plotted against real numbers $Z'(\omega)$, and the Bode plot, in which absolute values of impedance or phase angle are plotted against the frequency. Extraction of the system characteristics requires interpreting the Nyquist plot according to Equation 2.4. At high frequencies, the frequency dependent term of Equation 2.4 vanishes, resulting in $Z(\omega) = Z'(\omega) = R_s$, which is an intercept on the $Z'(\omega)$ axis on the high-frequency side ($\phi = 0$ or $Z''(\omega) = 0$). For $\omega \rightarrow 0$, Equation 2.3 becomes $Z(\omega) = R_s + R_p$, which is an intercept on the $Z'(\omega)$ axis on the low frequency side. At the frequency where a maximum $Z''(\omega)$ is observed, the straightforward relationship (Equation 2.4), which is the time constant of the electrochemical reaction, can be shown and indicates how fast the reaction takes place. Also, if R_p and C_d is known, C_d can be obtained because R_p is already known from the low-frequency intercept on the $Z'(\omega)$ axis.

$$R_p \text{g} C_d = 1/\omega_{\max} = 1/(2\pi f_{\max}) = \tau_{rxn} \quad \textbf{(2.4)}$$

The Nyquist plot gives all the necessary information about the electrode–electrolyte interface and the reaction. Similar information is obtained by examining the Bode diagram using Equation 2.2. log R_s and log (R_p+R_s) are obtained straightforwardly from the $Z(\omega)$ versus log ω plot at high and low frequencies from the same argument as the Nyquist plot. In the intermediate frequency region, an almost straight line with a slope of ~ –1.0 can be seen. The equation for this line is obtained by ignoring the frequency-independent terms, R_s and 1 in the denominator, of Equation 2.3 to yield 2.5

$$Z(\omega) = R_s + \frac{R_p}{1 + j\omega R_p C_d} \quad \textbf{(2.5)}$$

Taking the logarithm on both sides of the resulting equation yields $Z(\omega) = -\log\omega - \log C_d$, which says that $\log|Z(\omega)|$ vs. $\log\omega$ would have a slope of –1, and C_d can be obtained from the intercept of this line with the $Z(\omega)$ axis when $-\log\omega = 0$ at $\omega = 1$. Thus, the Bode plot provides the same information as the Nyquist plot. The ϕ vs. $\log\omega$ plot shows that the impedance responses are resistive primarily at high and low frequencies as indicated by practically no phase shifts, whereas at intermediate frequencies, they are mostly capacitive as their phase shifts get closer to 90°.

Contribution and the effect of the Warburg impedance can be important at low frequencies because the mass transport of the electroactive species may limit the electron-transfer process. The Warburg impedance is imparted by mass transfer and can be derived by

$$Z(\omega) = R_s + R_p\left[1 + \frac{\lambda}{\sqrt{2\omega}}\right] - R_p^2\lambda^2 C_d - \frac{jR_p\lambda}{\sqrt{2\omega}} \quad \textbf{(2.6)}$$

in which $\lambda = k_f/\sqrt{D_O} + k_b/\sqrt{D_R}$, and k_f and k_b are the forward and backward electron-transfer rate constants, respectively, and D_O and D_R are the diffusion coefficients for the oxidant O and the reductant R, respectively, for the reaction $O + ne^- \leftrightarrow R$. Here the frequency-dependent terms $\lambda/\sqrt{2\omega}$, appearing in both the real and the imaginary terms in Equation 2.5, are called the Warburg impedance. When $Z'(\omega)$ is plotted against $Z'(\omega)$with the Warburg component included, the high- and low-frequency intercepts on

the $Z'(\omega)$ axis are still R_s and $R_s + R_p$, as was the case without the Warburg impedance, and the plot of the Warburg components becomes a straight line with a slope of unity and an intercept of $R_s + R_p - R_p^2\lambda^2 C_d$. Thus we can calculate λ, and thereby the diffusion coefficient from λ when k_f is known, and k_f can be obtained from $i_f = nFAk_f C_O$, in which C_O is the bulk concentration of oxidant and A is the area. In other words, we now have a complete description of the electrochemical system.

2.3.2. Attenuated Total Reflectance (ATR)-FTIR

Attenuated total reflectance (ATR) spectroscopy, also known as internal reflection spectroscopy or multiple internal reflectances (MIR), is a versatile, nondestructive technique for obtaining the infrared spectrum of the surface of a material or the spectrum of materials either too thick or too strongly absorbing to be analyzed by standard transmission spectroscopy. ATR spectroscopy has been developed since 1959, when it was reported that optical absorption spectra could conveniently be obtained by measuring the interaction of the evanescent wave with the external less dense medium [64]. In this technique, the sample is placed in contact with the internal reflection element (IRE), the light is totally reflected, generally several times, and the sample interacts with the evanescent wave (Figure 2.15) resulting in the absorption of radiation by the sample at each point of reflection. The internal reflection element is made from a material with a high refractive index; zinc selenide (ZnSe), thallium iodide – thallium bromide (KRS-5), and germanium (Ge) are the most commonly used. To obtain total internal reflection the angle of the incident radiation θ must exceed the critical angle θ_c. The critical angle is defined as:

$$\theta_c = \sin^{-1}\frac{n_2}{n_1} \qquad \textbf{(2.7)}$$

where n_1 is the refractive index of the internal reflection element and n_2 is the refractive index of the sample.

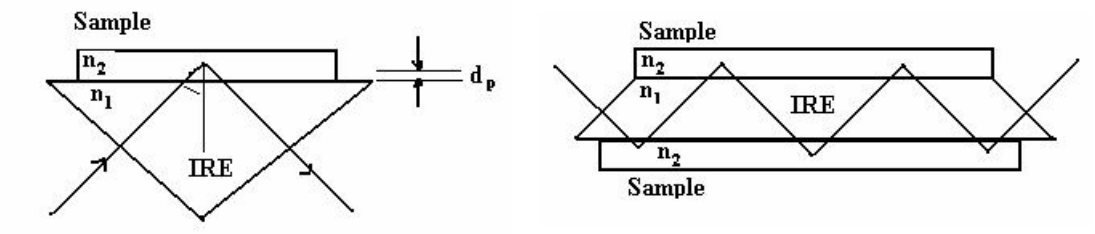

Figure 2.13: : Schematic representation of total internal reflection with: a) Single reflection; b) Multiple reflection IRE (internal reflection element) n_1=Refractive index of the internal reflection element; n_2=Refractive index of the sample with $n_2 < n_1$; θ = Angle of incidence; d_p=Depth of penetration.

What makes ATR a powerful technique is the fact that the intensity of the evanescent wave decays exponentially with the distance from the surface of the internal reflection element. As the effective penetration depth is usually a fraction of a wavelength, total internal reflectance is generally insensitive to sample thickness and so permits thick or strongly absorbing samples to be analyzed. The depth of penetration d_p, defined as the distance required for the electrical field amplitude to fall to e^{-1} of its value at the interface, is given by:

$$d_p = \frac{\lambda_1}{2\pi(\sin^2\theta - n_{21}^2)^{1/2}} \qquad \textbf{(2.8)}$$

where $\lambda_1 = \lambda/n_1$ is the wavelength in the denser medium, and $n_{21} = n_2 / n_1$ is the ratio of the refractive index of the less dense medium divided by that of the denser. Although ATR and transmission spectra of the same sample closely resemble each other, differences are observed because of the dependency of the penetration depth on wavelength: longer wavelength radiation penetrates further into the sample, so that in an ATR spectrum bands at longer wavelengths are more intense than those at shorter ones. The depth of penetration also depends on the angle of incidence; hence, an angle of 45°, which allows a large penetration depth, is generally used to analyze organic substances, rather than an angle of 60°, which results in a substantially weaker spectrum due to the decreased depth of penetration. The degree of physical contact between sample and internal reflection element determines the sensitivity of an ATR spectrum. To achieve this, a horizontal ATR accessory such as FastIR, in which the top plate is the sampling surface, is used; reproducible contact is ensured by a special sample clamp or powder press. Good quality spectra are thus obtained for many materials that present problems of analysis with routine transmission methods, e.g., powders, pastes, adhesives, coatings, rubbers, fibers, thick films, textiles, papers,

greases, foams, and viscous liquids. Liquid samples are also well suited to ATR analysis. Most liquids require a very short path length; aqueous samples, for instance, are measured at path lengths of no more than ca. 15 μm, which makes the design of transmission cells difficult because flow of liquids is hindered; they also exhibit interference fringes because of the small spacing between the high refractive index infrared windows. These problems are eliminated by using liquid ATR cells, a variant of solid ATR, in which the internal reflection element is surrounded by a vessel into which the liquid is poured.

2.4. Synthetic Routes

The synthesis of electrically conducting polymers with conjugated –HC=CH– bonds requires the controlled coupling of a large number of monomers (unsaturated compounds or compounds with difunctional groups). Alternatively, pendant groups attached to existing polymers can be cyclized to give conjugated systems. Polymerization of unsaturated monomers gives polymers with long chains that are often branched and cross-linked and therefore insoluble. Alkynes polymerize as follows:

1. $n\ HC{\equiv}CH \rightarrow \ {\left(CH{=}CH\right)}_n$ [65]
(2.9)

2. $n\ HC{\equiv}C{-}CH{=}CH_2 \rightarrow \ {\left(CH{=}CH{-}CH{=}CH\right)}_n$ [65]
(2.10)

3. $n\ RC{\equiv}CH \rightarrow \ {\left(CR{=}CH\right)}_n$ [66]
(2.11)

4. Alkyne or allene $\rightarrow$ 460 °C thermal polymerization, insoluble polyenes and aromatics [67]

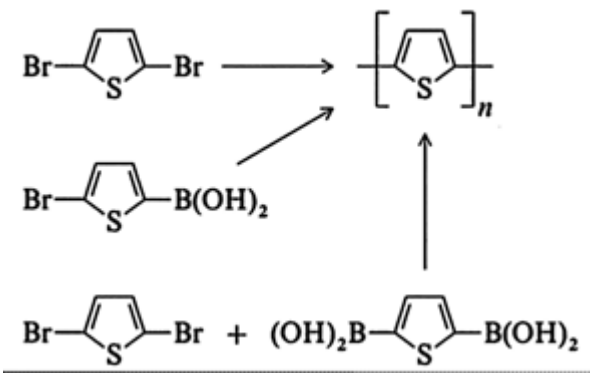

(2.12)

Stepwise coupling of monomers with difunctional groups runs in a more controlled fashion than polymerization of unsaturated monomers but problems are caused by low conversion rates and purification of the starting monomers. This method includes Wittig, MacMurry, retro Diels – Alder, and elimination reactions. It is accessible to a wide variety of soluble precursors and produces defined polymers. Examples follow:

1. Oxidative coupling [68] can be applied to pyrrole, thiophene, aromatic, and heteroaromatic systems (0 – 350 °C)

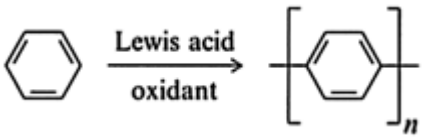

(2.13)

2. Grignard coupling [69]:

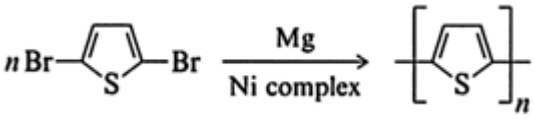

(2.14)

3. Boronic acid coupling [70]:

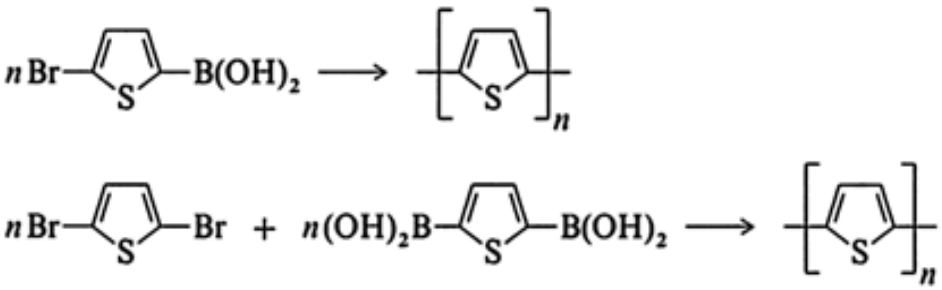

(2.15)

4. Stille reaction [71]:

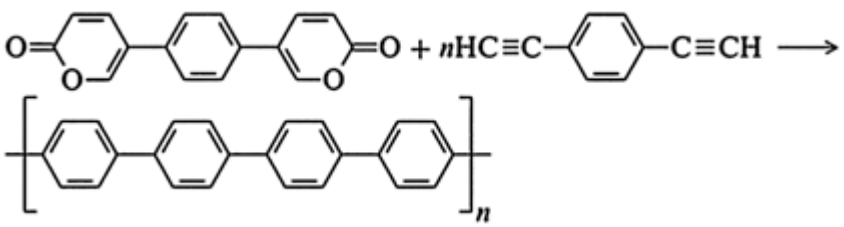

(2.16)

5. Elimination reactions [72]:

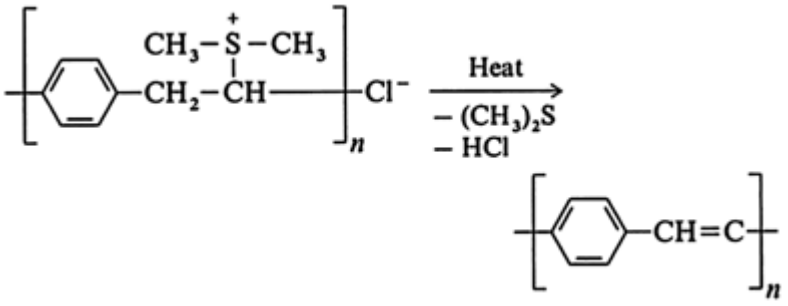

(2.17)

6. Feast reaction (retro- cycloaddition) [73]:

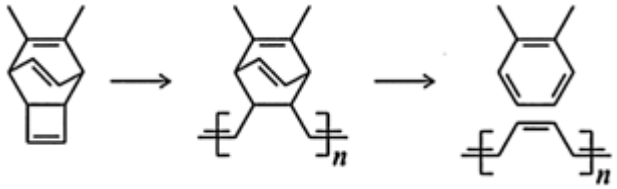

(2.18)

7. Grubb's method: polybenzvalene is isomerized to polyacetylene in the presence of $HgCl_2$ [74]:

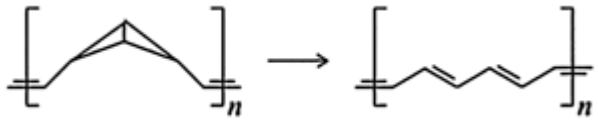

(2.19)

Cyclooctatetraene is also polymerized to give soluble polyenes [75]:

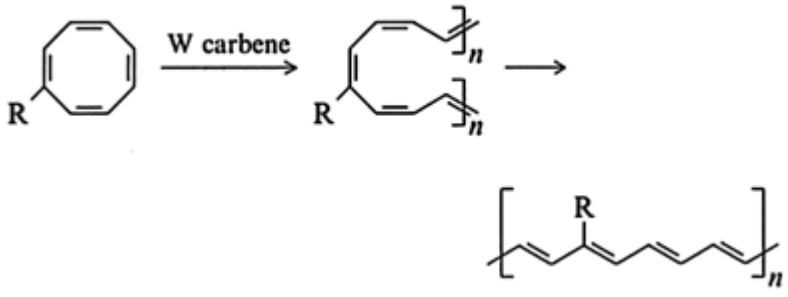

(2.20)

Polycyclization starts with polymers whose pendant side groups are cyclized to give condensed systems, often under pyrolytic conditions. Defects cannot be excluded. These methods lead to the basic structures of electrically conducting organic materials (ECOMs) and are reviewed in [65]. Examples follow [68]:

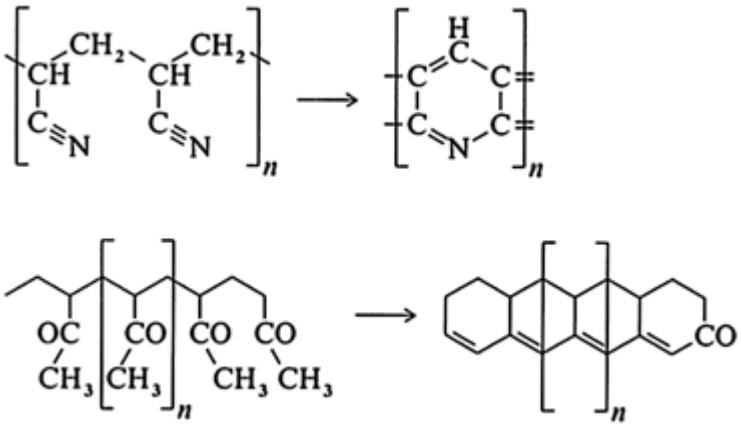

(2.21)

Analogous reactions occur with $-CH=CH_2$ pendant groups.

Monomers may also be cyclized [66], [76]:

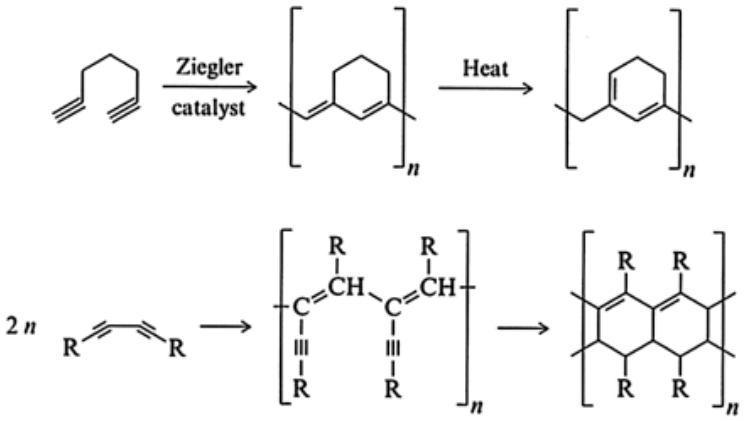

(2.22)

2.5. Cross-Coupling Reactions

The cross-coupling reaction accessible via a variety of organometallic reagents may provide a fundamentally common synthetic methodology. In 1972, Kumada and Tamao [77, 78] and Corriu [79] reported independently that the reaction of organomagnesium reagents with alkenyl or aryl halides could be markedly catalyzed by Ni(II) complex. Kochi [80-82] found the efficiency of Fe(III) catalyst for the cross-coupling of Grignard reagents with 1-halo-l-alkenes and Li_2-$CuCl_4$ catalyst for haloalkanes. The palladium-catalyzed reaction of Grignard reagents was first reported by Murahashi, [83] the synthetic utility of which was then amply demonstrated by Negishi [84, 85] on the reactions of organoaluminum, zinc, and zirconium reagents. After those discoveries, many other organometallic reagents have proven to be highly useful as nucleophiles for

the cross-coupling reaction, e.g., organolithiums by Murahashi, [86] organostannans by Migita [87, 88] and Stille, [89, 90] l-alkenylcopper(I) by Normant, [91] organosilicon compounds by Hiyama [92-94].

Palladium-catalyzed cross-coupling reactions of organohalides (or triflates) with organometallic reagents follow a general mechanistic cycle. The 14-electron Pd (0) [the active catalyst PdL is 6 electron when P (*o*-Tol)$_3$ is used as the ligand] catalyst 4 is sometimes reduced from a Pd(II) species 1 by an organometallic reagent R_1M (2). The transmetalation product 3 from 1 and 2 undergoes a reductive elimination, giving rise to Pd (0) species 4, along with the homocoupling product R_1-R_1. This is one of the reasons why the organometallic coupling partners are often used in a slight excess relative to the electrophilic partners. When the Pd(0) catalyst 4 is generated, the catalytic cycle goes through a three-step sequence,

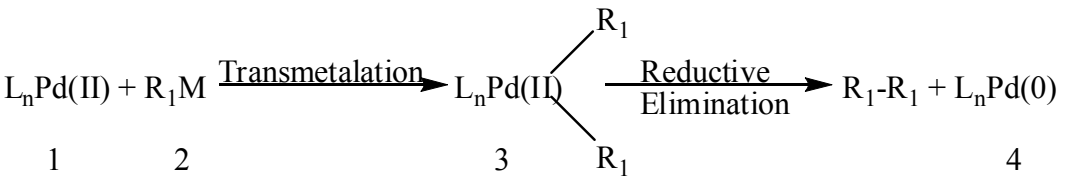

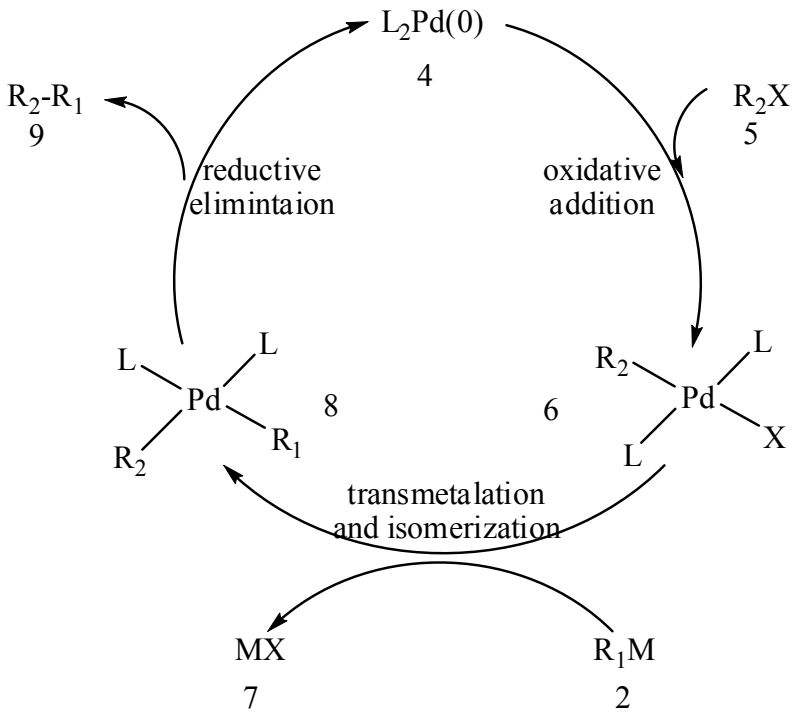

Figure 2.14. A general mechanistic cycle of palladium catalyzed cross-coupling reactions of organohalides with organometallic reagents.

a) Electrophile R_2-X (5) undergoes an oxidative addition to Pd(0) to afford a 16-electron Pd(II) intermediate 6;

b) Subsequently, 6 undergoes a transmetalation step with the organometallic reagent R_1M (2) to produce intermediate 8. When there is more than one group attached to metal M, the order of transmetalation for different substituents is:

alkynyl > vinyl > aryl> allyl ~ benzyl >> alkyl

The transmetalation step, often rate-limiting, is the step to which attention should be directed if the reaction goes awry;

c) Finally, with appropriate syn geometry, intermediate 8 undergoes a facile reductive elimination step to produce the coupling adduct R_2-R_1 (9), regenerating palladium (0) catalyst 4 to close the catalytic cycle.

2.5.1. Stille Coupling

Examples of the palladium-catalyzed coupling of organotin compounds with carbon electrophiles were first reported in 1977 by Kosugi, Shimizu and Migita[95-97]. The first study by Stille appeared in 1978 [98]. The early work of Beletskaya, using "ligandless" catalysts in cross-coupling reactions, also often employed organostannanes[99]. In recognition of Stille's comprehensive synthetic and mechanistic studies, this coupling is refered as the Stille reaction [100]. The stille reaction is schematcally defined in Eq. 2.23.

$$R^1Sn(R^2)_3 + R^3X \xrightarrow{Pd(0)L_n} R^1\text{-}R^3 + (R^2)_3SnX \qquad \textbf{(2.23)}$$

In equation 1, R^1 is typically an unsaturated moiety (e.g., vinyl, aryl, heteroaryl, alkynyl, allyl) or less often an alkyl group, and R^2, the nontransferable ligand, is almost always butyl or methyl. Elctrophiles participating in the coupling include halides(almost always bromides ar iodides) and sulfonates(most often used are the triflates). Other leaving groups have been used in special cases.

The stille reaction belongs to the larger family of palladium- and nickel –catalyzed cross-coupling reactions which features, e.g., organomagnesium [101], organozinc[102], organoboron[103], and organosilicon reagents[104].

Organotin reagents are air and moisture-stable organometallics, and can be conveniently purified and stored. Since they do not react with most common functional groups, the use of protecting groups is almost always unnecessary in conjuction with the stille reaction. This is a very unusual and attractive feature for an organometallic process. Also, the reaction is often neither air nor moisture sensitive. In some cases, water and oxygen have actually been shown to promote the coupling. Although the reaction as initially described by Stille is often carried out under rather drastic conditions(temperatures of >100º are not uncommon), newly developed ligands[105] and the addition of copper (I) salts have solved some of the problems associated with low reactivity. The utility and mildness of the Stille reaction are demonstrated by its frequent use in the final stages of complex natural product synthesis. The reaction was reviewed by Stille in 1986 [100], and by mitchell in 1992 [107] ; a rather comprehensive account by Farina and Roth has appeared more recently[108].

2.5.2. Mechanistic Considerations, Regiochemistry, and Stereochemistry

The three –step catalytic cycle proposed for the Stille reaciton follows the general principles of transition metal- mediated cross- coupling reactios and is shown in Figure 2.15 [100].

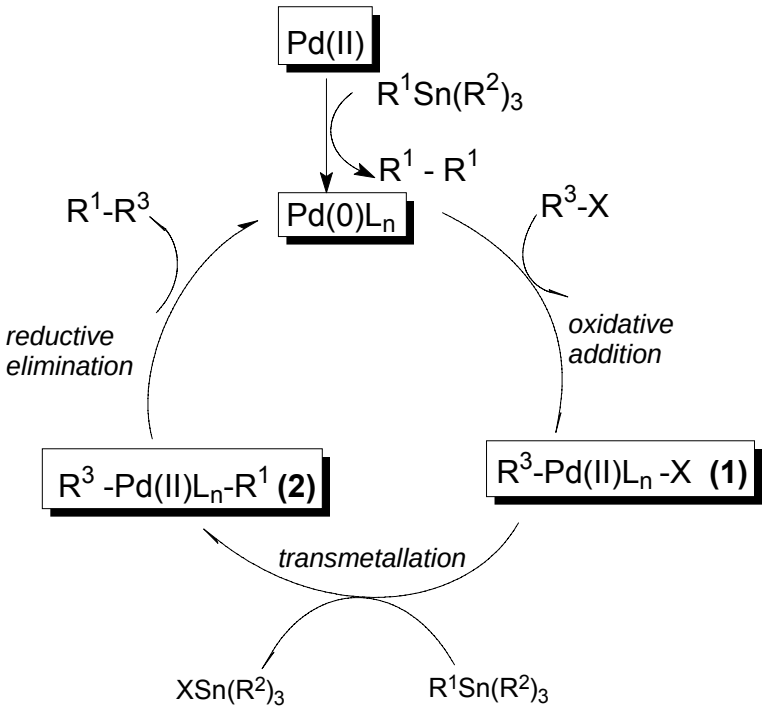

Figure 2.15. Catalytic cycle of the stille reaction.

When the catalyst is introduced as Pd(II), fast reduction by the stannane to a Pd(0) complex ensues, and the resulting Pd(0) species enters the cycle. Alternatively, the catalyst can be introduced directly as Pd(0). The rate or yield differences sometimes observed between Pd(II) and Pd(0) catalyst are not likely to be due to the initial difference in oxidation state, but rather to the stoichiometric ratio of palladium to ligand or other factors[105].

The first step of the cycle is termed oxidative addition and is quite general process for low-valent transition metal complexes[109]. The reaction is represented as a simple process in scheme 1, but is likely to be rather complex one. There is substantial evidence that a coordinatively unsaturated Pd(0) species for example $Pd(PPh_3)_2$, is responsible for the oidative process[110]. When the substrate is an aryl iodide, the reaction is accelerated by electron-withdrawing substituents on the ring ($\rho = +2$) [111].

Oxidative additions are also accelerated by electron – rich phosphorus ligads on the palladium center[112]. In the coupling of aryl bromides with tetramethylstanne, the overall rate is strongly enhanced by electron- withdrawing groups on the aryl moiety ($\rho = +3.38$), suggesting that in this case the oxidative addition is rate limiting[113].

At least with alkenyl halides, the oxidative addition may be a reversible process. Such a reaction generally proceeds with retention of olefin geometry[114].

Benzylic bromides undergo oxidative addition with partial or total racemization[115]; this has been explained by invoking a one – electron transfer procss for this oxidative addition[116], and CIDNP studies have supported the suggestions[117]. In these cases, the oxidative addition may be accelerated by the presence of oxygen in solution[113]. Intermediate 1 (Figure 2.17) is generally formed as a trans square-planar complex, i.e., the two phosphine moietes are *trans* to each other, although the intermediacy of the less stable cis complex is assumed [100].

In allylic systems, i.e., allylic chlorides, the oxidative addition was initially shown to proceed with cmplete inversion of configuration, through the intermediacy of η^3 – complexes[118], but subsequent studies have revealed a more complex situation (Eq. 2.24) [119].

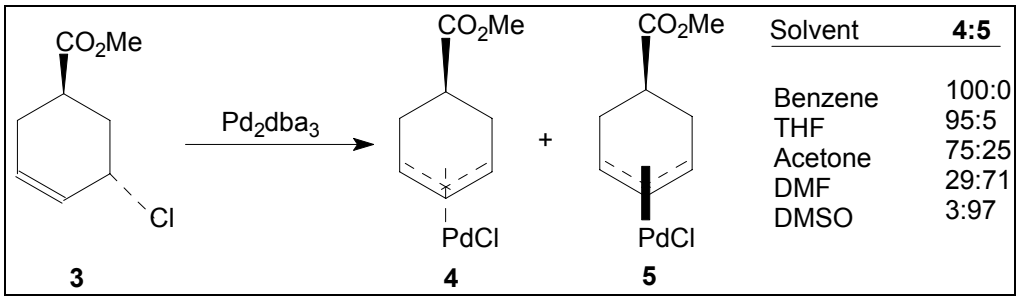

(2.24)

Specifially, it was shown that, in the absence of strong coodinating ligands, the stereochemistry depends on the solvent, nonpolar solvents favorig retention and polar onesleading to inversion. Furthermore, olefin ligands promote syn oxidative addition, and phosphines favor the anti pathway [120].

Although it is known that the transmetallation is very often the rate-determining step of the Stille reaction, much less is known mechanistically about this metathesis reaction.

In early studies, Stille et. al. Showed that showed that, in the coupling of benzylic stannanes with acid chlorides, electron – releasing substituents slightly increased the transmetallation rate ($\rho = +1.2$), suggesting that carbon-tin bond breaking precedes palladium-carbon bond formation. The sterechemical outcome with benzylic stannnes is predominantly inversion at the tin – bearing carbon, suggesting an "open" S_E2 mechanism [121].

More recently, it has been shown that the transmetallation of 1 to 2 proceeds via prior ligand dissociation and that ligands with lower donicity toward Pd(II) than PPh_3 can lead to major rate enhancements in the transetallation [105]. With these ligands, many Stille couplings previously requiring vigorous conditions can be performed at room temperature.

In studies of the synthtically important coupling of organic triflates [122,123], LiCl is necessary to induce couping of organic triflates in THF as solvent. This has been rationalized by postulating that the initial oxidative addition product (Figure 2.16), which was isolated in one case, is catalytically incompetent, whereas ligand substitution with chloride ion leads to the reactive species **7** [28].

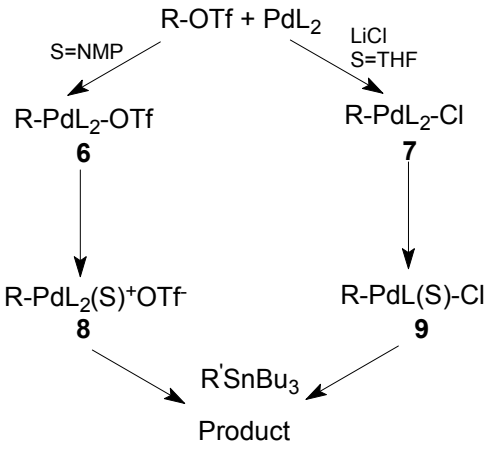

Figure 2.16. Two possible pathways in the stille coupling with organic triflates.

More, recently, it has been found that addition of LiCl is often not necessary when operating in highly polar solvents like NMP, and in many cases LiCl is actually an inhibitor of the coupling. This was explained by invoking two pathways in the transmetallation, i.e... a faster one proceeding via cationic species **8** and a slower one (with L=PPh_3) proceeding via ligand dissociation (through **9**). Hammet studies confirmed that there are two pathways with opposite electronic demands. Thus, in the absence of chloride the reaction is faster when the arylstanne contains electron-releasing groups (ρ = - 0,89), whereas in the presence of LiCl, electron-withdrawing substituents also enhanced the rate. The transmetallation is affected n a complex way by the combination of LiCl, ligads and solvent and the highest rates are obtained with $AsPh_3$ as ligand. With this superior ligand, the effect of halide additives on the rate of the transmetallation is minimal [124].

Intramolecular couplings o triflates with stannes do not require LiCl even in THF [125]. The recently reported ability of Ag(**I**) salts to improve some Stille couplings may also be explained by a switch of the transmetallation pathway via **8** away from **9** (scheme 2) [126].

The cocatalytic effect of Cu(I) in the Stille coupling was reported by Liebesking and Fengl [106]. Later studies have shown that Cu(**I**) performs a dual role: In ethereal solvents (THF, dioxane) and in conjuction with highly coordinating ligands (PPh_3), Cu(I) acts as a ligand scavenger to facilitate formation of the coordinatively unsaturated Pd(**II**) intermediate (**9** in the scheme) needed to effect transmetallation, where as in highly dipolar solvents (NMP) in the presence of "soft" ligands ($AsPh_3$) formation of an organocopper species s likely [127]. Thus, it seems simply that in the presence of

inorganic Cu(I) salts, an organostanne may be in equilibrium with an organocopper species (Eq. 2.24). Another important role of Cu(I), enhancing the selectivity of group transfer in the Stille reaction, s discussed ina later section.

$$RsnBu_3 + CuI \underset{\leftarrow}{\overset{NMP}{\rightarrow}} RCu + IsnBu_3 \qquad \textbf{(2.24)}$$

Similar transmetallations have been postulated in order to explain the beneficial effect of stoichiometric Zn(II) salts on certain Stille couplings, but no experimental evidence is available[122].

From the standpoint of the stereochemistry at Pd(II), the transmetallation usually proceeds with retention of configuration and is probably followed by cis-trans isomerization. The reductive elimination that follows probably proceeds through a T-shaped intermediate via prior ligand dissociation at Pd(II) [109]. Pd(IV) species have been implicated as intermediates in the reductive elimination [128], but factors that influence this step are not discussed further since reductive elimination is not rate determining in the Stille coupling. In the coupling of allylic electrophiles, however, reductive elimination will determine the regşochemistry of coupling, and in this case detailed understanding of this step is very important.

Allylic halides, typically chlorides, couple smoothly with organostannanes under normal conditions, and the regiochemistry of the coupling is usually the one resulting from attack of the organostanne at the less hşndered terminus of the allylic moiety (Eqs 2.25 and 2.26) [118].

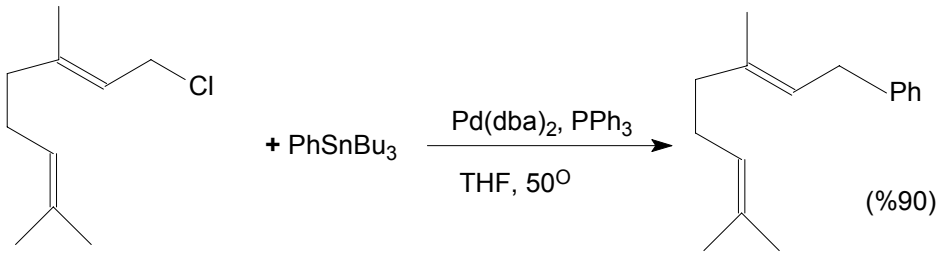

(2.25)

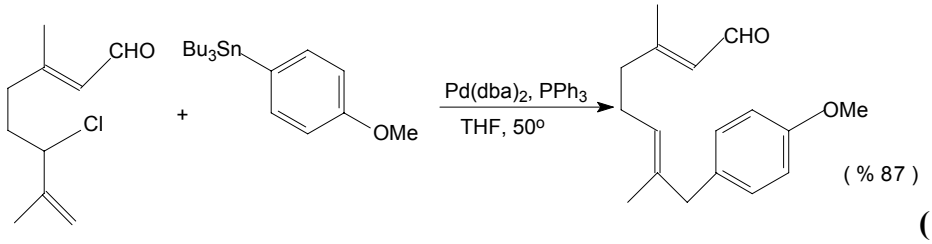

(2.26)

When the organostanne is also allylic, the situation is more complicated. Apparently, the coupling is somewhat regiospecific, and the C-C bond is formed between the more substituted end of the allylic stannane and the less substituted one in the allylic halide [129,130]. To explain the predominant allylic transposition of the stannane, both Stille and Trost postulated a direct attack of the stannane at the carbon terminus of an intermediate π – allyl complex, but there is no proof for such a mechanism. Indeed, indicator substrates for nucleophilic attack at π – allyl complexes classify allylstannanes as reacting directly at Pd(II) and not at carbon [131]. This mechanistic issue is still unresolved, even though a simple stereochemical probe could resolve the issue. On the other hand, in the presence of maleic anhydride the coupling takes place in a preferred head- to- head mode, and the stereochemistry indicates attack of the stannane at the Pd center of the π – allyl complex, followed by reductive elimination with retention of configuration [132,133].

One must also note that the two regiochemistries are interconvertible by Cope rearrangement [134].

An important mechanistic issue that has recently begun to be addressed by several investigators concerns the effect of nucleophilic assistance at tin(IV) during the transmetallation. Two studies [135,136] have independently shown that a nucleophilic moiety placed within the stannane considerably enhances transmetallation rates, whereas other studies in related systems have failed to detect such enhancements [124]. The increased reactivity of stannanes **10** has been explained by invoking internal N-Sn coordination in the transition state [135], and a similar rationalization has been applied to the increased reactivity of systems such as **11** [136].

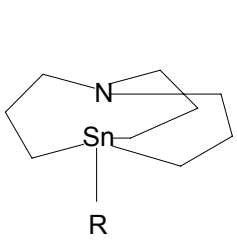

10

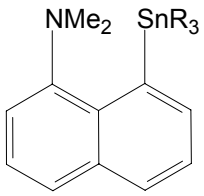

11

(2.27)

These stannanes are able to effect transfers of alkyl moieties, which occur sometimes with difficulty or not at all using traditional Stille chemistry.

3. EXPERIMENTAL WORK

3.1. Materials

N.methyl Pyrrole (N-Py), Br_2, BuLi (2.5 M in hexane) was used as received from Lancester and Aldrich Chemicals with a purity of higher than 99%. Electrolytes, tetrabutylammonium hexafluorophosphate (Bu_4NPF_6), Tetrabutylammoniumperchlorate (Bu_4NclO_4), sodiumperchlorate ($NaClO_4$), Butanone, dithioxamide, trimethyltinstanne, sudium sulphate ($NaSO_4$), magneisum sulphate ($MgSO_4$), sodiımbisulphate ($NaHSO_3$), potasyumchromate (K_2CO_3) were supplied from Fluka Chemicals and were used after drying in vacuum oven without further purification with a ratio of 99% purity. $NaClO_4$, Acetic acid were used from Riedel-de Haen Chemicals as pure. Chemicals: Synthesis procedures for all of the comonomers were given in the results and discussion chapter. All other chemicals were analytical grade and were used without further purification.

Dichloromethane (DCM), acetonitrile (ACN), diethylether was used as received from either Riedel-de Haen Chemical or Merck. Tetrahydrofuran (THF) and toluen were received from Sigma-Aldrich and purified by refluxing with, and distilling with metallic sodium wire which removes water and other impurities.

3.2. Characterizations

Polymerization reactions were performed electrochemically in proper solvent i.e., ACN, DCM, solution with different electrolyte systems such as containing 0.1M $LiClO_4$, 0.1M $NaClO_4$, 0.1M Et_4NBF_4 for various electrodes with different monomer concentrations and scan rates. Cyclic voltammogram (CV), of the polymers was performed on a GAMRY reference 600 model potentiostat, which is a self-contained unit that combines potentiostatic circuitry with phase-sensitive detection (Faraday cage that BAS Cell Stand C3). A three-electrode system employing a platinum button electrode (BASi stationary voltammetry electrodes; diameter 1.6 mm, area 0.02 cm^2) as working electrode, Platinum wire as counter electrode, and a Ag wire as a reference electrode. EIS measurements were also performed with GAMRY reference 600 model

potentiostat with a EIS software package. Both polymers and copolymers electrocoated onto platinum surface were analyzed by FT-IR reflectance spectrophotometer. (Perkin Elmer, Spectrum One; with a Universal ATR attachment with a diamond and ZnSe crystal C70951).

Electrochemical Impedance Spectroscopy (EIS): EIS measurements were taken at room temperature (23±2ºC) using a conventional three electrode cell configuration. The electrochemical cell was connected to a Potentiostat (GAMRY reference 600 model potentiostat) with interfaced to a PC. An electrochemical impedance software Potentioastatic EIS was used to carry out impedance measurements between 0,01Hz and 100000 Hz. The AC amplitude voltage used for the experiments was 10mV and DC potential referenced versus Ag/AgCl electrode. Galvanostatic DC charge/discharge experiments were carried out at constant current of ±1 mA cm^{-2}.

^{1}H NMR spectra were collected on a Varian 400 MHz spectrometer and referenced to the residual proton solvent resonance.

3.3. Electropolymerizations and Characterizations of the Monomers

A platinum wire was used as a counter electrode and Ag wire was used as a reference electrode. Cyclic voltammetry (CV) experiments, chronoamperometry (CA) and electropolymerizations were performed with a GAMRY reference 600 model potentiostat /galvanostat interfaced to a PC computer and controlled Gamry Frame Work software package in a three-electrode setup employing a platinum button electrode (BASi stationary voltammetry electrodes; diameter 1.6 mm, area 0.02 cm^2) as the working electrode, a platinum wire electrode as the counter electrode, and a silver wire as the pseudo reference electrode.

3.4. Doping Degree

We have done the doping degree experiments by Chronoamperometry (CA). We have coated the electrode with the polymer same as the polymer growth experiment with 5, 15 and 30 seconds. Then we obtained the ΔQ_{pg} from the polymer growth graph for each different time. Then we dip the coated polymer into the monomer free solution and rescanned it between 0,0 V and -1,0 V. Then we get the graph on which we obtained ΔQ_{fd} .By the help of these two measurements we have obtained the dopping degree (y) with underbelow formula (Equation 3.1).

$$DD = \frac{2.\ |\Delta Qfd|}{(\Delta Qpg - |\Delta Qfd|)} \quad (1mC = 10^3\ \mu C) \qquad (3.1)$$

3.5. Electrochemical Impedance Spectroscopy Study

Electrochemical Impedance Spectroscopy (EIS) measurements were performed at open circuit potential in the range of 10 kHz-10 mHz (application of amplitude of 10mV) for P(NMePyEBTNMePy), P(NMePy) electrochemically obtained at different charges (number of cycles, polymerization time) with the most appropriate scan rates for each monomer.

4. RESULTS AND DISCUSSION

4.1. Synthesis and electrochemical characterization of pyrrole – biethlythiazole pyrrole

We have planned to synthesize donor-acceptor-donor type (DAD) comonomers. synthesis of a novel comonomer based on N-methyl pyrrole and thiazole moieties. It was anticipated that NmePy_EBT_NMePy would result in well-defined polymers with well-ordered linkages. The alkyl chains on the thiazole moieties were expected to improve solubility of the comonomer and to reduce the polymer's band gap. Thus the comonomer is expected to yield regioregular polymers which should be well ordered and exhibit high conductivity.

In the first two steps, ethylbithiazole moiety of the target comonomer was synthesized via similar procedures as previously reported. A long alkyl chain was integrated to four position of the thiazole ring via 2-bromounbutanone, afterwards the 4,4'-diethyl-2,2'-bithiazole was brominated. The synthesis of trimethlystanne N-methylpyrrole was performed at the fourth step of the procedure and at the final step the palladium-catalysed cross coupling reaction were performed to integrate N-methylpyrrole rings to the 4,4'-diethyl-2,2'-bithiazole in order to obtain a mixed donor-acceptor comonomer based on N-methylpyrrole and ethylthiazole rings. The product was re-crystallized in ethanol and was characterized by ^{1}H-NMR. The NMePyEBTNMePy comonomer is soluble in DCM and insoluble or scarcely soluble in the other organic solvents tested.

4.1.1. Synthesis of 1-bromobutanone

A 500 mL Schlenk flask equipped with a magnetic stirring bar was filled with 2-butanone (22 mL, 242 mmol) and urea (24,17 g, 402mmol) in acetic acid (125 mL). This mixture was stirred for 20 minutes. The Schlenk flask was equipped with pressure equalizing additional funnel, to this funnel 30mL of acetic acid and 13,59 mL of Br_2 was added dropwise over a period of about an hour. Then, the mixture was allowed to stir and come to room temperature. After 7 h, the mixture solution was poured into ice-

water mixture and was filtered. And the final product was crystallized over ethanol. Synthesis of 1-bromobutanone is given in equation 4.1. Yield = 20% white crystals.

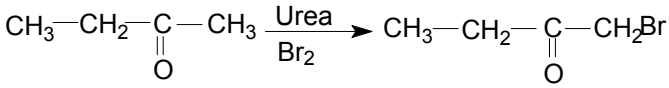

(4.1)

4.1.2. Synthesis of Ethylbithiazole

A 250 mL 3-necked flash equipped with a condenser, a stir bar, N_2 was filled with 6,05 g of 1-bromobutanone, 2.41 g of dithioxamide and absolute ethanol (106 mL). The mixture was heated to reflux for 5 hours, was poured into ice. The solid was filtered and stirred in CH_2Cl_2 over $NaSO_4$ and decolorizing carbon. The mixture was filtered and solvent removed by vacuum. The water layer was dried over $MgSO_4$ and the precipitate was crystallized in methanol. Synthesis ofethylbithiazole is illustrated in equation 4.2. Yield = 4,056 g (60.0%).

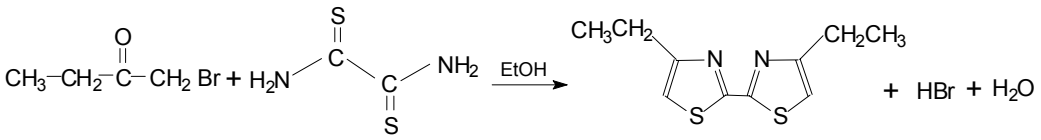

(4.2)

ATR-FTIR spectrum of EBT is seen in Figure 4.1. FTIR measurement was made using solid EBT powder. The peaks of the EBT populated into three region, the peaks around 2900cm^{-1} assigned to alkyl chain, the absorption in the region of 1506cm^{-1} is ascribed to thiazole ring. That is streching and in plane vibration of the –C=N and in plane vibration of the –C=C-fracitons of the thiazole ring.

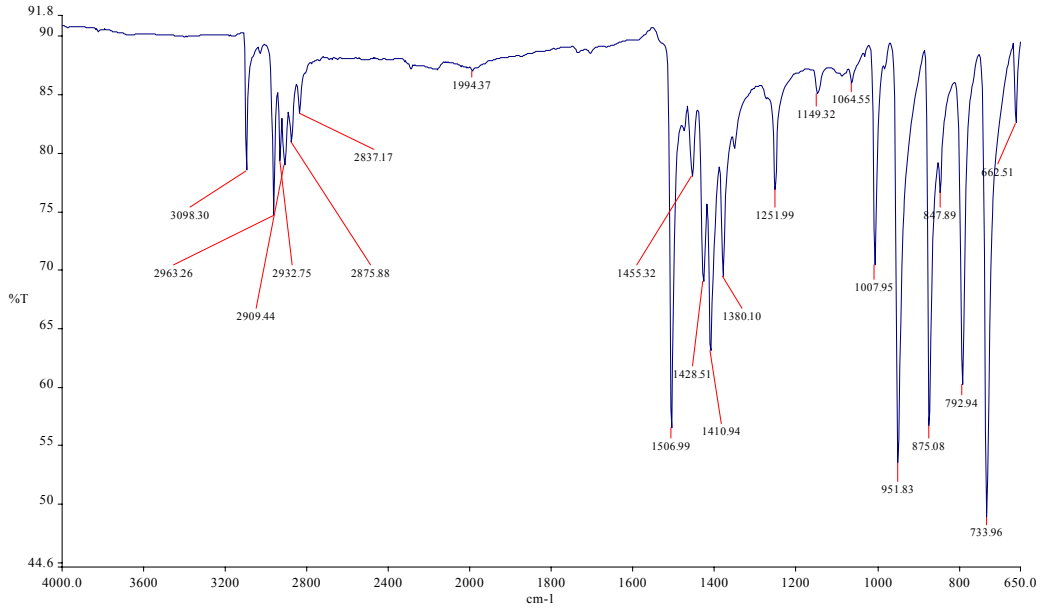

Figure. 4.1 ATR-FTIR spectrum of ethylbithiazole.

4.1.3. Bromination of Ethylbithiazole

A 100 mL round bottom 3-neck flask equipped with an addition funnel was charged with 0,5 g (2.23 mmol) EBT and 20 mL $CHCl_3$. 0,3ml (4,46mmol) bromine was added in $CHCl_3$ (20 mL) dropwise over 15 minutes. A precipitate was formed during addition. The reaction was refluxed for 2 hours. At which time the solution was allowed to cool diluted with 40 mL of $CHCl_3$ and washed with (3x100 mL) $NaHSO_3$, (2x50 mL) K_2CO_3 and (2x100 mL) H_2O. The $CHCl_3$ layer was dried over $MgSO_4$ and filtered. Solvent was removed via vacuum to get pure product. The solid was recrystallized from acetonitrill. Bromination equation of ethylbithiazole is illustrated in equation 4.3. Yield = 1.06g (76.8%).

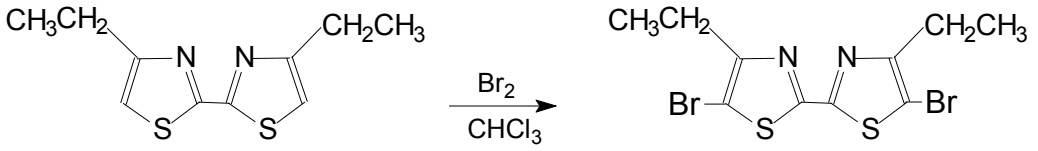

(4.3)

In appendix A.1. FT-IR spectrum of BrEBTBr is seen. H-NMR of the BrEBTBr in $CDCl_3$, δ1,565 ppm(m,4H),δ1,257 ppm(t, 6H).

4.1.4. Synthesis of trimethylstannanyl-N-methlypyrrole

8ml of BuLi (2.5 M in hexane) was added dropwise over a period of 1 hto an ice-cooled stirred solution of 1,8ml of N-MePy in THF (40 mL) at -78°C, the mixture was stirred for five hour prior to refluxing over an oil bath for 20 h, during which period the reaction mixture turned turbid. The mixture was cooled with an ice-salt mixture, and a solution of trimethyltin chloride in dry THF was added with vigorous strirring. After the additon, the reaction mixture was diluted with THF, washed with water, dried over $MgSO_4$, and concentrated to afford a red viscous liguid. Synthesis of 2 trimethylstannanyl-N-methlypyrrole is illustrated in equation 4.4.

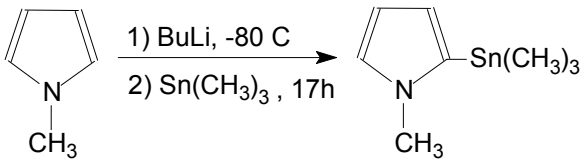

(4.4)

ATR-FTIR spectrum of Trimethyl trimethylstannanyl-N-methlypyrrole is seen in Figure 4.2.

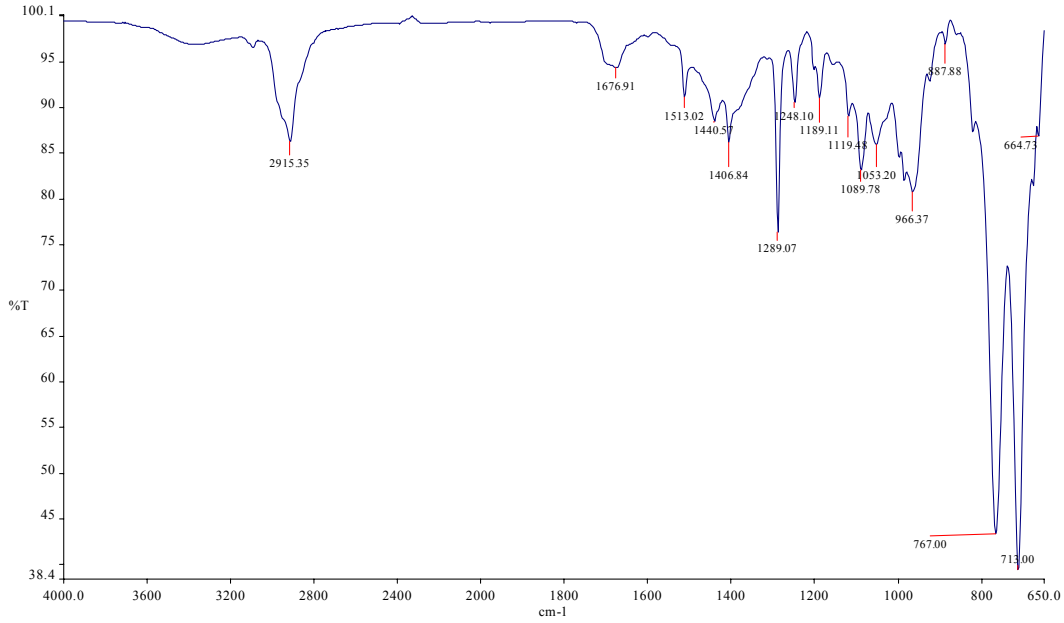

Figure 4.2. ATR-FTIR spectrum of Trimethyl trimethylstannanyl-N-methlypyrrole

4.1.5. Synthesis of N-methyl pyrrole – biethlythiazole –N-methyl pyrrole

In a dry schlenk flask equipped with stir bar, N_2, condenser was added ~60mL of toluen (dry), 0.4 g (2 mmol) of Br-EBT-Br, 0.4939 g of (4 mmol) of N-Py-$SnMe_3$ and 35.3 mg (0.05 mmol) of Pd(II) catalyst ($Pd(PPh_3)_2Cl_2$). After cooling down to room temperature, reaction mixture was poured into water. Chloroform were added and the organic phase was extracted, then organic phase was washed with water again and was dried with $MgSO_4$ and the solvent rotary evaporated. The product was re-crystallized in ethanol. Cross coupling reaction of N-MePyEBTN-MePy synthesis is given in equation 4.5. The characteristic peaks of stretching vibration of Pyrrole ring are shown around1638cm^{-1}, 1527cm^{-1} and 1471cm^{-1}. The characteristic peaks of thiazole ring are shown around 3103cm^{-1}, 1509cm^{-1}, 1402cm^{-1}, 1258cm^{-1}.

ATR-FTIR spectrum of N-methyl pyrrole – biethlythiazole –N-methyl pyrrole is seen at Figure 4.3.

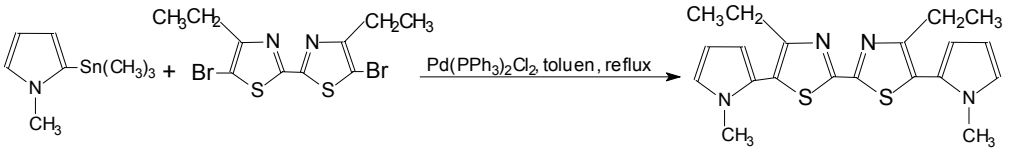

(4.5)

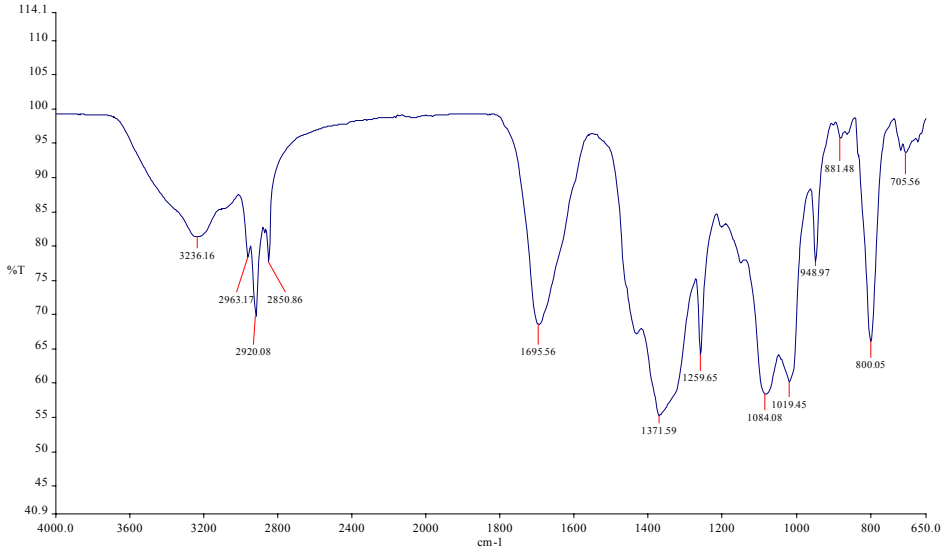

Figure 4.3. ATR-FTIR spectrum of N-methyl pyrrole – biethlythiazole –N-methyl pyrrole

4.2. Electropolymerization of P(NMePyEBTNMePy)

Electropolymerization of NMePyEBTNMePy was achieved under several conditions. A possible polymerization mechanism of NMePYEBTNMePy is given at Figure 4.4.

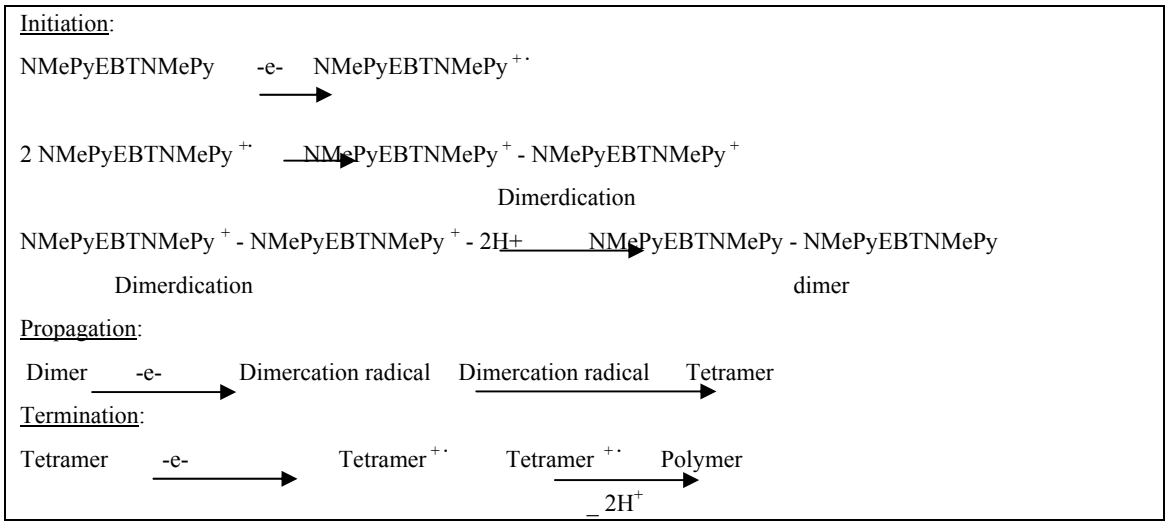

Figure 4.4. Posisible electropolymerization mechanism of NMePyEBTNMePy

4.2.1. Potentiodynamically Electropolymerization of P(NMePyEBTNMePy)

Firstly, polymerization of NMePyEBTNMePy was obtained by potentiodynamically methods. Electropolymerization of NMePyEBTNMePy comonomer was achieved in $TBAClO_4$ in DCM After several attempts electrodepositon of comonomer at a scan rate

of 100 mV/sn between -0,5 V and 1,1 V was found suitable. At the Figure 4.5 ramp curve is seen which point outs the potential values of polymerization. Nmepy and NMePyEBTNMePy ramp curves are discussed EBT group in the NmePy ring increases oxidation potential that is due to N atoms in the EBT ring. NmePy E_{onset} value is 1,079 V unfortunately NMePyEBTNMePy E_{onset} value is 1,12 V.

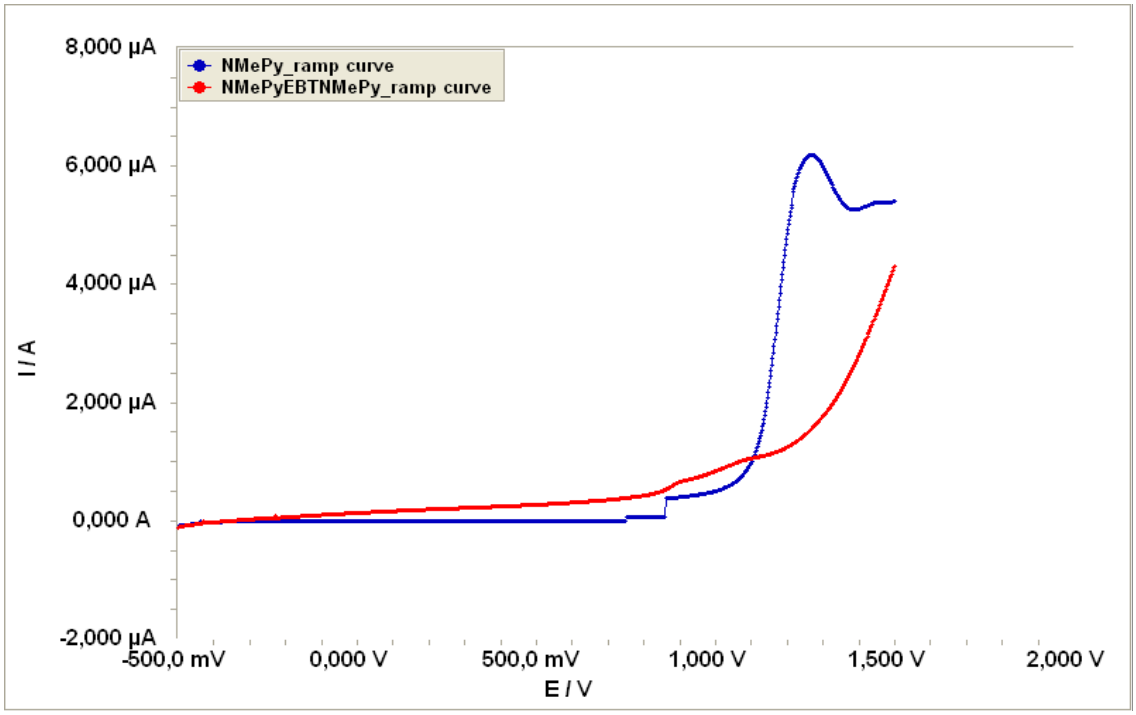

Figure 4.5. Ramp curve of 0,0001M NMePyEBTNMePy in 0,1M $TBAClO_4$/DCM.

4.2.1.1. Scan Rate Dependence on Polymerization of NMePyEBTNMePy

We have investigate scan rate dependence on the electropolymerization of NMePyEBTNMePy. In figure 4.6 cyclic voltammogram of 2 cycle electrodeposition of NMePyEBTNMePy is seen. Electropolymerization of P(NMePyEBTNMePy) comonomer was achieved from a 0,001M solution of comonomer by cyclic voltammetry in 0,1M $TBAPF_6$/DCM at 50mV/sn at bare platin botton electrode .

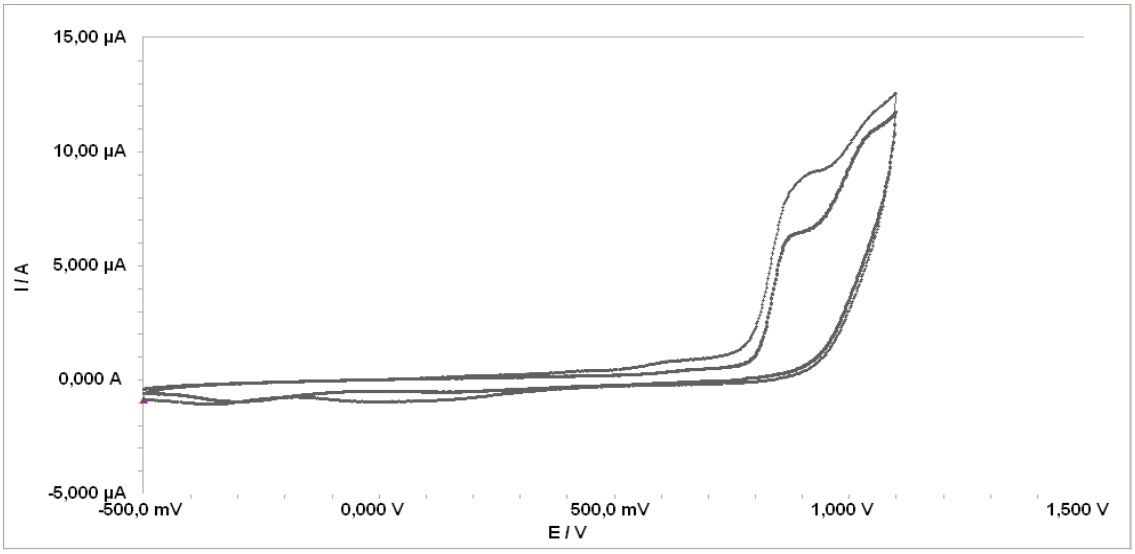

Figure 4.6. Electropolymerization of NmePy_EBT_NMePy comonomer by cyclic voltammetry from a 0.001M solution of comonomer in 0.1 M $TBAClO_4$/DCM at 50 mV s^{-1} onto platin botton electrode (area ~0.0024 cm^2).

The comonomer oxidation on to bare electrode starts (E_{onset} of NMePyEBTNMePy) at 795 mV vs Ag wire reference electrode. Scanning range from the -0,5-1,1V generates a broad cathodic peak at around 63 mV on the return scan. The increase in the size of this peak indicates that it is due to the electroactive film formed at the electrode surface.

The polymer films were washed with monomer-free electrolyte solution, and their redox behavior was investigated in the same solution by cyclic voltammetry. Figure 4.7. Presents cyclic voltammograms of a P(NMePyEBTNMePy) polymer film on the platin botton electrode in the monomer free solution at different scan rates.

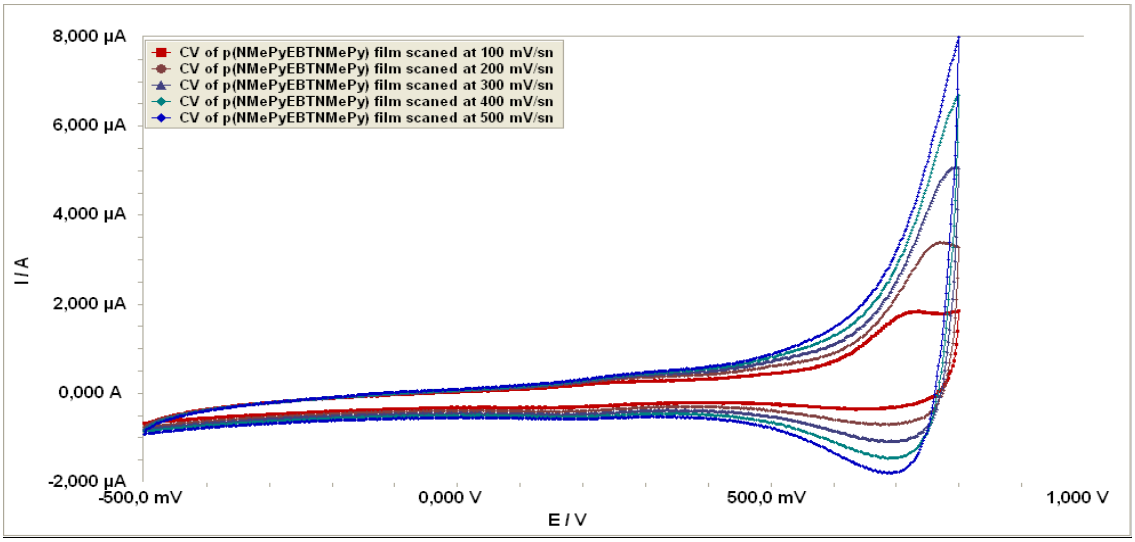

Figure 4.7 CV of the P(NMePy_EBT_NMePy) film in a monomer free electrolyte solution (0,1M $TBAClO_4$ in DCM) scanned at (a) 100, (b) 200, (c) 300, (d) 400, (e) 500 $mV.sn^{-1}$.

As seen in the Figure 4.7 there is no redox behaviour occurs greater than 200mV/sn. Redox behaviour of P(NMePyEBTNMePy) film damages with increasing scan rates. Greater than 200 mV/sn rates there are no oxidation peaks which corresponds to oxidation of copolymer and defines reversibility of copolymer.

Figure 4.8 shows cyclic voltammograms on platin button electrode containing 0,001M NMePyEBTNMePy comonomer in 0,1M $TBAClO_4$ in DCM scaned for 2 cycles at 100mV/sn.

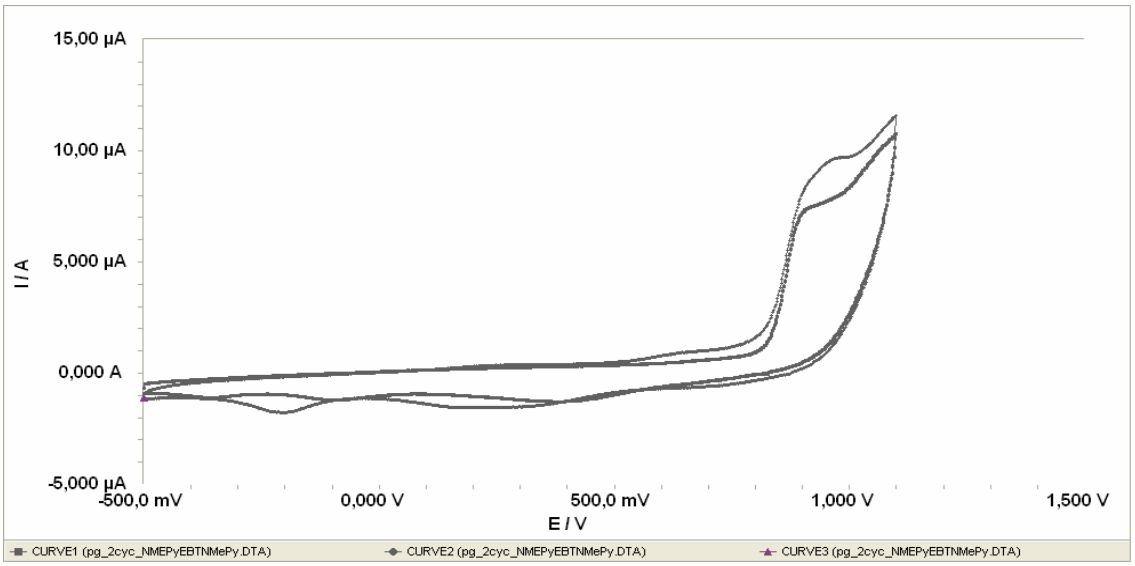

Figure 4.8. Electropolymerization of NmePy_EBT_NMePy comonomer by cyclic voltammetry from a 0.001M solution of comonomer in 0.1 M $TBAClO_4$/DCM at 100 mV s^{-1} onto platin botton electrode (area ~0.0024 cm^2).

The comonomer oxidation on to bare electrode starts (E_{onset} of NMePyEBTNMePy) at 814 mV vs Ag wire reference electrode. Scanning range from the -0,5-1,1V generates a broad cathodic peak at around 230 mV on the return scan. The increase in the size of this peak indicates that it is due to the electroactive film formed at the electrode surface.

The polymer films were washed with monomer-free electrolyte solution, and their redox behavior was investigated in the same solution by cyclic voltammetry. Figure 4.9. Presents cyclic voltammograms of a P(NMePyEBTNMePy) polymer film on the platin botton electrode in the monomer free solution at different scan rates.

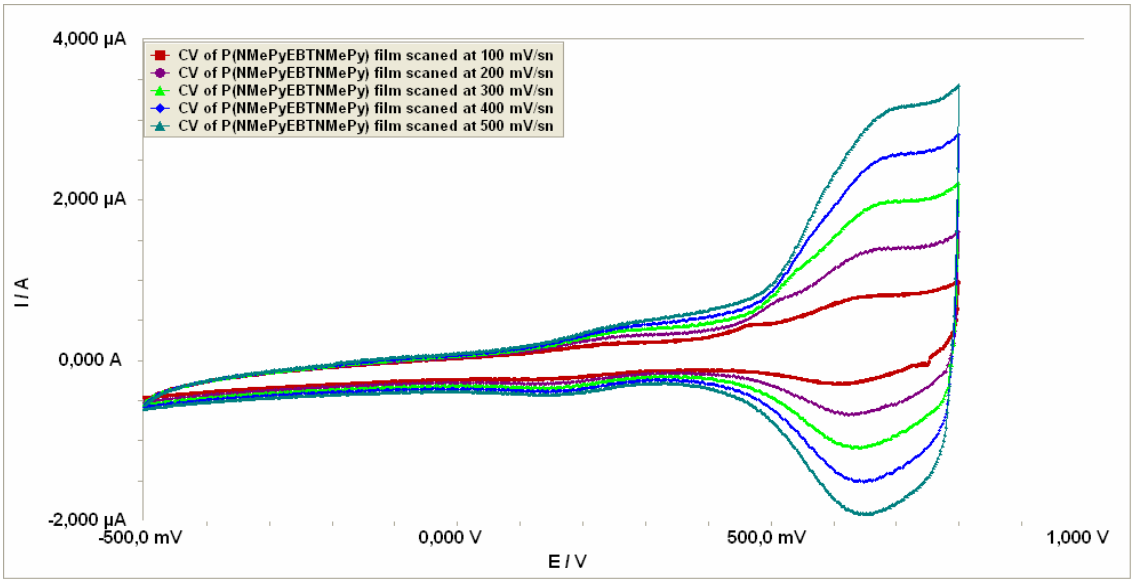

Figure 4.9. CV of the P(NMePy_EBT_NMePy) film(electropolymerization given in Figure 4.8) in a monomer free electrolyte solution (0,1M $TBAClO_4$ in DCM) scanned at (a) 100, (b) 200, (c) 300, (d) 400, (e) 500 $mV.sn^{-1}$.

Figure 4.10. scan rate dependencies of both the oxidation and reduction peaks of the polymer were calculated using current density values with respect to square root of the scan rate. A linear relationship was found between the peak current density and scan rate, indicating that the electroactive polymer films are well adhered and the redox processes are non-diffusion limited.

E_a, E_c, I_a, I_c, ΔE, E_{onset}, E_o, I_a/I_c, I_p values of polymer films are listed in Table 4.1.

Table 4.1. E_a, E_c, I_a, I_c, ΔE, E_{onset}, E_o, I_a/I_c, I_p values of P(NMePyEBTNMePy) films scaned at 100, 200, 300, 400, 500 mV/sn scan rates.

scanrate ($mV.sn^{-1}$)	**E_{anodic} mV**	**$E_{cathodic}$ mV**	**ΔE mV**	**I_{anodic} µA**	**$I_{cathodic}$ µA**	**$I_{anodic}/I_{cathodic}$**	**E_o mV**
100	652	612	40	0,8	-0,3	2,6	632
200	666	624	42	1,4	-0,683	2,04	645
300	683	631	52	1,9	-1,1	1,72	657
400	695	643	52	2,5	-1,5	1,6	669
500	700	655	45	3,2	-1,9	1,7	678

Scan rate dependence of polymer films were investigated in the Figure 4.10 As shown in the figure current densities and square root of scan rate is in a linear relationship which is significiant with Randles-sevcik equation.

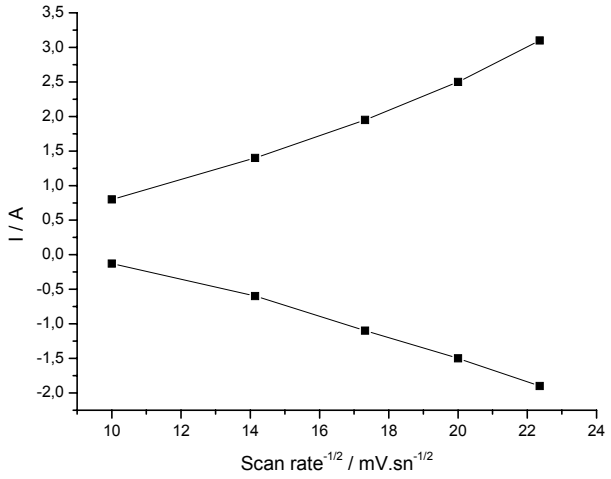

Figure 4.10. Scan rate depence of P(NMePyEBTNMePy) films scaned at different scan rates.

According to the ΔE, I_a/I_c and scan rate dependence plot, it is clearly seen that P(NMePyEBTNMePy) films are reversible.

Figure 4.11 shows cyclic voltammograms on platin button electrode containing 0,001M NMePyEBTNMePy comonomer in 0,1M $TBAClO_4$ in DCM scaned for 2 cycles at 200mV/sn.

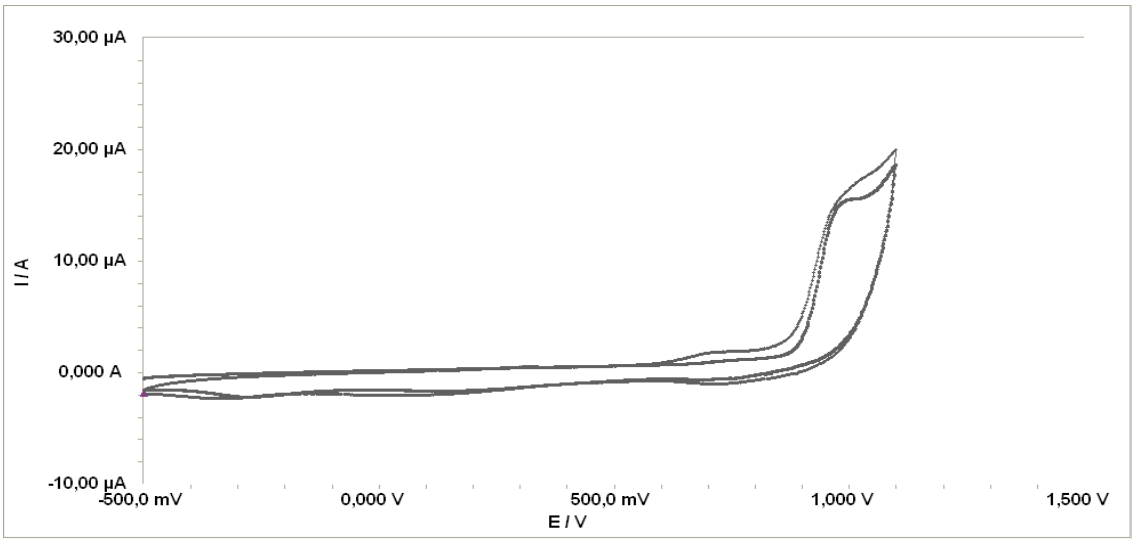

Figure 4.11. Electropolymerization of NmePy_EBT_NMePy comonomer by cyclic voltammetry from a 0.001M solution of comonomer in 0.1 M $TBAClO_4$/DCM at 200 mV s^{-1} onto platin botton electrode (area ~0.0024 cm^2).

The comonomer oxidation on to bare electrode starts (E_{onset} of NMePyEBTNMePy) at 875 mV vs Ag wire reference electrode. Scanning range from the -0,5-1,1V generates a broad cathodic peak at around 749 mV on the return scan. The increase in the size of this peak indicates that it is due to the electroactive film formed at the electrode surface.

The polymer films were washed with monomer-free electrolyte solution, and their redox behavior was investigated in the same solution by cyclic voltammetry. Figure 4.12 Presents cyclic voltammograms of a P(NMePyEBTNMePy) polymer film on the platin botton electrode in the monomer free solution at different scan rates.

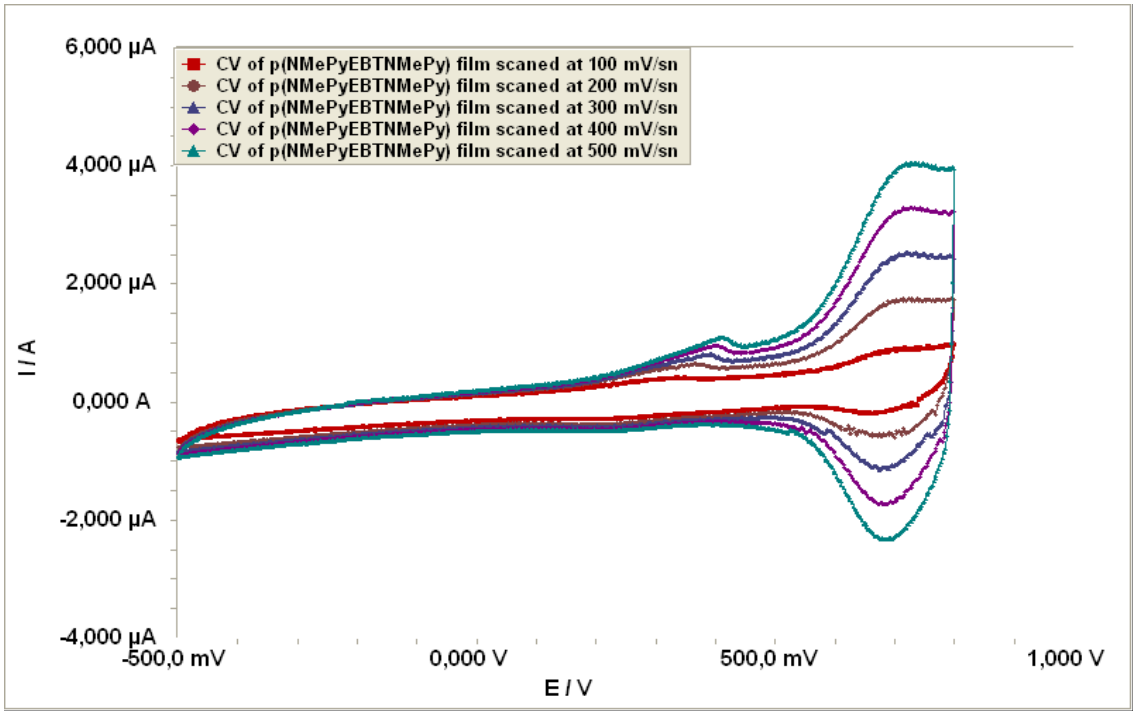

Figure 4.12 CV of the P(NMePy_EBT_NMePy) film(electropolymerization given in Figure..) in a monomer free electrolyte solution (0,1M $TBAClO_4$ in DCM) scanned at (a) 100, (b) 200, (c) 300, (d) 400, (e) 500 $mV.sn^{-1}$.

Figure 4.13 scan rate dependencies of both the oxidation and reduction peaks of the polymer were calculated using current density values with respect to square root of the scan rate. A linear relationship was found between the peak current density and scan rate, indicating that the electroactive polymer films are well adhered and the redox processes are non-diffusion limited. E_a, E_c, I_a, I_c, ΔE, E_{onset}, E_o, I_a/I_c, I_p values of polymer films are listed in Table 4.2.

Table 4.2. E_a, E_c, I_a, I_c, ΔE, E_{onset}, E_o, I_a/I_c, I_p values of P(NMePyEBTNMePy) films scaned at 100, 200, 300, 400, 500 mV/sn scan rates.

scanrate (mV.sn-1)	Eanodic mV	Ecathodic mV	ΔE mV	Ianodic µA	Icathodic µA	Ianodic/ Icathodic	Eo mV
100	700	662	38	0,89	0,2	4,45	681
200	718	678	40	1,74	0,58	3	698
300	728	676	52	2,5	1,15	2,17	702
400	726	681	45	3,3	1,7	1,94	703
500	728	683	45	4	2,32	1,72	705

Scan rate dependence of polymer films were investigated in the Figure 4.13. As shown in the figure current densities and square root of scan rate is in a linear relationship which is significiant with Randles-sevcik equation.

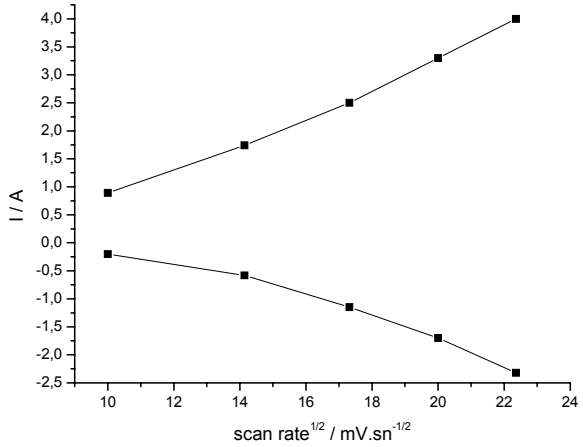

Figure 4.13 Scan rate depence of P(NMePyEBTNMePy) films scaned at different scan rates.

According to the ΔE, I_a/I_c and scan rate dependence plot, it is clearly seen that P(NMePyEBTNMePy) films are reversible.

Figure 4.14 shows cyclic voltammograms on platin button electrode containing 0,001M NMePyEBTNMePy comonomer in 0,1M $TBAClO_4$ in DCM scaned for 2 cycles at 300mV/sn.

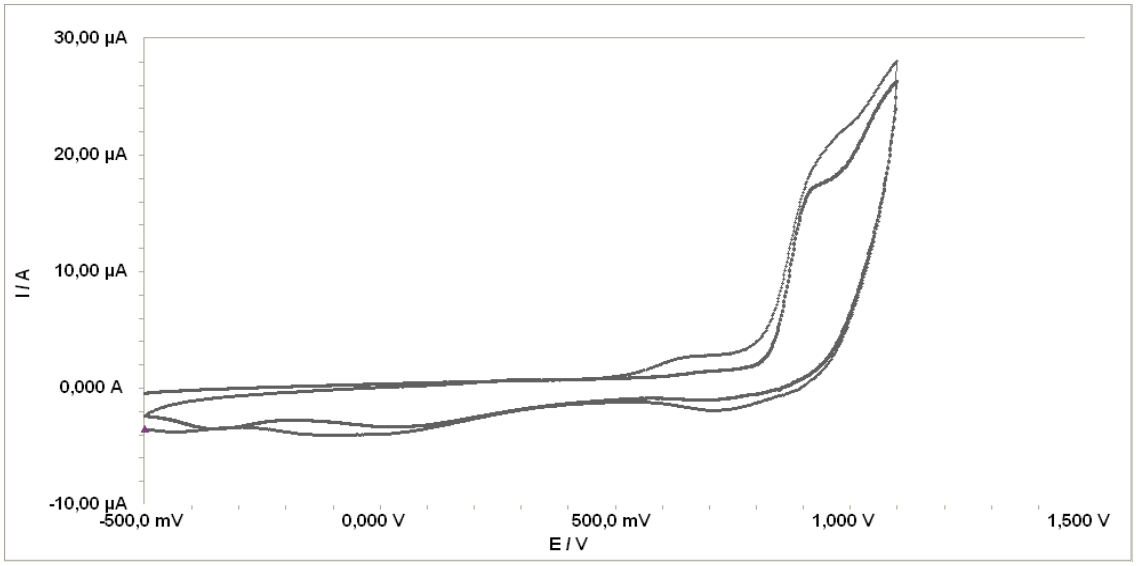

Figure 4.14 Electropolymerization of NmePy_EBT_NMePy comonomer by cyclic voltammetry from a 0.001M solution of comonomer in 0.1 M $TBAClO_4$/DCM at 300 mV s^{-1} onto platin botton electrode (area ~0.0024 cm^2).

The comonomer oxidation on to bare electrode starts (E_{onset} of NMePyEBTNMePy) at 812mV vs Ag wire reference electrode. Scanning range from the -0,5-1,1V generates a broad cathodic peak at around 712 mV on the return scan. The increase in the size of this peak indicates that it is due to the electroactive film formed at the electrode surface.

The polymer films were washed with monomer-free electrolyte solution, and their redox behavior was investigated in the same solution by cyclic voltammetry. Figure 4.15 Presents cyclic voltammograms of a P(NMePyEBTNMePy) polymer film on the platin botton electrode in the monomer free solution at different scan rates.

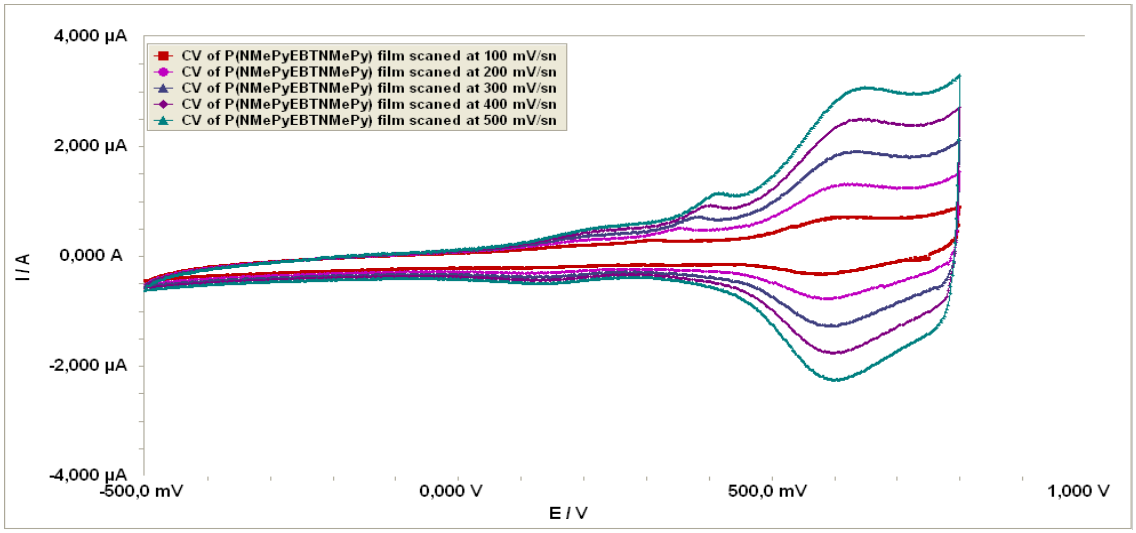

Figure 4.15. CV of the P(NMePy_EBT_NMePy) film in a monomer free electrolyte solution (0,1M $TBAClO_4$ in DCM) scanned at (a) 100, (b) 200, (c) 300, (d) 400, (e) 500 mV.sn^{-1}.

Figure 4.16 scan rate dependencies of both the oxidation and reduction peaks of the polymer were calculated using current density values with respect to square root of the scan rate. A linear relationship was found between the peak current density and scan rate, indicating that the electroactive polymer films are well adhered and the redox processes are non-diffusion limited. E_a, E_c, I_a, I_c, ΔE, E_{onset}, E_o, I_a/I_c, I_p values of polymer films are listed in Table 4.3.

Table4.3. E_a, E_c, I_a, I_c, ΔE, E_{onset}, E_o, I_a/I_c, I_p values of P(NMePyEBTNMePy) films scaned at 100, 200, 300, 400, 500 mV/sn scan rates.

scanrate (mV.sn-1)	**E_{anodic} mV**	**$E_{cathodic}$ mv**	**ΔE mV**	**I_{anodic} µA**	**$I_{cathodic}$ µA**	**$I_{anodic}/I_{cathodic}$**	**E_o mV**
100	617	577	40	0,724	0,33	2,19	597
200	619	586	33	1,3	0,77	1,68	602
300	629	591	38	1,9	1,28	1,48	610
400	640	598	42	2,49	1,75	1,42	619
500	645	603	42	3	2,27	1,32	624

Scan rate dependence of polymer films were investigated in the Figure 4.16. As shown in the figure current densities and square root of scan rate is in a linear relationship which is significiant with Randles-sevcik equation.

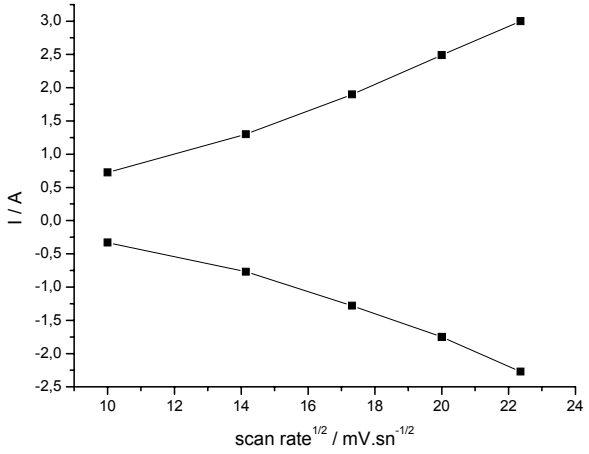

Figure 4.16. Scan rate depence of P(NMePyEBTNMePy) films scaned at different scan rates.

According to the ΔE, I_a/I_c and scan rate dependence plot, it is clearly seen that P(NMePyEBTNMePy) films are reversible.

If we compare the results, although maximum current is observed in P(NMePyEBTNMePy) film which was polymerize at 50 mV/sn, the most reversible behaviour is gained in P(NMePyEBTNMePy) film which was polymerize at 300 mV/sn but the currents were lower than the P(NMePyEBTNMePy) film which was polymerize at 100mV/sn. Therefore, we continue electropolymerization at 100 mV/sn scan sate. In Figure 4.17 polymerization scan rate effect is seen.

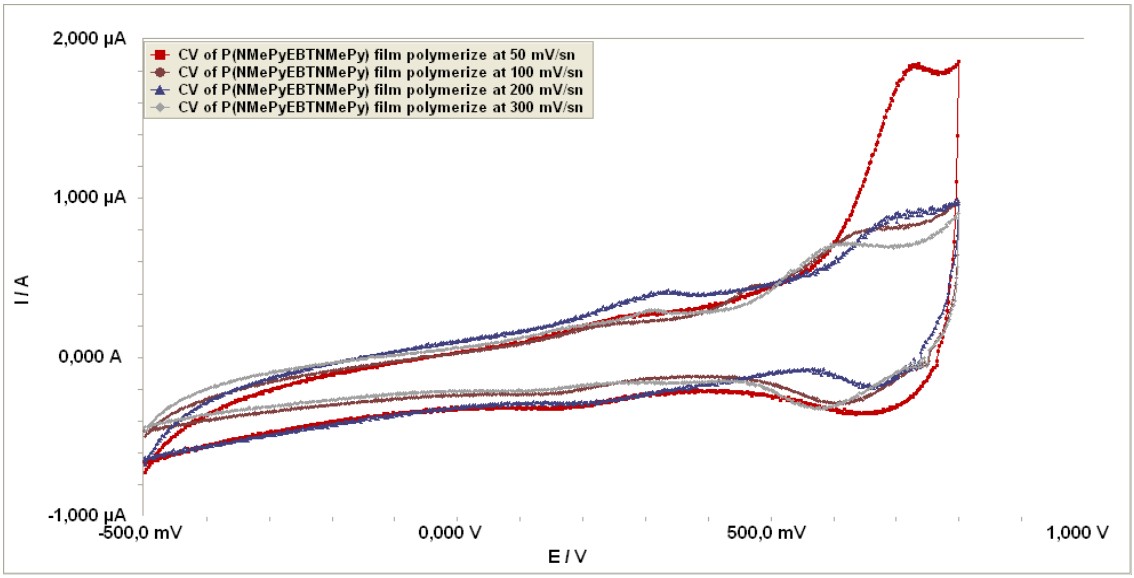

Figure 4.17. CV of P(NMePyEBTNMePy) films polymerize at different scan rates.

4.2.1.2. Thickness effect on redox behaviour of P(NMePyEBTNMePy) in $TBACIO_4$/DCM media

We have obtained polymers which have different thicknesses by appliying different cycles. 2,3 and 4 cycle polymers were obtained and redox behaviour of that polymers were investigated. In Figure 4.18 cyclic voltammograms of 0,001M NMePYEBTNMePy comonomer in 0,1M $TBACIO_4$/DCM scaned for 3 times is seen.

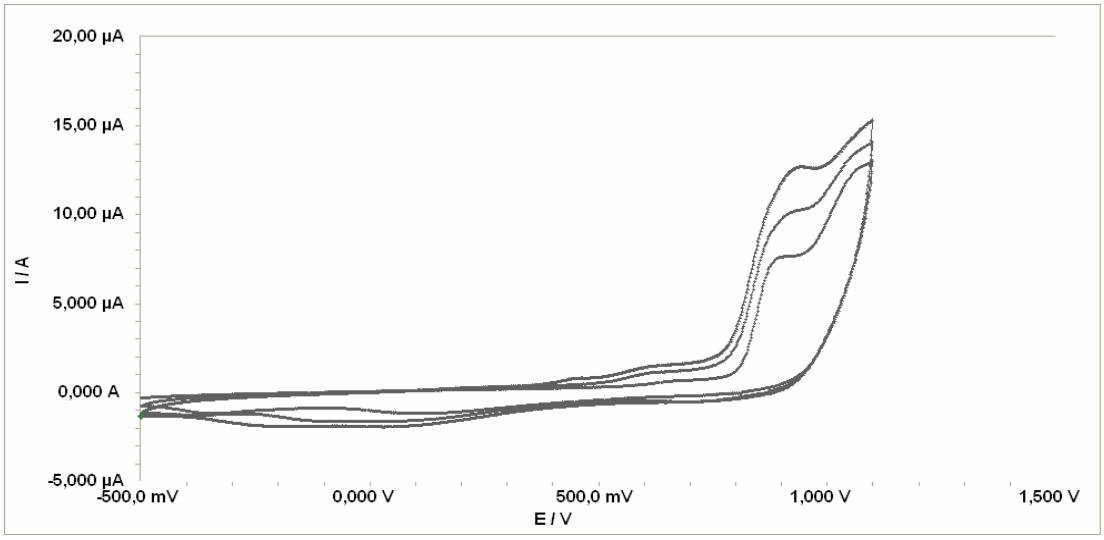

Figure 4.18 Electropolymerization of NmePy_EBT_NMePy comonomer by cyclic voltammetry from a 0.001M solution of comonomer in 0.1 M $TBAClO_4$/DCM at 100 mV s^{-1} onto platin botton electrode.

The comonomer oxidation on to bare electrode starts (E_{onset} of NMePyEBTNMePy) at 805 mV vs Ag wire reference electrode. Scanning range from the -0,5-1,1V generates a broad cathodic peak at around 746 mV on the return scan. The increase in the size of this peak indicates that it is due to the electroactive film formed at the electrode surface.

The polymer films were washed with monomer-free electrolyte solution, and their redox behavior was investigated in the same solution by cyclic voltammetry. Figure 4.19 Presents cyclic voltammograms of a P(NMePyEBTNMePy) polymer film on the platin botton electrode in the monomer free solution at different scan rates.

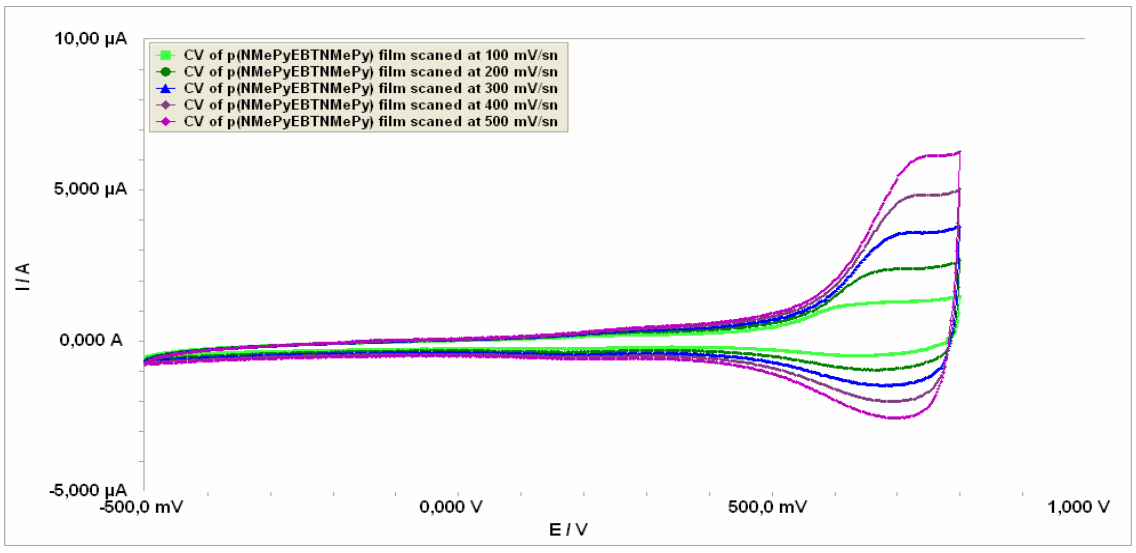

Figure 4.19. CV of the P(NMePy_EBT_NMePy) film(electropolymerization given in Figure 4.18) in a monomer free electrolyte solution (0,1M $TBAClO_4$ in DCM) scanned at (a) 100, (b) 200, (c) 300, (d) 400, (e) 500 mV.sn^{-1}

Figure 4.20 scan rate dependencies of both the oxidation and reduction peaks of the polymer were calculated using current density values with respect to square root of the scan rate. A linear relationship was found between the peak current density and scan rate, indicating that the electroactive polymer films are well adhered and the redox processes are non-diffusion limited. E_a, E_c, I_a, I_c, ΔE, E_{onset}, E_o, I_a/I_c, I_p values of polymer films are listed in Table 4.4

Table4.4 E_a, E_c, I_a, I_c, ΔE, E_{onset}, E_o, I_a/I_c, I_p values of P(NMePyEBTNMePy) films scaned at 100, 200, 300, 400, 500 mV/sn scan rates.

scanrate (mV.sn-1)	**E_{anodic} mV**	**$E_{cathodic}$ mV**	**ΔE mV**	**I_{anodic} µA**	**$I_{cathodic}$ µA**	**$I_{anodic}/I_{cathodic}$**	**E_o mV**
100	645	640	5	1,2	0,49	2,4	642
200	671	669	2	2,32	0,98	2,36	670
300	712	681	31	3,5	1,4	2,5	696
400	728	697	31	4,8	2,0	2,4	712
500	740	704	36	6	2,6	2,3	722

Scan rate dependence of polymer films were investigated in the Figure 4.20. As shown in the figure current densities and square root of scan rate is in a linear relationship which is significiant with Randles-sevcik equation.

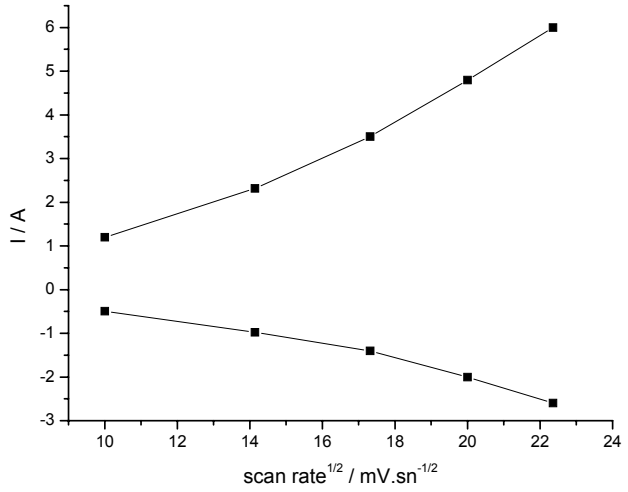

Figure 4.20. Scan rate depence of P(NMePyEBTNMePy) films scaned at different scan rates.

According to the ΔE, I_a/I_c and scan rate dependence plot, it is clearly seen that P(NMePyEBTNMePy) films are reversible.

In Figure 4.21 electropolymerization of 0,001M NMePYEBTNMePy comonomer in 0,1M $TBAClO_4$/DCM scaned 4 times is seen.

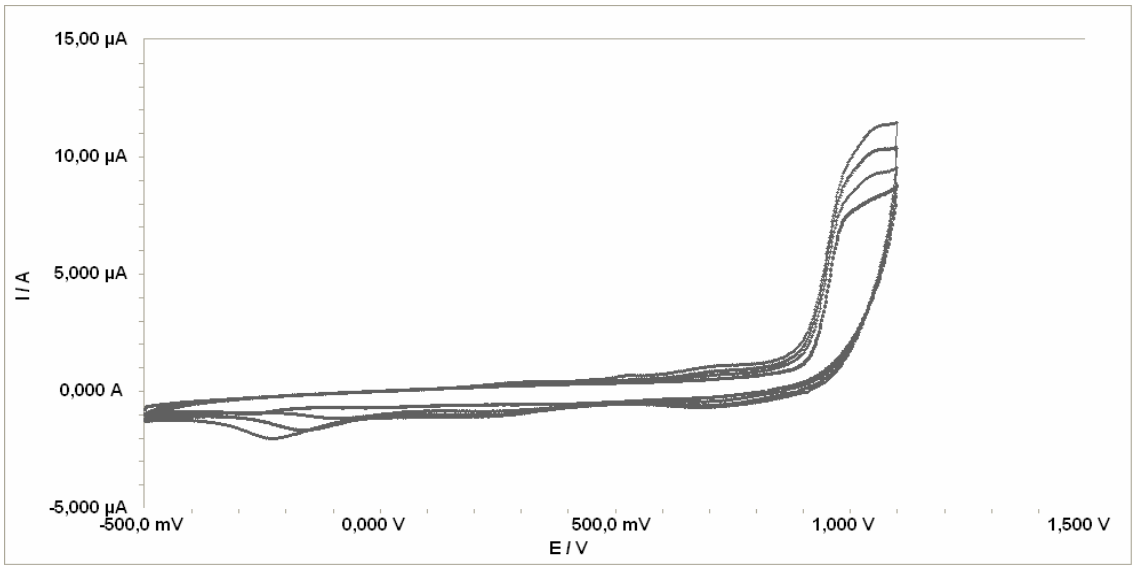

Figure 4.21. Electropolymerization of NmePy_EBT_NMePy comonomer by cyclic voltammetry from a 0.001M solution of comonomer in 0.1 M $TBAClO_4$/DCM at 100 mV s^{-1} onto platin botton electrode (area ~0.0024 cm^2).

The comonomer oxidation on to bare electrode starts (E_{onset} of NMePyEBTNMePy) at 897 mV vs Ag wire reference electrode. Scanning range from the -0,5-1,1V generates a broad cathodic peak at around 722 mV on the return scan. The increase in the size of this peak indicates that it is due to the electroactive film formed at the electrode surface.

The polymer films were washed with monomer-free electrolyte solution, and their redox behavior was investigated in the same solution by cyclic voltammetry. Figure 4.22 Presents cyclic voltammograms of a P(NMePyEBTNMePy) polymer film on the platin botton electrode in the monomer free solution at different scan rates.

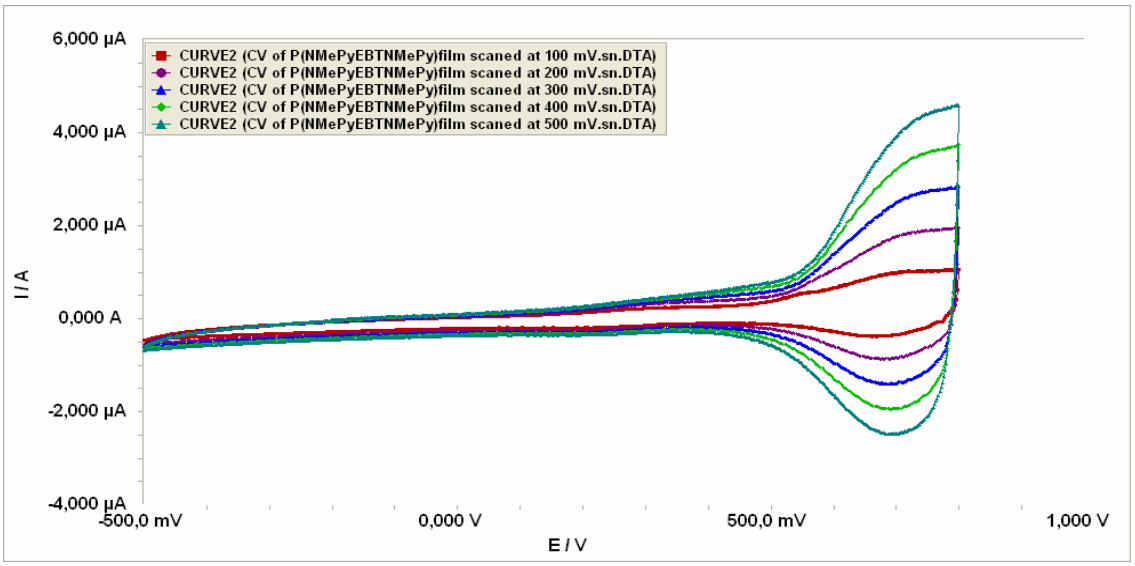

Figure 4.22 CV of the P(NMePy_EBT_NMePy) film in a monomer free electrolyte solution (0,1M $TBAClO_4$ in DCM) scanned at (a) 100, (b) 200, (c) 300, (d) 400, (e) 500 $mV.sn^{-1}$

Figure 4.23 scan rate dependencies of both the oxidation and reduction peaks of the polymer were calculated using current density values with respect to square root of the scan rate. A linear relationship was found between the peak current density and scan rate, indicating that the electroactive polymer films are well adhered and the redox processes are non-diffusion limited. E_a, E_c, I_a, I_c, ΔE, E_{onset}, E_o, I_a/I_c, I_p values of polymer films are listed in Table 4.5.

Table4.5 E_a, E_c, I_a, I_c, ΔE, E_{onset}, E_o, I_a/I_c, I_p values of P(NMePyEBTNMePy) films scaned at 100, 200, 300, 400, 500 mV/sn scan rates.

scanrate (mV.sn-1)	**E_{anodic} mV**	**$E_{cathodic}$ mV**	**ΔE mV**	**I_{anodic} µA**	**$I_{cathodic}$ µA**	**$I_{anodic}/I_{cathodic}$**	**Eo mV**
100	711	673	38	1	0,39	2,5	692
200	732	682	50	1,8	0,87	2,06	707
300	734	693	41	2,7	1,4	1,92	713
400	732	693	39	3,5	1,9	1,8	712
500	750	700	50	4,45	2,4	1,85	725

Scan rate dependence of polymer films were investigated in the Figure 4.23. As shown in the figure current densities and square root of scan rate is in a linear relationship which is significiant with Randles-sevcik equation.

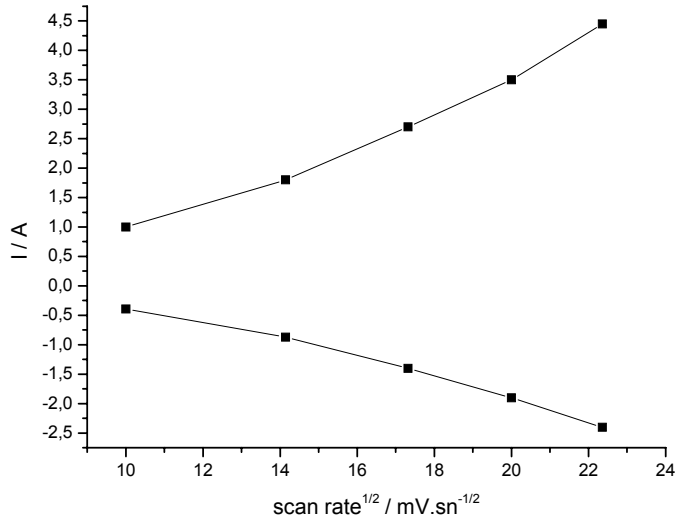

Figure4.23 Scan rate depence of P(NMePyEBTNMePy) films scaned at different scan rates.

According to the ΔE, I_a/I_c and scan rate dependence plot, it is clearly seen that P(NMePyEBTNMePy) films are reversible.

The difference in CV of P(NMePyEBTNMePy) films scaned at 300 mV/sn is seen in the Figure 4.24.

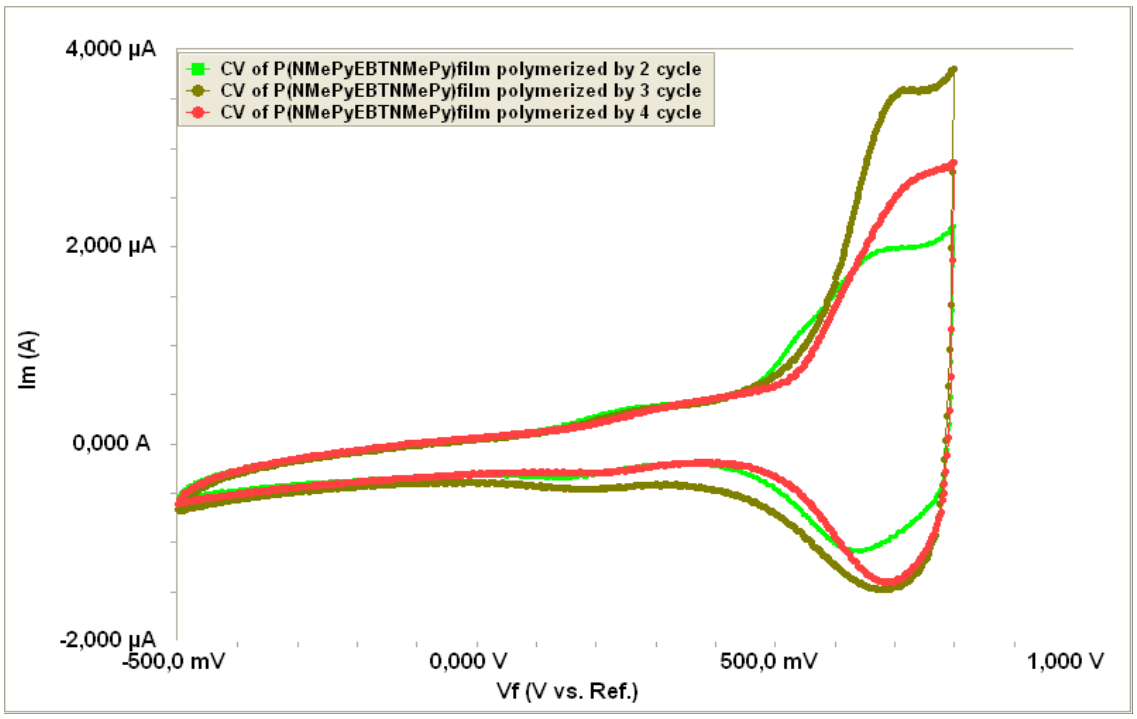

Figure 4.24. CV of P(NMePyEBTNMePy) films scaned at 300 mV/sn. (a) electropolymerization was achieved by appliying 2 cycles, (b) electropolymerization was achieved by appliying 3 cycles, (c) electropolymerization was achieved by appliying 4 cycles.

Although, increase with cycle number increase in current is seen. More reversible peaks are observed in the least polymerize cycle number. E_a, E_c, I_a, I_c, ΔE, E_{onset}, E_o, I_a/I_c, I_p values of P(NMePyEBTNMePy) films scaned at 300 mV/sn are given in Table 4.6.

Table4.6. E_a, E_c, I_a, I_c, ΔE, E_{onset}, E_o, I_a/I_c, I_p values of P(NMePyEBTNMePy) films scaned at 300 mV/sn.

Cycle number	E_{anodic}	$E_{cathodic}$	ΔE	I_{anodic}	$I_{cathodic}$	$I_{anodic}/I_{cathodic}$	E_o
2	683	631	52	1,9	1,1	1,72	657
3	712	681	31	3,5	1,4	2,5	696
4	734	693	41	2,7	1,4	1,92	713

According to results, thinner P(NMePyEBTNMePy) films show more reversible behaviour than the thicker ones. Altough 3cycle polymerized polymer film has higher current values than the other 2 and 4 cycle. 2 cycle polymerized polymer film has better redox behaviour than 3 cycle. As can be seen from the Figure 4.24. when the comonomer is cycled by 4 scanes the current decreases that is because of the polymer film destroyes over oxidation. Because of this we could not be able to polymerize comonomer for 6 nor 8 cycles.

4.2.1.3. Thickness effect on redox behaviour of P(NMePyEBTNMePy) in $TBAPF_6$/DCM media

Oxidative electropolymerization of NMePyEBTNMePy was carried out in DCM with 0,1M $TABPF_6$ as electrolyte. Figure 4.25 shows first two cycle of the anodic electropolymerization by cylic voltammetry at 100mV/sn of a 0,001M solution of NMePyEBTNMePy onto a platin botton electrode.

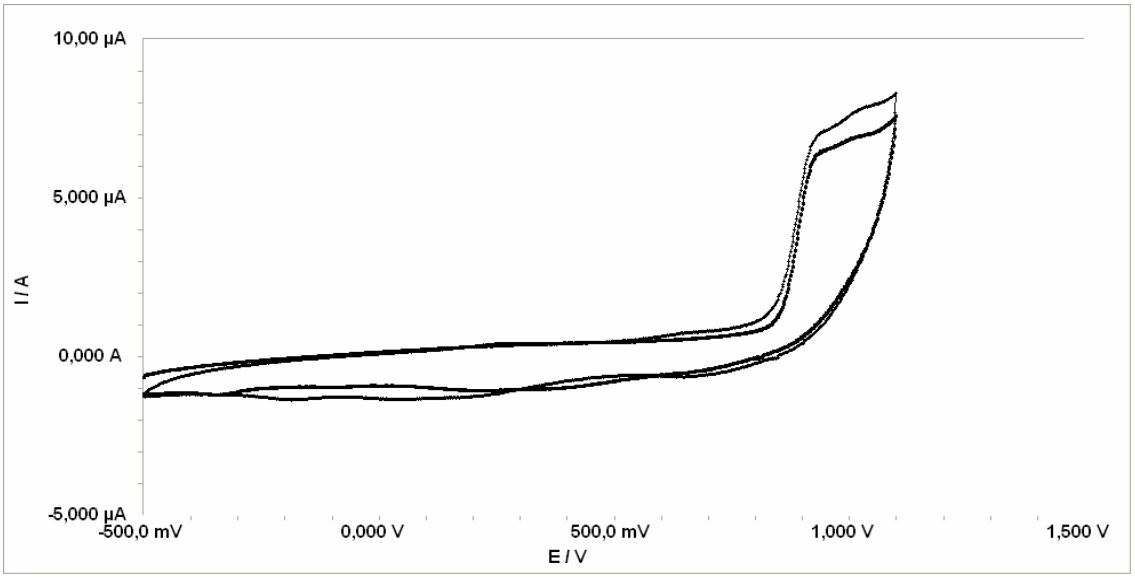

Figure 4.25 Electropolymerization of NmePy_EBT_NMePy comonomer by cyclic voltammetry from a 0.001M solution of comonomer in 0.1 M $TBAPF_6$/DCM at 100 mV s^{-1} onto PBE (area ~0.0024 cm^2).

The polymeric films of P(NMePyEBTNMePy) were deposited by cylic voltammetry over 2 cycles from 0,1 M solution of comonomer in 0,1M $TBAPF_6$/DCM electrolyte. Investigation of the polymer films in monomer free electrolyte solution for their redox switching showed a well defined redox process. Figure 4.26 shows the cyclic voltammogram of this polymer film at scan rates of 100, 200, 300, 400, 500 mV/sn in 0,1M $TBAPF_6$/DCM. It is significiant that the polymer exhibits very well defined and reversible redox processes.

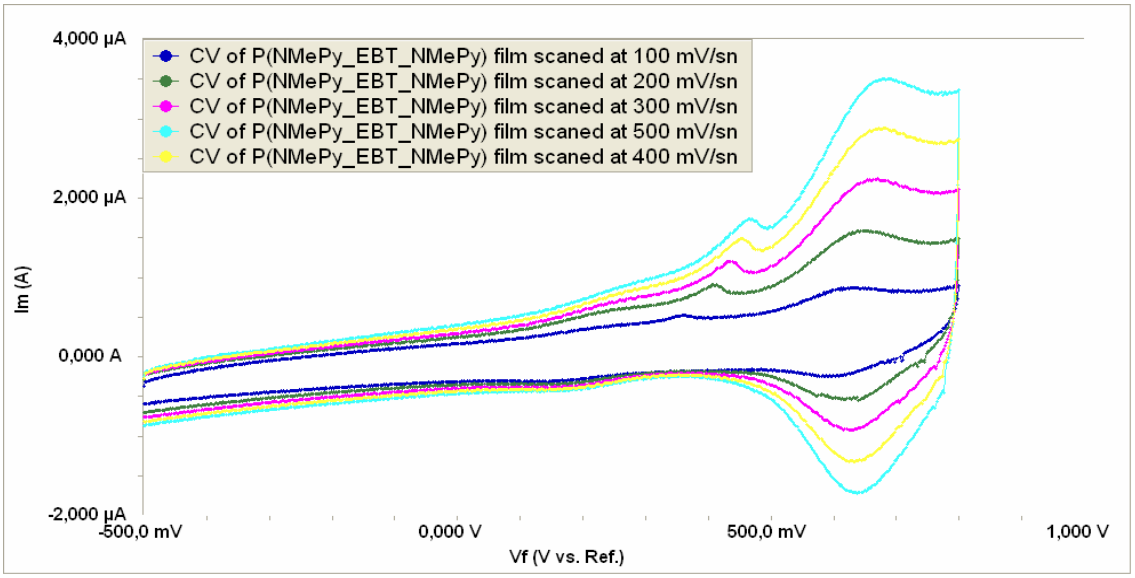

Figure4.26. CV of the P(NMePy_EBT_NMePy) film a monomer free electrolyte solution (0,1M $TBAPF_6$ in ACN) scanned at (a) 100, (b) 200, (c) 300, (d) 400, (e) 500 $mV.sn^{-1}$.

The half-wave oxidation potentials of the polymer (E_o) was observed at 613 V at the scan rate of 100mV/sn. E_a, E_c, I_a, I_c, ΔE, E_{onset}, E_o, I_a/I_c, I_p values of polymer films are listed in Table 4.7. The other oxidation peak which is over 475 mV formation is cause of scanning from negative potentials to positive potentials called cation trapping.

Table4.7. E_a, E_c, I_a, I_c, ΔE, E_{onset}, E_o, I_a/I_c, I_p values of P(NMePyEBTNMePy) films scaned at 100, 200, 300, 400, 500 mV/sn scan rates.

scanrate ($mV.sn^{-1}$)	**E_{anodic} mV**	**$E_{cathodic}$ mV**	**ΔE mV**	**I_{anodic} µA**	**$I_{cathodic}$ µA**	**$I_{anodic}/I_{cathodic}$**	**E_o mV**
100	629	598	31	0,827	0,253	3,27	613
200	645	624	21	1,6	0,535	2,99	634
300	662	624	38	2,22	0,911	2,44	643
400	678	633	41	2,9	1,3	2,23	654
500	674	636	42	3,5	1,72	2,03	657

Scan rate dependence of polymer films were investigated in the Figure 4.27. As shown in the figure current densities and square root of scan rate is in a linear relationship which is significiant with Randles-sevcik equation.

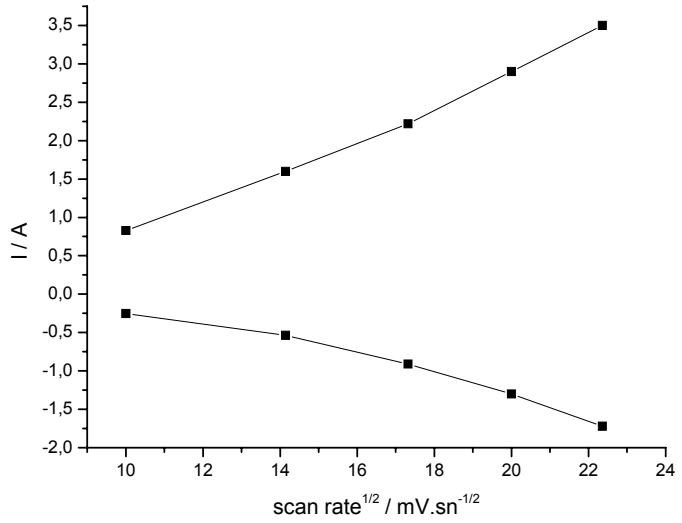

Figure 4.27. Scan rate depence of P(NMePyEBTNMePy) films scaned at different scan rates.

The current response of the film was directly proportional to the scan rate, indicating that the polymer film is electroactive and very well adhered to the electrode. The scan rate dependence of the peak currents both anodic and cathodic peaks shows linear dependence.

Oxidative electropolymerization of NMePyEBTNMePy was carried out in DCM with 0,1M $TABPF_6$ as electrolyte. Figure 4.28. shows first four cycle of the anodic electropolymerization by cylic voltammetry at 100mV/sn of a 0,001M solution of NMePyEBTNMePy onto a platin botton electrode.

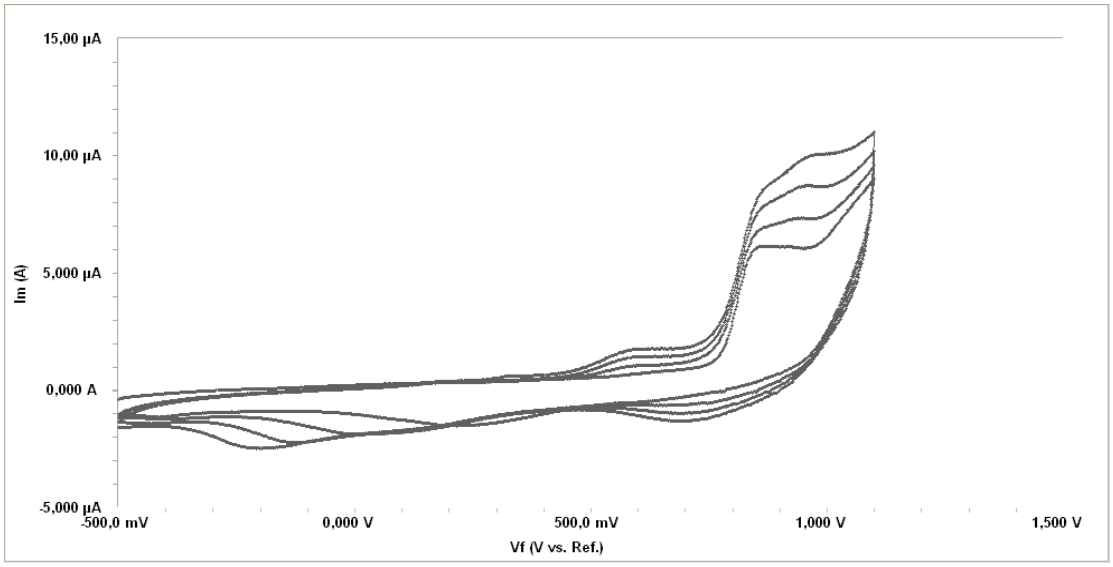

Figure 4.28. Electropolymerization of NmePy_EBT_NMePy comonomer by cyclic voltammetry from a 0.001M solution of comonomer in 0.1 M $TBAPF_6$/DCM at 100 mV s^{-1} onto PBE (area ~0.0024 cm^2). Q_{dep}=3.2x10^{-3} C cm^{-2}.

The polymeric films of P(NMePyEBTNMePy) were deposited by cylic voltammetry over 3 cycles from 0,1 M solution of comonomer in 0,1M $TBAPF_6$/DCM electrolyte. Investigation of the polymer films in monomer free electrolyte solution for their redox switching showed a well defined redox process. Figure 4.29. shows the cyclic voltammogram of this polymer film at scan rates of 100, 200, 300, 400, 500 mV/sn in 0,1M $TBAPF_6$/DCM. It is significiant that the polymer exhibits very well defined and reversible redox processes.

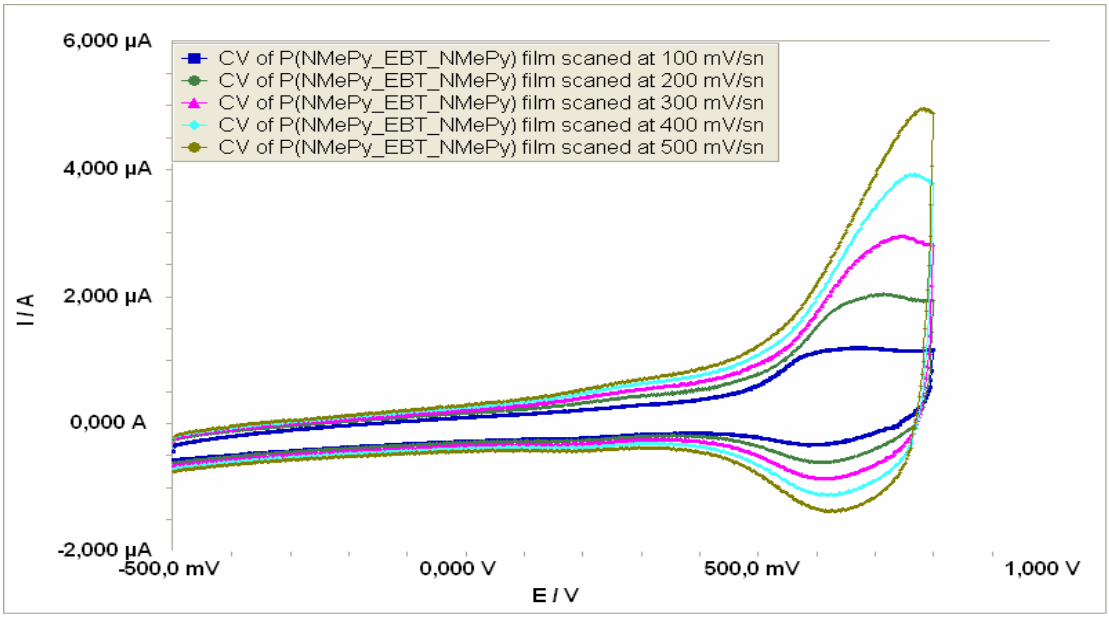

Figure 4.29. CV of the P(NMePy_EBT_NMePy) film(polymerization show in Figure 4.28) in a monomer free electrolyte solution (0,1M $TBAPF_6$ in ACN) scanned at (a) 100, (b) 200, (c) 300, (d) 400, (e) 500 $mV.sn^{-1}$.

E_a, E_c, I_a, I_c, ΔE, E_{onset}, E_o, I_a/I_c, I_p values of polymer films are listed in Table 4.8.

Table4.8. E_a, E_c, I_a, I_c, ΔE, E_{onset}, E_o, I_a/I_c, I_p values of P(NMePyEBTNMePy) films scaned at 100, 200, 300, 400, 500 mV/sn scan rates.

scanrate (mV.sn-1)	**E_{anodic} mV**	**$E_{cathodic}$ mV**	**ΔE mV**	**I_{anodic} µA**	**$I_{cathodic}$ µA**	**$I_{anodic}/I_{cathodic}$**	**E_o mV**
100	666	596	70	1,19	0,322	3,69	631
200	716	615	101	2	0,614	3,26	665
300	744	615	129	2,9	0,880	3,29	679
400	761	622	139	3,945	1,1	3,58	691
500	780	631	149	4,9	1,376	3,56	705

Scan rate dependence of polymer films were investigated in the Figure 4.30. As shown in the figure current densities and square root of scan rate is in a linear relationship which is significiant with Randles-sevcik equation.

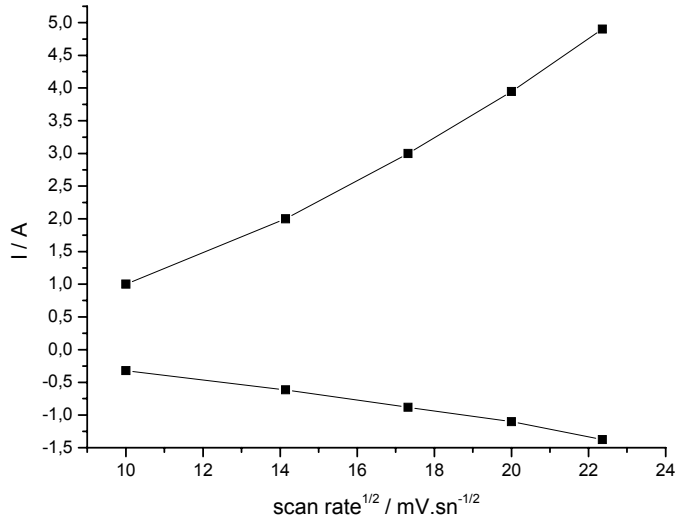

Figure 4.30. Scan rate depence of P(NMePyEBTNMePy) films scaned at different scan rates.

The current response of the film was directly proportional to the scan rate, indicating that the polymer film is electroactive and very well adhered to the electrode. The scan rate dependence of the peak currents both anodic and cathodic peaks shows linear dependence.

Oxidative electropolymerization of NMePyEBTNMePy was carried out in DCM with 0,1M $TABPF_6$ as electrolyte. Figure 4.31 shows first 8 cycle of the anodic electropolymerization by cylic voltammetry at 100mV/sn of a 0,001M solution of NMePyEBTNMePy onto a platin botton electrode.

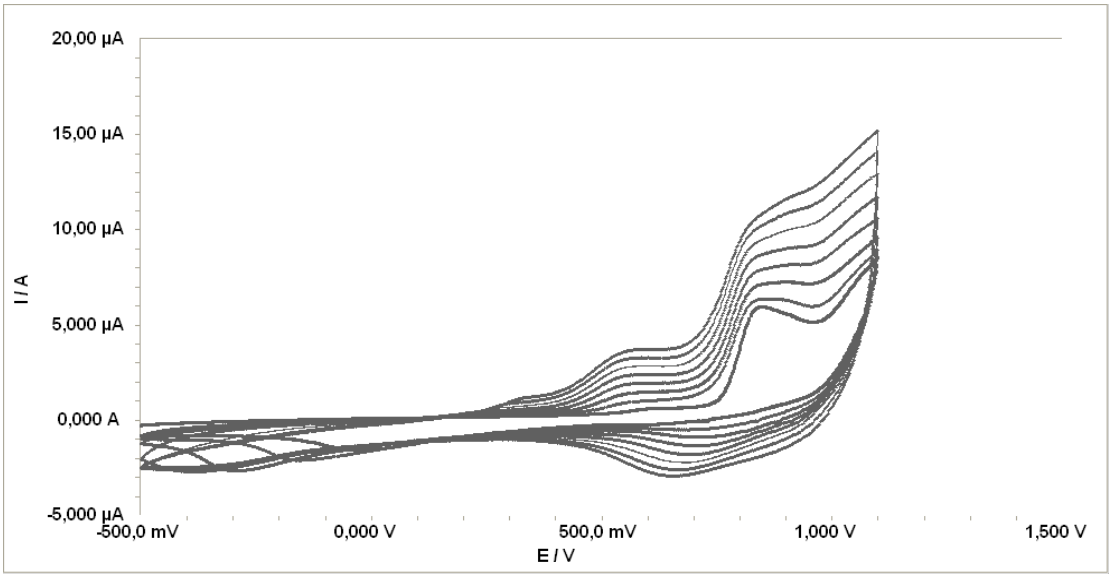

Figure 4.31. Electropolymerization of NmePy_EBT_NMePy comonomer by cyclic voltammetry from a 0.001M solution of comonomer in 0.1 M $TBAPF_6$/DCM at 100 mV s^{-1} onto PBE (area ~0.0024 cm^2).

The polymeric films of P(NMePyEBTNMePy) were deposited by cylic voltammetry over 2 cycles from 0,1 M solution of comonomer in 0,1M $TBAPF_6$/DCM electrolyte. Investigation of the polymer films in monomer free electrolyte solution for their redox switching showed a well defined redox process. Figure 4.32 shows the cyclic voltammogram of this polymer film at scan rates of 100, 200, 300, 400, 500 mV/sn in 0,1M $TBAPF_6$/DCM. It is significiant that the polymer exhibits very well defined and reversible redox processes.

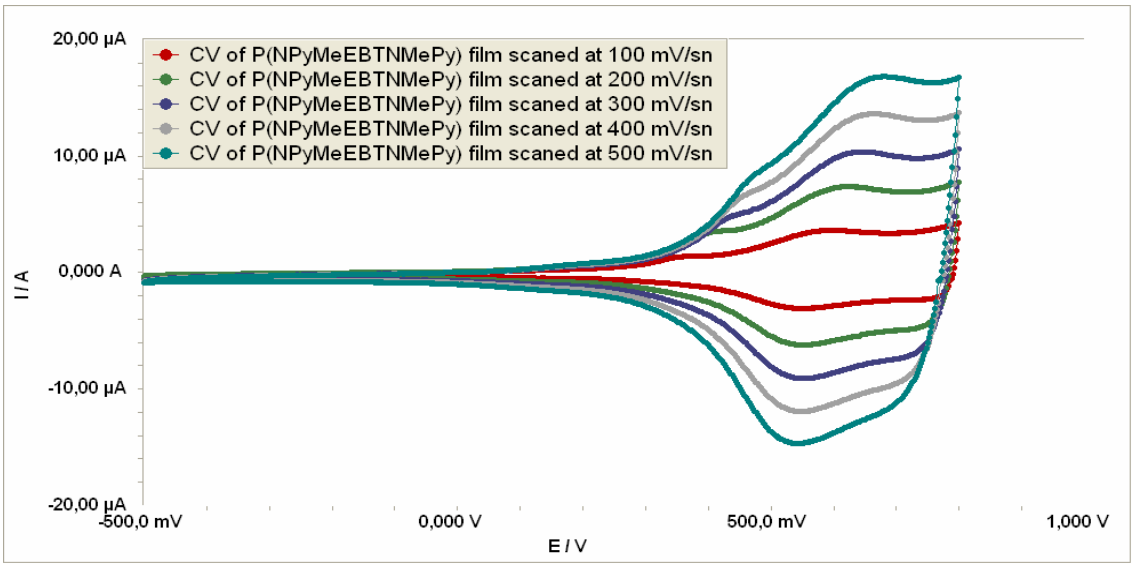

Figure 4.32. CV of the P(NMePy_EBT_NMePy) film(8cyc polymerization) in a monomer free electrolyte solution (0,1M $TBAPF_6$ in ACN) scanned at 100, 200, 300, 400, 500 $mV.sn^{-1}$.

E_a, E_c, I_a, I_c, ΔE, E_{onset}, E_o, I_a/I_c, I_p values of polymer films are listed in Table 4.9.

Table 4.9. E_a, E_c, I_a, I_c, ΔE, E_{onset}, E_o, I_a/I_c, I_p values of P(NMePyEBTNMePy) films scaned at 100, 200, 300, 400, 500 mV/sn scan rates.

scanrate ($mV.sn^{-1}$)	E_{anodic} mV	$E_{cathodic}$ mV	ΔE mV	I_{anodic} µA	$I_{cathodic}$ µA	$I_{anodic}/I_{cathodic}$	E_o mV
100	591	548	43	3,64	3,1	1,17	569
200	617	551	66	7	6	1,16	584
300	645	548	97	10,37	9	1,15	596
400	659	544	115	13,58	12	1,13	602
500	676	539	137	16,97	15	1,13	608

Scan rate dependence of polymer films were investigated in the Figure 4.33. As shown in the figure current densities and square root of scan rate is in a linear relationship which is significiant with Randles-sevcik equation.

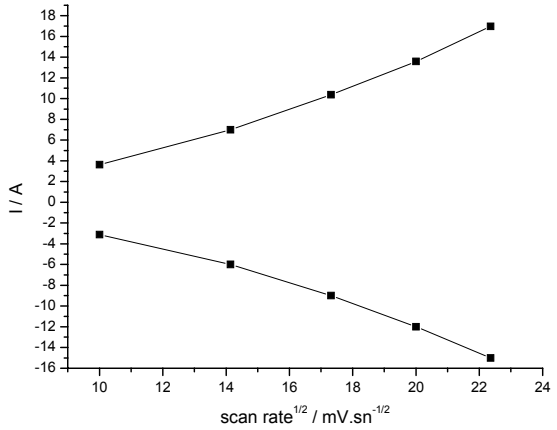

Figure 4.33 Scan rate depence of P(NMePyEBTNMePy) films scaned at different scan rates.

The current response of the film was directly proportional to the scan rate, indicating that the polymer film is electroactive and very well adhered to the electrode. The scan rate dependence of the peak currents both anodic and cathodic peaks shows linear dependence.

The difference in CV of P(NMePyEBTNMePy) films scaned at 100 mV/sn is seen in the Figure 4.34.

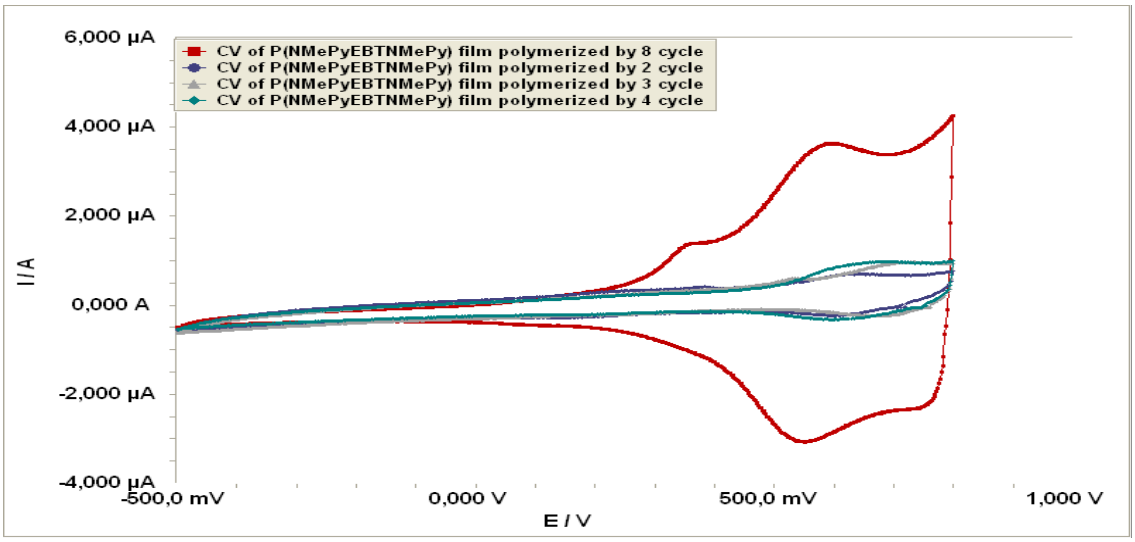

Figure 4.34. CV of P(NMePyEBTNMePy) films scaned at 100 mV/sn. (a) electropolymerization was achieved by appliying 8 cycles, (b) electropolymerization was achieved by appliying 2cycles, (c) electropolymerization was achieved by appliying 3 cycles, (d) electropolymerization was achieved by appliying 4 cycles

Doping with PF_6^- makes possible to polymerize wtih 8 cycles. If we look at Figure 4.34 and table 4.10 it is seen that 8 cycled polymerize film has better redox behaviour than the other 2 and 4 cycle polymerized polymer films. However, we could not be able to polymerize 8 cycles with ClO_4^- dopant ion we were able to in PF_6^- case that colud be because of the larger group of PF_6^- ion.

Table 4.10. E_a, E_c, I_a, I_c, ΔE, E_{onset}, E_o, I_a/I_c, I_p values of P(NMePyEBTNMePy) films scaned at 100 mV/sn.

Cycle number	E_{anodic}	$E_{cathodic}$	ΔE	I_{anodic}	$I_{cathodic}$	$I_{anodic}/I_{cathodic}$	E_o
3	645	548	97	10,37	9	1,15	596
4	744	615	129	2,9	0,880	3,29	679
8	662	624	38	2,22	0,911	2,44	643

4.2.2. Galvanostically Electropolymerization of P(NMePyEBTNMePy)

We have also tested method differences on electropolymerization of P(NMePyEBTNMePy). For that purpose adding to cylic voltammetry measurements, we have also tried to polymerize our copolymer by galvanostically measurements. In following sections electropolymerization by chronoamperometry is described.

4.2.2.1. Thickness effect on redox behaviour of P(NMePyEBTNMePy) in $TBACIO_4$/DCM media

We have obtained different thicknesses by appliying constant potential 1,1V for this case, for changing times. 5,15,30 seconds were applied for this porpose resulting polymers redox behaviour was investigated.

The electrodeposition of P(NMePyEBTNMePy) onto platin botton electrode was performed by chronoamperometry for 5seconds at a constant potential of 1,1V. Current versus time plot seen at Figure 4.35 which was performed from 0,1M $TBACIO_4$/DCM electrolyte solution containg 0,001M NMePyEBTNMePy for 5 seconds at 1,1 V .

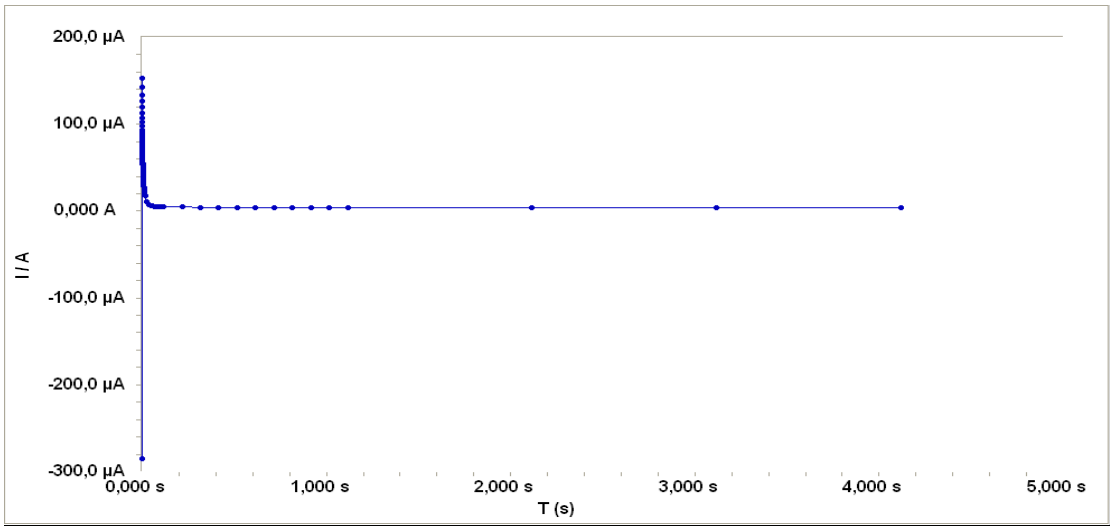

Figure 4.35. Chronoamperometry curve for NMePyEBTNMePy in 0,1M $TBAClO_4$/DCM electrolyte solution containing 0,001M NMePyEBTNMePy. (ΔI =147,8 µA)

Figure 4.35 illustrates electropolymerization of the comonomer, as seen above the plot reaches a maximum current value than decreases than stays constant. This incearese and decrease in the current value is because of the Nerst diffusion layer. The difference between maximum and minimum current values defines us that polymerization occurs. That is 147,8 µA for Figure 4.35.

The polymer films were washed with monomer-free electrolyte solution, and their redox behaviour was investigated with in the same solution by cyclic voltammetry. Figure 4.36 presents cyclic voltammogram of P(NMePyETNMePy) in the monomer free solution at different rates.

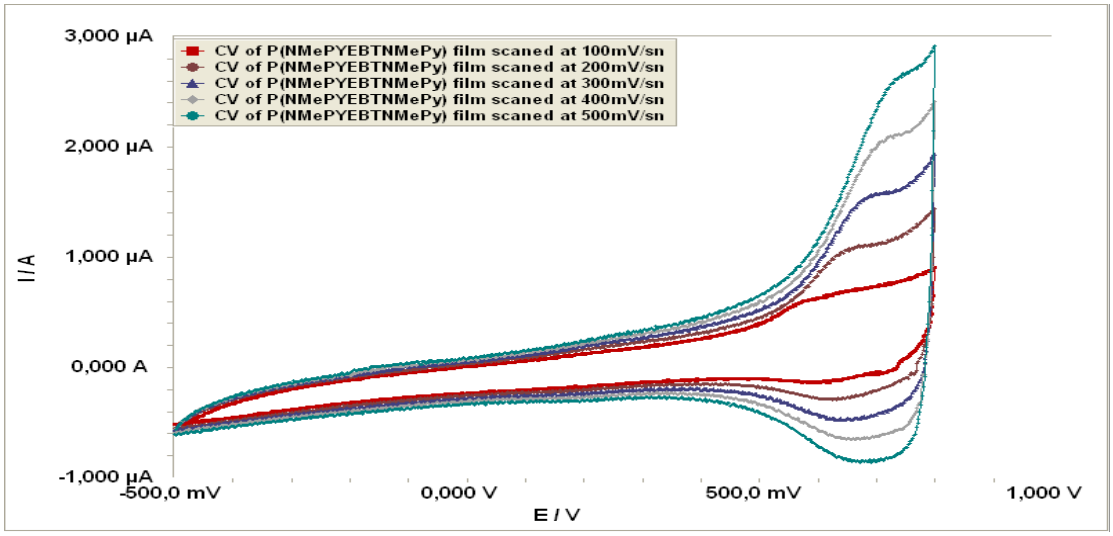

Figure 4.36. Cyclic voltammogram of the electrochemically polymerized P(NMePyEBTNMePy) filmin a monomer free electrolyte solution scaned at different rates.

P(NMePyEBTNMePy) films exhibit well defined oxidation and reduction peaks. Figure 4.37 scan rate dependencies of both oxidaiton and reduction peaks of the polymer were calculated using current values with respect to square root of the scan rate. The half-wave oxidation potentials of the polymer (E_o) was observed at 0,620V at the scan rate of 100mV/sn. E_a, E_c, I_a, I_c, ΔE, E_{onset}, E_o, I_a/I_c, I_p values of polymer films are listed in Table 4.11.

Table 4.11 E_a, E_c, I_a, I_c, ΔE, E_{onset}, E_o, I_a/I_c, I_p values of P(NMePyEBTNMePy) films scaned at 100, 200, 300, 400, 500 mV/sn scan rates.

scanrate ($mV.sn^{-1}$)	**E_{anodic} mV**	**$E_{cathodic}$ mV**	**ΔE mV**	**I_{anodic} µA**	**$I_{cathodic}$ µA**	**$I_{anodic}/I_{cathodic}$**	**E_o mV**
100	644	597	47	0,709	0,152	4,66	620
200	664	633	31	1,1	0,309	3,56	648
300	693	658	35	1,6	0,500	3,2	675
400	716	673	43	2	0,676	2,95	695
500	746	695	51	2,6	0,885	2,94	720

The current response of the film was directly proportional to the scan rate, indicating the the polymer film is electroactive and very well adhered to the electrode. The scan rate dependence of the peak currents of both the anodic and cathodic peaks shows linear dependence.

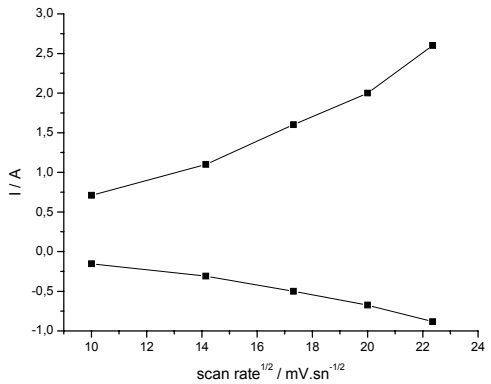

Figure 4.37 Scan rate depence of the cyclic voltammogram given in Figure 4.36

The electrodeposition of P(NMePyEBTNMePy) onto platin botton electrode was performed by chronoamperometry for 15 seconds at a constant potential of 1,1V. Current versus time plot seen at Figure 4.38 which was performed from 0,1M $TBAClO_4$/DCM electrolyte solution containg 0,001M NMePyEBTNMePy for 15 seconds at 1,1 V .

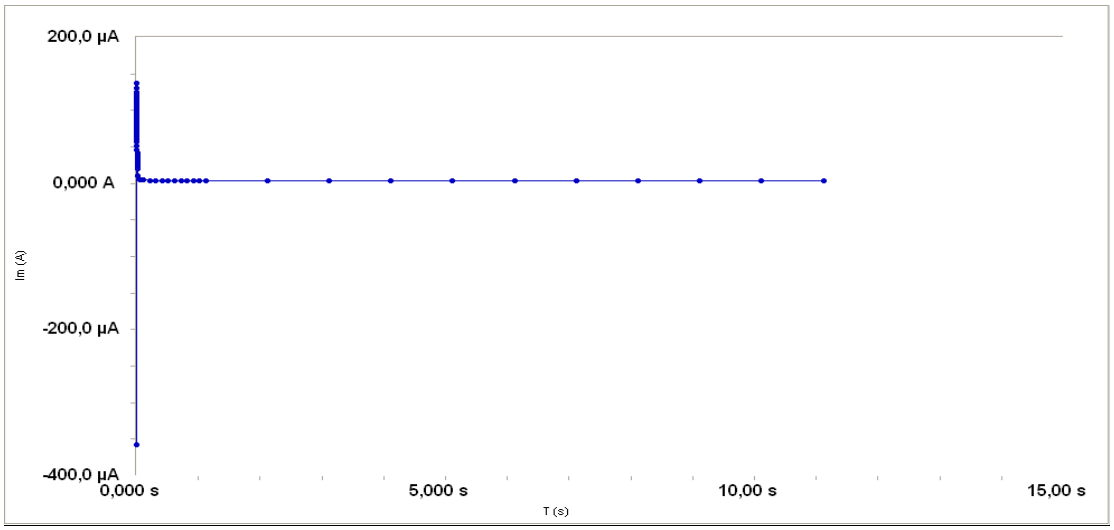

Figure 4.38. Chronoamperometry curve for NMePyEBTNMePy in 0,1M $TBAClO_4$/DCM electrolyte solution containing 0,001M NMePyEBTNMePy. (ΔI =134,314 µA)

Figure 4.38 illustrates electropolymerization of the comonomer, as seen above the plot reaches a maximum current value than decreases than stays constant. This incearese and decrease in the current value is because of the Nerst diffusion layer. The difference between maximum and minimum current values defines us that polymerization occurs. That is 134,314µA for Figure 4.38.

The polymer films were washed with monomer-free electrolyte solution, and their redox behaviour was investigated with in the same solution by cyclic voltammetry. Figure 4.39 presents cyclic voltammogram of P(NMePyETNMePy) (polymerize by chronoamperometry seen in Figure 4.38) in the monomer free solution at different rates.

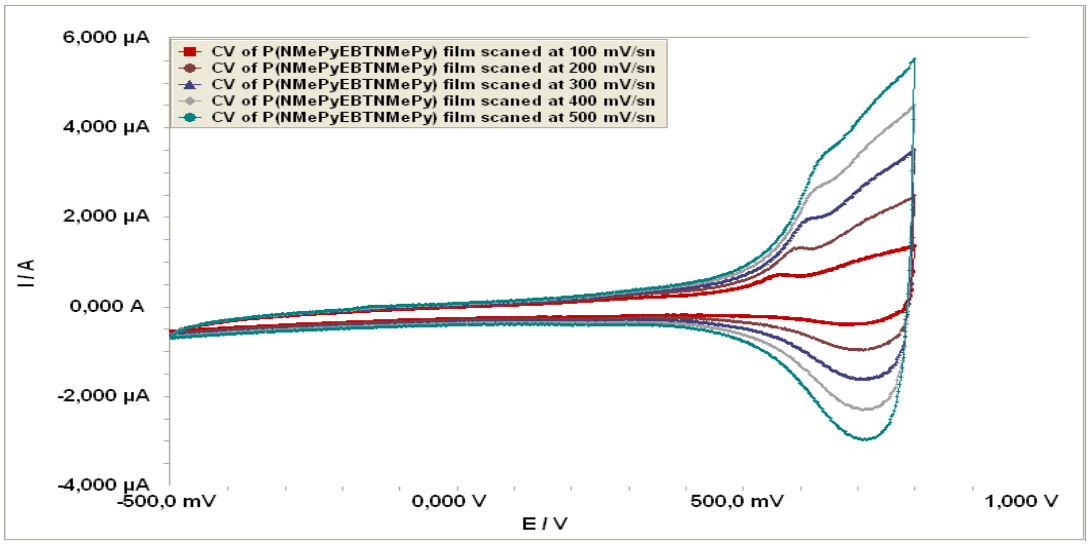

Figure 4.39. Cyclic voltammogram of the electrochemically polymerized P(NMePyEBTNMePy) filmin a monomer free electrolyte solution scaned at different rates.

P(NMePyEBTNMePy) films exhibit well defined reduction peaks but no fine oxidation peak. So it could be sad that while time increases in polymerization by chronoamperometry polymer films redox behaviour gets worsen. It is also seen in ΔI value Figure 4.38. the current difference is 135 µA which is a lower value than 5 second polymerization with chronoamperometry.

The electrodeposition of P(NMePyEBTNMePy) onto platin botton electrode was performed by chronoamperometry for 30 seconds at a constant potential of 1,1V. Current versus time plot seen at Figure 4.40 which was performed from 0,1M $TBAClO_4$/DCM electrolyte solution containg 0,001M NMePyEBTNMePy for 30 seconds at 1,1 V .

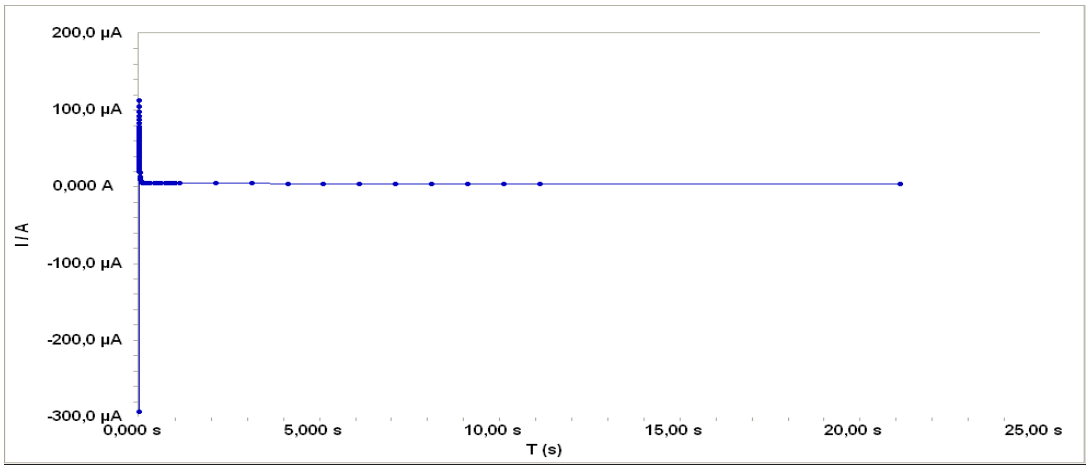

Figure 4.40 Chronoamperometry curve for NMePyEBTNMePy in 0,1M $TBAClO_4$/DCM electrolyte solution containing 0,001M NMePyEBTNMePy. (ΔI =110 µA)

Figure 4.40 illustrates electropolymerization of the comonomer, as seen above the plot reaches a maximum current value than decreases than stays constant. This incearese and decrease in the current value is because of the Nerst diffusion layer. he difference between maximum and minimum current values defines us that polymerization occurs. That is 110 µA for Figure 4.40.

The polymer films were washed with monomer-free electrolyte solution, and their redox behaviour was investigated with in the same solution by cyclic voltammetry. Figure 4.41 presents cyclic voltammogram of P(NMePyETNMePy) (polymerize by chronoamperometry seen in Figure 4.40) in the monomer free solution at different rates.

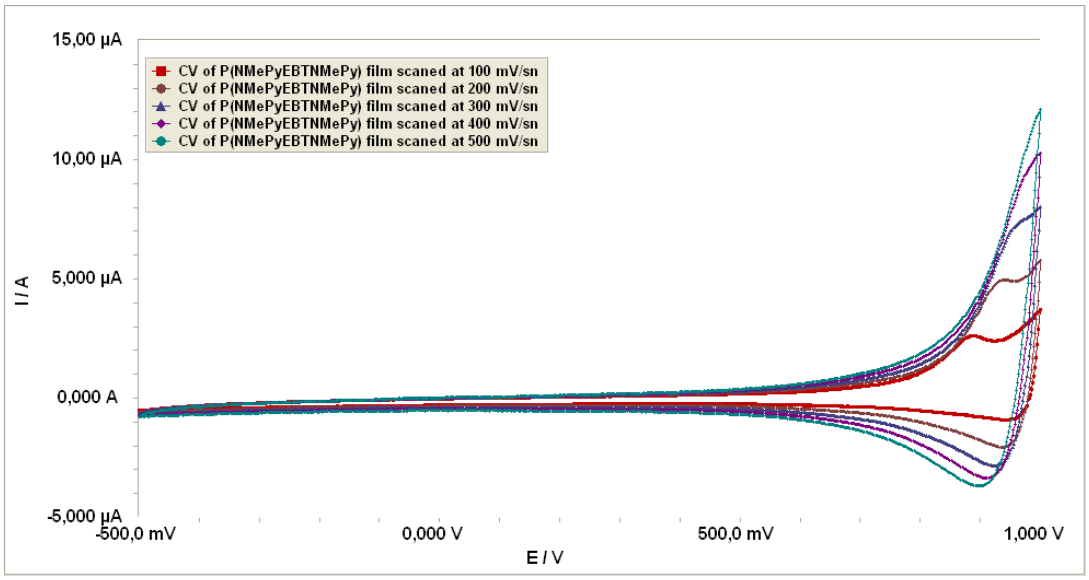

Figure 4.41. Cyclic voltammogram of the electrochemically polymerized P(NMePyEBTNMePy) filmin a monomer free electrolyte solution scaned at different rates.

P(NMePyEBTNMePy) films exhibit well defined reduction peaks but no fine oxidation peak. So it could be sad that while time increases in polymerization by chronoamperometry polymer films redox behaviour gets worsen. It is also seen in ΔI value Figure 4.40. the current difference is 110 µA which is a lower value than 5 second polymerization with chronoamperometry.

As seen in the Figure 4.41 redox behaviour of P(NMePyEBTNMePy) film damages with increasing scan rates. Greater than 300 mV/sn rates there are no oxidation peaks which corresponds to oxidation of copolymer and defines reversibility of copolymer.

The difference in CV of P(NMePyEBTNMePy) films scaned at 100 mV/sn is seen in the Figure 4.42. Although, with increasing times currents of polymer films increases. Well redox behaviour is seen with the 5 second potential treatment polymer film.

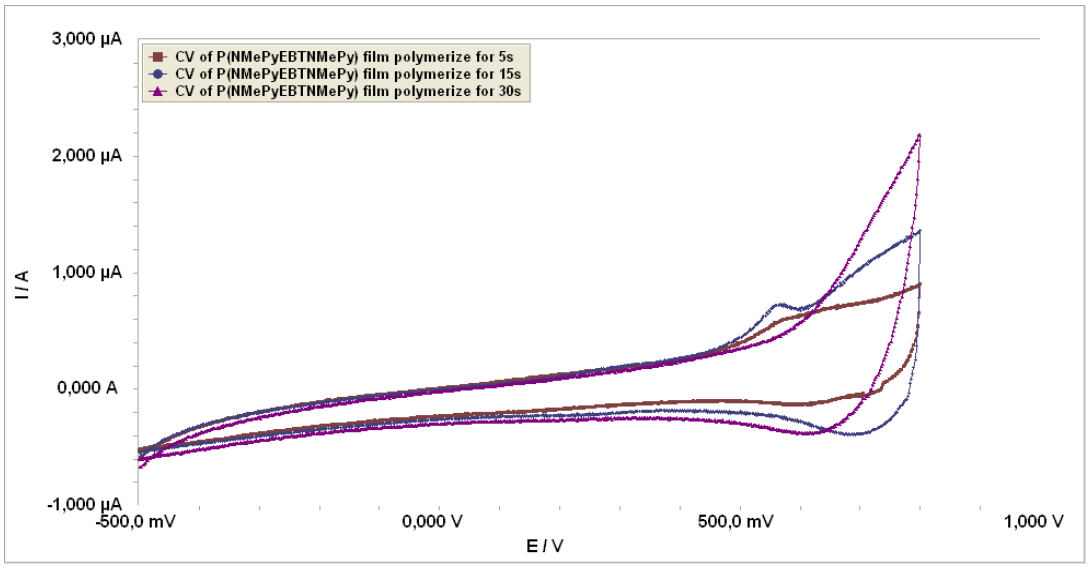

Figure 4.42. CV of P(NMePyEBTNMePy) films scaned at 1,1V (a) electropolymerization was achieved by appliying 5 second, (b) electropolymerization was achieved by appliying 15 second, (c) electropolymerization was achieved by appliying 30 second.

4.2.2.2. Thickness effect on redox behaviour of P(NMePyEBTNMePy) in $TBAPF_6$/DCM media

We have obtained different thicknesses by appliying constant potential 1,1V for this case, for changing times. 5,15,30 seconds were applied for this porpose resulting polymers redox behaviour was investigated.

The electrodeposition of P(NMePyEBTNMePy) onto platin botton electrode was performed by chronoamperometry for 5seconds at a constant potential of 1,1V. Current versus time plot seen at Figure 4.43 which was performed from 0,1M $TBAClO_4$/DCM electrolyte solution containg 0,001M NMePyEBTNMePy for 5 seconds at 1,1 V .

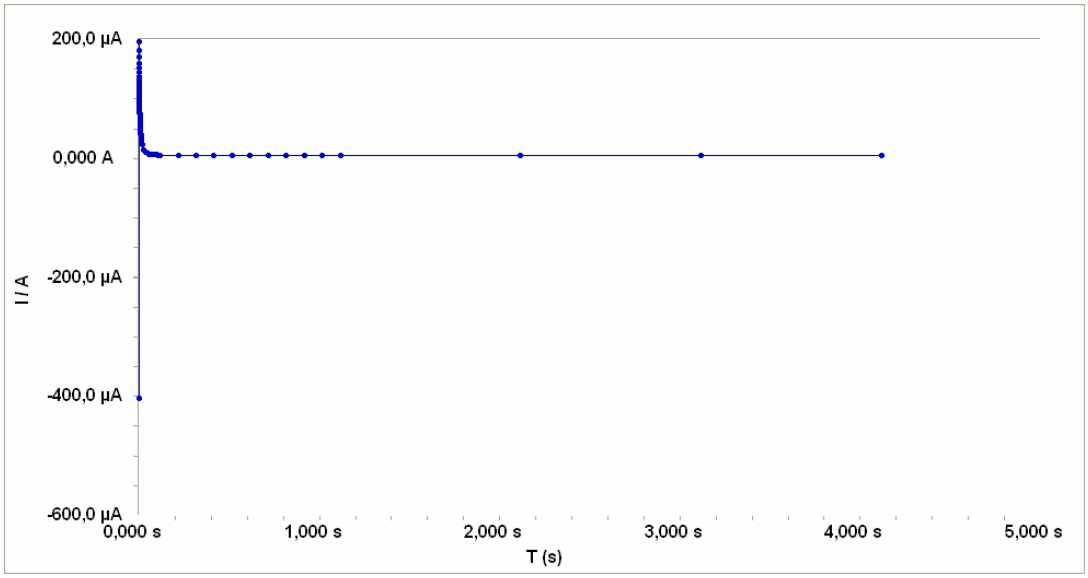

Figure 4.43. Electropolymerization of NmePy_EBT_NMePy comonomer by chronoamperometry from a 0,001M solution of comonomer in 0.1 M $TBAPF_6$/DCMfor 5 seconds onto PBE.

Figure 4.43 illustrates electropolymerization of the comonomer, as seen above the plot reaches a maximum current value than decreases than stays constant. This incearese and decrease in the current value is because of the Nerst diffusion layer. The difference between maximum and minimum current values defines us that polymerization occurs. That is 194,50µA for Figure 4.43.

The polymer films were washed with monomer-free electrolyte solution, and their redox behaviour was investigated with in the same solution by cyclic voltammetry. Figure 4.44 presents cyclic voltammogram of P(NMePyETNMePy) in the monomer free solution at different rates.

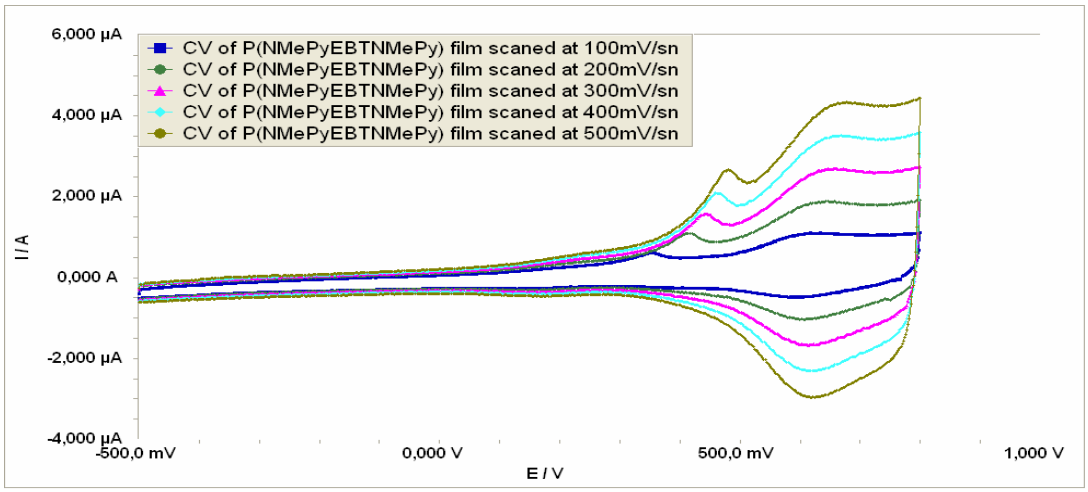

Figure 4.44. CV of the P(NMePy_EBT_NMePy) film(5 s) in a monomer free electrolyte solution (0,1M $TBAPF_6$ in DCM) scanned at 100, 200, 300, 400, 500 $mV.sn^{-1}$.

P(NMePyEBTNMePy) films exhibit well defined oxidation and reduction peaks. Figure 4.45 scan rate dependencies of both oxidaiton and reduction peaks of the polymer were calculated using current values with respect to square root of the scan rate. The half-wave oxidation potentials of the polymer (E_o) was observed at over 630 mV and E_a, E_c, I_a, I_c, ΔE, E_{onset}, E_o, I_a/I_c, I_p values of polymer films are listed in Table 4.12.

Table 4.12. E_a, E_c, I_a, I_c, ΔE, E_{onset}, E_o, I_a/I_c, I_p values of P(NMePyEBTNMePy) films scaned at 100, 200, 300, 400, 500 mV/sn scan rates.

scanrate ($mV.sn^{-1}$)	**E_{anodic}**	**$E_{cathodic}$**	**ΔE**	**I_{anodic}**	**$I_{cathodic}$**	**$I_{anodic}/I_{cathodic}$**	**E_o**
100	624	594	30	1,11	0,501	2,22	609
200	646	605	41	1,89	1,05	1,8	626
300	650	608	42	2,7	1,67	1,61	629
400	658	620	38	3,5	2,3	1,52	639
500	670	620	50	4,35	2,97	1,46	645

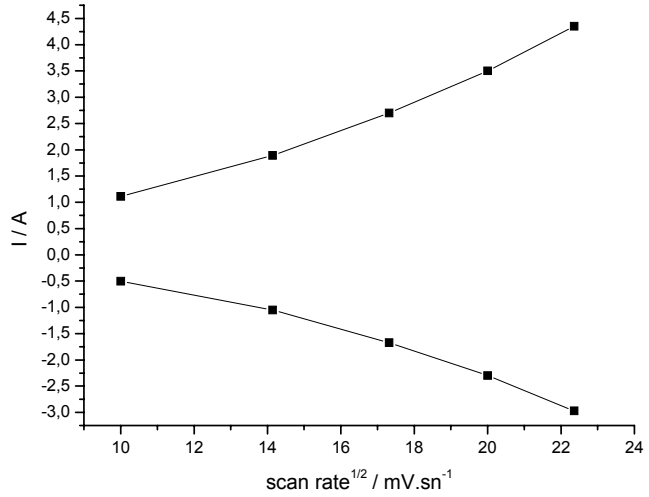

Figure4.45. Scan rate depence of the cyclic voltammogram given in Figure 4.44.

The current response of the film was directly proportional to the scan rate, indicating the the polymer film is electroactive and very well adhered to the electrode. The scan rate dependence of the peak currents of both the anodic and cathodic peaks shows linear dependence.

The electrodeposition of P(NMePyEBTNMePy) onto platin botton electrode was performed by chronoamperometry for 15seconds at a constant potential of 1,1V. Current versus time plot seen at Figure 4.46 which was performed from 0,1M $TBAClO_4$/DCM electrolyte solution containg 0,001M NMePyEBTNMePy for 15 seconds at 1,1 V .

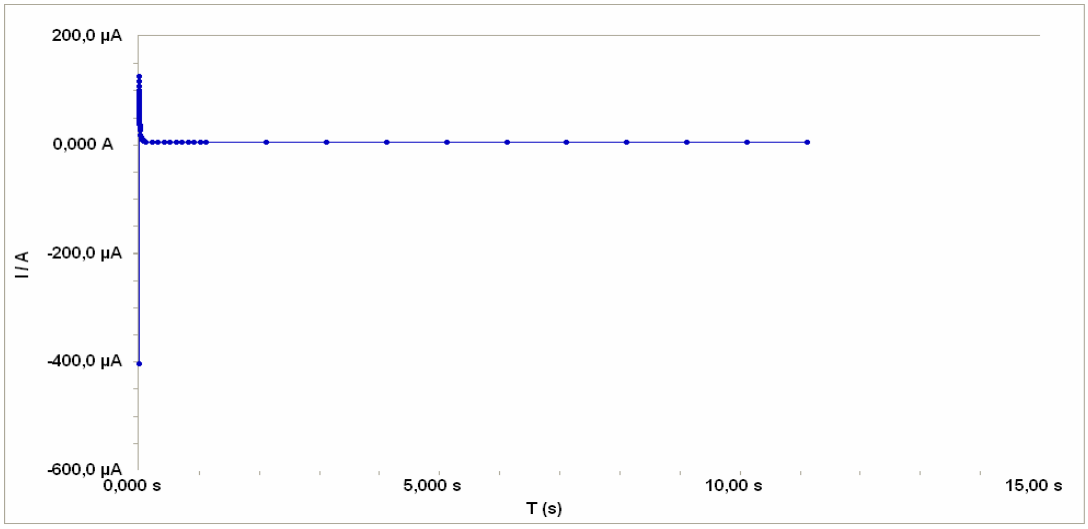

Figure 4.46. Electropolymerization of NmePy_EBT_NMePy comonomer by chronoamperometry from a 0,001M solution of comonomer in 0.1 M $TBAPF_6$/DCMfor 15 seconds onto PBE.

Figure 4.46 illustrates electropolymerization of the comonomer, as seen above the plot reaches a maximum current value than decreases than stays constant. This incearese and decrease in the current value is because of the Nerst diffusion layer. The difference between maximum and minimum current values defines us that polymerization occurs. That is 123 µA for Figure 4.46.

The polymer films were washed with monomer-free electrolyte solution, and their redox behaviour was investigated with in the same solution by cyclic voltammetry. Figure 4.47 presents cyclic voltammogram of P(NMePyETNMePy) (polymerize by chronoamperometry seen in Figure 4.46) in the monomer free solution at different rates.

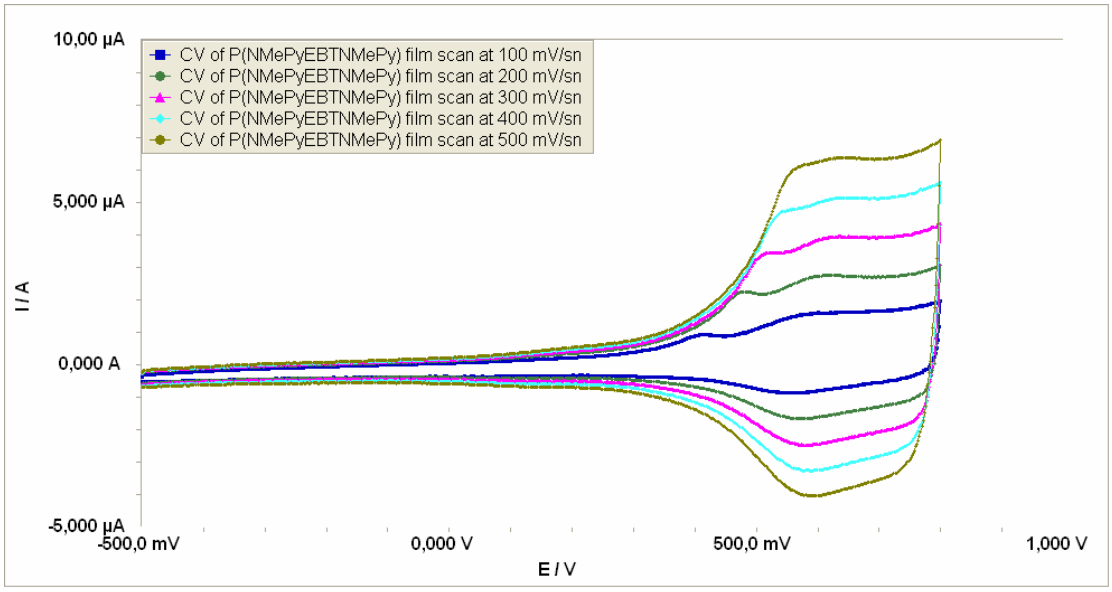

Figure 4.47. CV of the P(NMePy_EBT_NMePy) film(15 s) in a monomer free electrolyte solution (0,1M $TBAPF_6$ in DCM) scanned at 100, 200, 300, 400, 500 $mV.sn^{-1}$.

P(NMePyEBTNMePy) films exhibit well defined oxidation and reduction peaks. Figure 4.48 scan rate dependencies of both oxidaiton and reduction peaks of the polymer were calculated using current values with respect to square root of the scan rate. E_a, E_c, I_a, I_c, ΔE, E_{onset}, E_o, I_a/I_c, I_p values of polymer films are listed in table 4.13.

Table 4.13. E_a, E_c, I_a, I_c, ΔE, E_{onset}, E_o, I_a/I_c, I_p values of P(NMePyEBTNMePy) films scaned at 100, 200, 300, 400, 500 mV/sn scan rates.

scanrate (mV.sn^{-1})	**E_{anodic} mv**	**$E_{cathodic}$ mv**	**ΔE mV**	**I_{anodic} µA**	**$I_{cathodic}$ µA**	**$I_{anodic}/I_{cathodic}$**	**E_o mV**
100	603	560	43	1,58	0,889	1,7	582
200	615	577	38	2,76	1,67	1,65	596
300	633	579	54	3,98	2,5	1,59	606
400	638	572	66	5,17	3,31	1,56	605
500	638	594	44	6,42	4	1,60	616

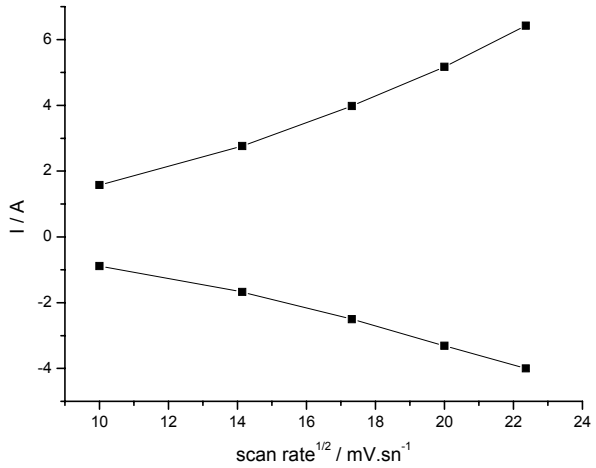

Figure 4.48. Scan rate depence of the cyclic voltammogram given in Figure 4.47.

The current response of the film was directly proportional to the scan rate, indicating the the polymer film is electroactive and very well adhered to the electrode. The scan rate dependence of the peak currents of both the anodic and cathodic peaks shows linear dependence.

The electrodeposition of P(NMePyEBTNMePy) onto platin botton electrode was performed by chronoamperometry for 30 seconds at a constant potential of 1,1V. Current versus time plot seen at Figure 4.49 which was performed from 0,1M $TBAPF_6$/DCM electrolyte solution containg 0,001M NMePyEBTNMePy for 30 seconds at 1,1 V .

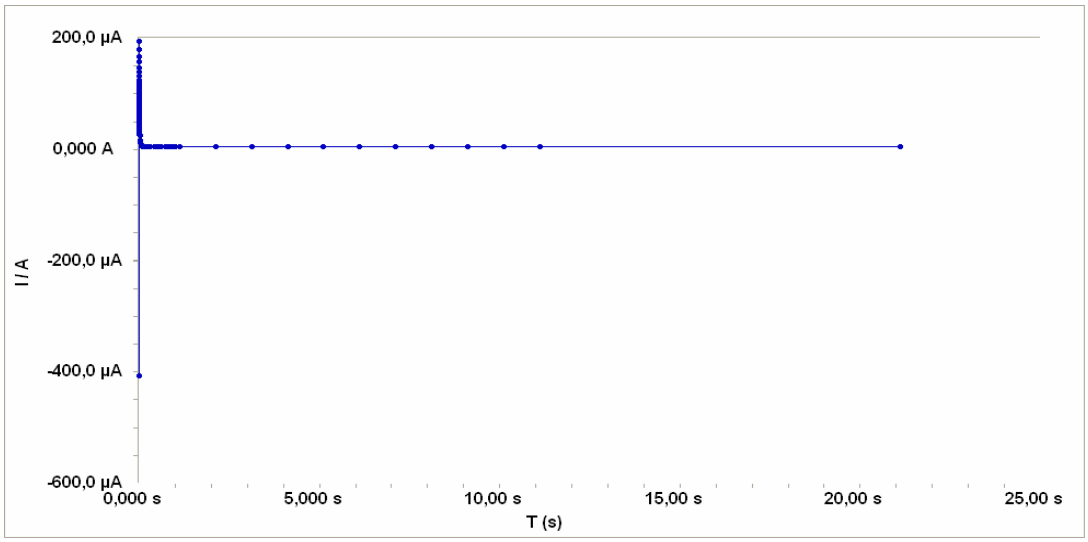

Figure 4.49. Electropolymerization of NmePy_EBT_NMePy comonomer by chronoamperometry from a 0,001M solution of comonomer in 0.1 M $TBAPF_6$/DCMbfor 30 seconds onto PBE.

Figure 4.49 illustrates electropolymerization of the comonomer, as seen above the plot reaches a maximum current value than decreases than stays constant. This incearese and decrease in the current value is because of the Nerst diffusion layer. The difference between maximum and minimum current values defines us that polymerization occurs. That is 188,35 µA for Figure 4.49.

The polymer films were washed with monomer-free electrolyte solution, and their redox behaviour was investigated with in the same solution by cyclic voltammetry. Figure 4.50 presents cyclic voltammogram of P(NMePyETNMePy) (polymerize by chronoamperometry seen in Figure 4.49) in the monomer free solution at different rates.

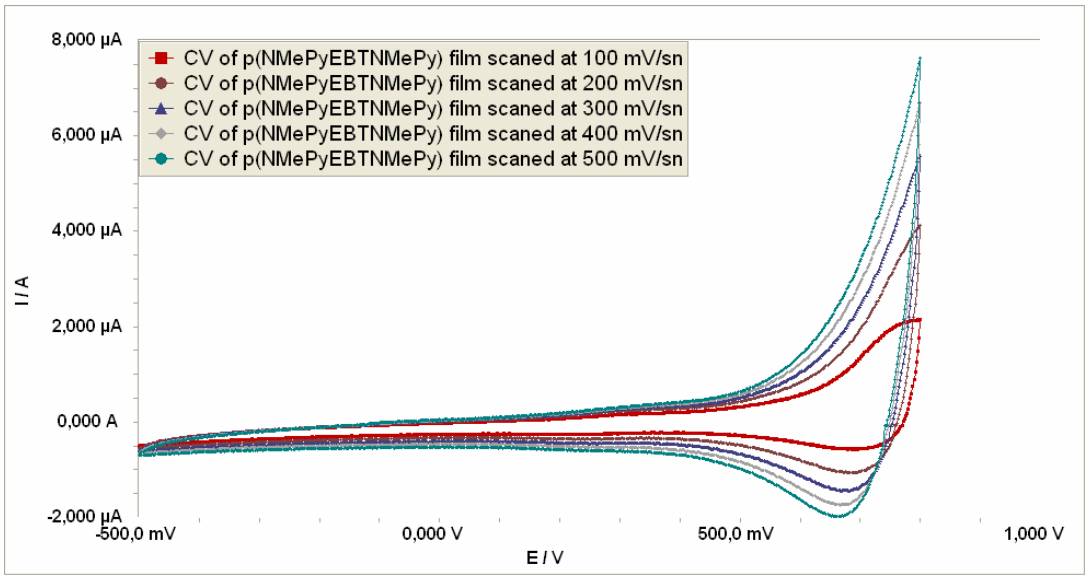

Figure 4.50. CV of the P(NMePy_EBT_NMePy) film (30 s) in a monomer free electrolyte solution (0,1M $TBAPF_6$ in ACN) scanned at 100, 200, 300, 400, 500 $mV.sn^{-1}$

P(NMePyEBTNMePy) films exhibit well defined oxidation and reduction peaks. The half-wave oxidation potentials of the polymer (E_o) was observed at 743 mV at the scan rate of 100mV/sn. E_a, E_c, I_a, I_c, ΔE, E_{onset}, E_o, I_a/I_c, I_p values of polymer film is listed in Table 4.14.

Table 4.14. E_a, E_c, I_a, I_c, ΔE, E_{onset}, E_o, I_a/I_c, I_p values of P(NMePyEBTNMePy) films scaned at 100, 200, 300, 400, 500 mV/sn scan rates.

scanrate ($mV.sn^{-1}$)	**E_{anodic} mV**	**$E_{cathodic}$ mV**	**ΔE mV**	**I_{anodic} µA**	**$I_{cathodic}$ µA**	**$I_{anodic}/I_{cathodic}$**	**E_o mV**
100	788	698	90	2,14	0,581	3,68	743

The scan rate dependence of the peak currents of both the anodic and cathodic peaks is seen only for 100 mv/sn scan rate. After that scan rate values, anodic and cathodic peaks become visible. So the polymer film does not have good redox properties.

As seen in the Figure 4.50 redox behaviour of P(NMePyEBTNMePy) film damages with increasing scan rates. Greater than 100 mV/sn rates there are no oxidation peaks which corresponds to oxidation of copolymer and defines reversibility of copolymer.

The difference in CV of P(NMePyEBTNMePy) films scaned at 100 mV/sn is seen in the Figure 4.51.

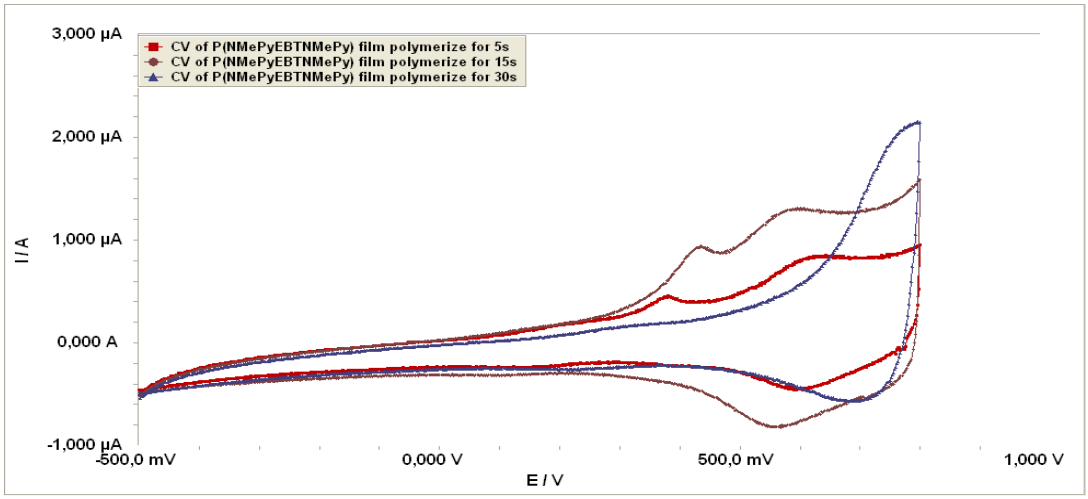

Figure 4.51. CV of P(NMePyEBTNMePy) films scaned at 100 mV/sn. (a) electropolymerization was achieved by appliying 8 cycles, (b) electropolymerization was achieved by appliying 2cycles, (c) electropolymerization was achieved by appliying 3 cycles, (d) electropolymerization was achieved by appliying 4 cycles

Although, increase with time increase in current is seen. More reversible peaks are observed in the5 second polymerization condition. E_a, E_c, I_a, I_c, ΔE, E_{onset}, E_o, I_a/I_c, I_p values of P(NMePyEBTNMePy) films scaned at 100 mV/sn are given in Table 4.15.

Table 4.15. E_a, E_c, I_a, I_c, ΔE, E_{onset}, E_o, I_a/I_c, I_p values of P(NMePyEBTNMePy) films scaned at 100 mV/sn.

Time	E_{anodic} mV	$E_{cathodic}$/ mV	ΔE / mV	I_{anodic} / µA	$I_{cathodic}$ / µA	I_{anodic}/ $I_{cathodic}$	E_o / mV
5	624	594	30	1,11	0,501	2,22	609
15	603	560	43	1,58	0,889	1,7	582
30	788	698	90	2,14	0,581	3,68	743

According to the results above polymerization with 15 seconds gives the best result for reversible systems. Although 30 second has the highest value its redox parameters are dicordant with reversible conditions. If we compare results of $TBAClO_4$/DCM and $TBAPF_6$/DCM PF_6^- ion is a better dopant for CA method. If we compare 5 second polymerization wtih each other. It can be seen that ΔE and E_o has lower values in PF_6^- dopant system. Polymer oxidation is more easy in PF_6^- ions. Also, polymer films are more reversible compared to ClO_4^- dopants.

It is possible with cyclic voltametry to gain thicker polymer films. For PF_6^- dopant, for 8 cycle polymerization ΔQ is 171,26 μC but for 30 seconds polymerization with CA method, it is only 99,46 μC. In spite of having lower charge value polymer films polymerized for 30 seconds does not show good redox properties than 8 cycle polymerization with CV method.

It is a better way to polymerize NMePyEBTNMePy comonomer with PF_6^- dopant by CV method. Dedoping process of polymerization with CV makes polymer films more stable for voltage and scan rate changes.

4.3. Doping proces of P(NMePyEBTNMePy)

The negative doping appears as a reduction wave at low potentials -1,12V and -0,23V. It corresponds to the injection of electrons into the polymer and to the insertion of cations from the electrolyte into the electrode to preserve the electroneutrality (Eq.(4.6)).

$$\text{Polymer}^{(0)} + e^- + Na^+ \underset{\text{undoping}}{\overset{\text{doping}}{\rightleftharpoons}} \text{Polymer}^-, Na^+ \quad \textbf{(4.6)}$$

This leads toa change in the electronic structure of the polymer and it becomes electronically conductive. The negative undoping process appears as an oxidation peak on the reverse scan, at -1,12V for copolymer and corresponds to electron extraction from the polymer, and to the removal of cations. The polymer returns to its neutral and isolating state.

The bithiazole group (electron acceptor group) confers to P(NMePyEBTNMePy) a higher and more stable n-doping process leading to a beter cyclability than P(NMePy).

For the positive doping, the same process of insertion of ion occurs, but the electrons are now extracted from the polymer and anions are inserted in the electrode (Eq.(4.7)). He p-doping of copolymer appears as an oxidation wave begining 0,645V and undoping as a reduction peak at 0,600V. It represents the removal of anions while electrons are injected into the polymer.

$$\text{Polymer}^{(0)} + ClO_4^- \underset{\text{undoping}}{\overset{\text{doping}}{\rightleftharpoons}} \text{Polymer}^+, ClO_4 + e^- \quad \textbf{(4.7.)}$$

4.3.1. n-Doping Properties of P(NMePyEBTNMePy)

We have also investigate n-doping properties of P(NMePyEBTNMePy). The resulting copolymer structure has the both the electron donating N-Methyl Pyrrole unit and the electron accepting bithiazole unit. Although the presence of nitrogen in the bithiazole ring increases the oxidation potential and renders the material with respect to p-doping however n- doping is possible.

Figure 4.52. shows a representative electropolymerization attempt of NMePyEBTNMePy comonomer. Electropolymerization was achieved in 0,1M $NaClO_4$/ACN electrolyte solution with 0,001M NMePyEBTNMePy comonomer.

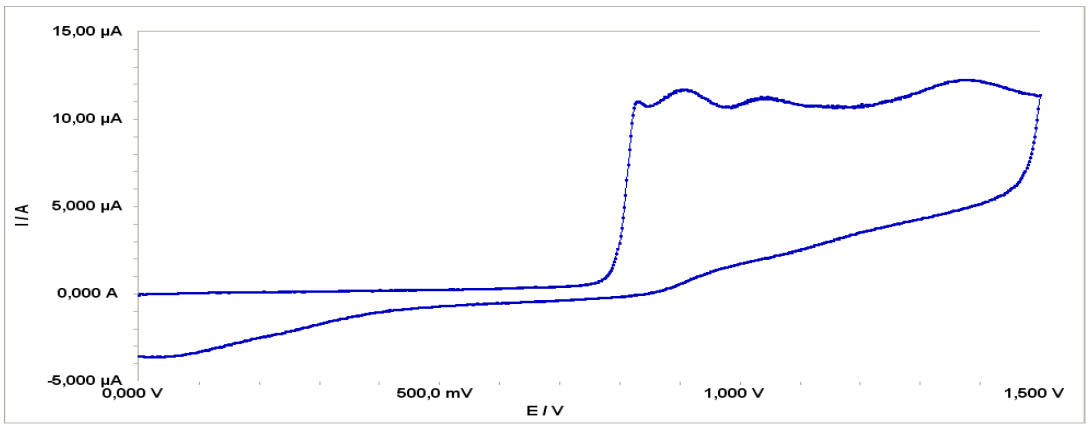

Figure 4.52. Electrodeposition of NMePyEBTNMePy by potentiodynamic deposition from a 0,001M solution of monomer in 0,1M $NaClO_4$/ACN at 100 mV/sn onto platin botton electrode.

Investigation of the polymer films in monomer free electrolyte solution for their redox behaviour showed a well defined p-doping and n-doping. Figure 4.53 shows the cyclic voltammogram of this polymer at scan rates of 100, 200, 300, 400, 500 mV/sn in 0,1M $NaClO_4$/ACN. It is significiant that polymer exhibits well defined and reversible n-doping process.

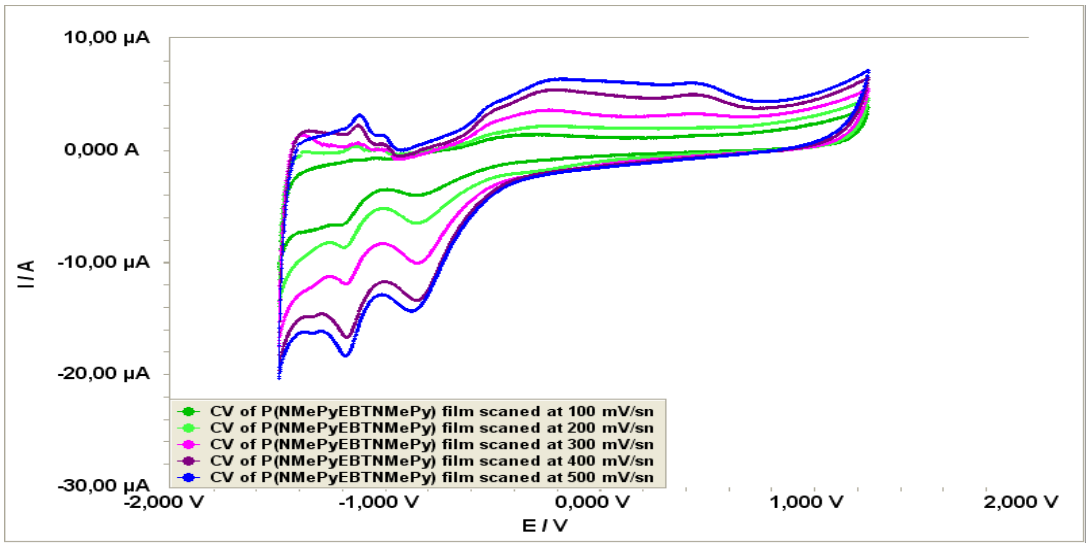

Figure 4.53. CV of the P(NMePy_EBT_NMePy) film(polymerization given in Figure 4.52) in a monomer free electrolyte solution (0,1M $TBAPF_6$ in ACN) scanned at 100, 200, 300, 400, 500 $mV.sn^{-1}$.

4.3.2. E_g value of P(NMePyEBTNMePy)

Figure 4.54 shows the cyclic voltammogram of P(NMePyEBTNMePy) film scaned at 500 mV/sn in 0,1M $NaClO_4$/ACN electrolyte solution. Sweep was started from an initial potential of -1,5V to 1,5V at a scan rate of 500 mV/sn.

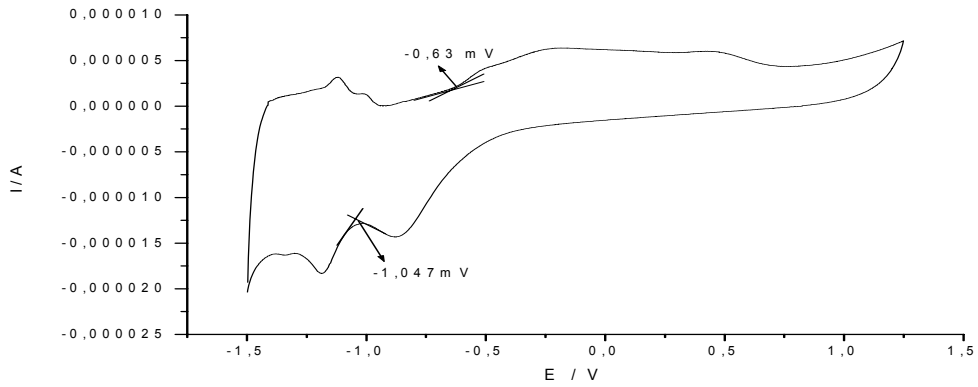

Figure 4.54. P(NMePyEBTNMePy) film in 0,1M $NaClO_4$/ACN at a scan rate of 500mV/sn from -1,5 to 1,5V .

The P(NMePyEBTNMePy) film exhibited a broad oxidation peak cause of different chain lenghts in the polymer at -0,63Vand a reduction peak at -1,047 V. These results support the structure of the polymer having both the electron donating NMePy unit and the electron acepting thiazole unit. From the potential difference between the onset of the p-doping and that of the main n-doping peak, the band gap of P(NMePyEBTNMePy) is determined at about 0,417eV.

4.4. Doping Degree Properties of P(NMePyEBTNMePy)

We have also investigated doping degree properties of P(NMePyEBTNMePy) films by linear sweep voltammetry method. We have polymerize P(NMePyEBTNMePy) films by chronoamperometry method wtih different times to obtain different thicker polymers. Than the polymer films were washed monomer free electrolyte solution and linear sweep plots were gained between 0 and -1 V. It corresponds to doping and than undoping process for electrically conductive polymers.

In table 4.16.ΔQ_{pg}, $|\Delta Q_{fd}|$, D.D. values of P(NMePyEBTNMePy) is listed which was electropolymerize on PBE from 0,001M NMePyEBTNMePy in 0,1M $TBAClO_4$/DCM by galvonistatically with 5, 15 , 30 seconds.

Table 4.16 ΔQ_{pg}, $|\Delta Q_{fd}|$, D.D. values of P(NMePyEBTNMePy) deposited on platium boton electrode from 0,001M NMePyEBTNMePy in 0,1M $TBAClO_4$/DCM and 0,1M $TBAPF_6$ / DCM by galvonistatically with different times.

	Time	y (DD)
P(NMePyEBTNMePy) in $TBAClO_4$ / DC M	5	
	15	0,8600
	30	0,4800
P(NMePyEBTNMePy) in $TBAPF_6$ / DC M	5	0,3900
	15	0,2400
	30	0,2200

As the polymerization time of P(NMePyEBTNMePy) increases, polymer film gets thicker fastly therefore it gets unable to give doped anions into the solution. Hence doping degree of the polymer film decreases as time increases.

4.5. Electrochemical Impedance Spectroscopy

Electrochemical Impedance Spectroscopy (EIS) measurements were performed at open circuit potential in the range of 10 mHz-100 kHz (application of amplitude of 10mV) for P(NMePyEBTNMePy)electrochemically obtained at different cycles and times.

4.5.1. Electrochemical Impedance Spectroscopy (EIS) Measurement with Appliying Potential on P(NMePyEBTNMePy)

Electrochemical Impedance Spectroscopy (EIS) measurements were performed at different applied potentials in the range of -0.4 V to 0,8 V with a potential step of 0.2V in parallel to cyclic voltammogram of the P(NMePyEBTNMePy) in monomer

free electrolyte solution where stability of the film exhibit electroactivity without undergoing deformation.

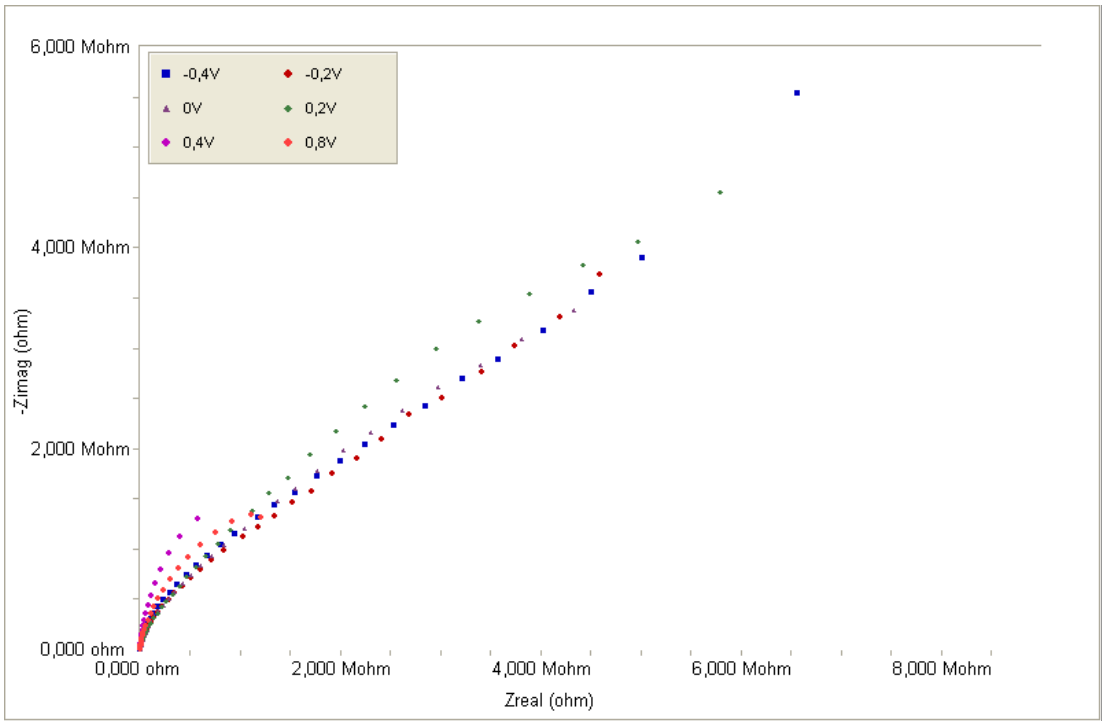

Figure 4.55. Nyquist plots at -0.4 V to 0,6V V for a P(NMePyEBTNMePy)film deposited at deposited at 100 mV/s, 2cycle in 0.1 M $TBAPF_6$/DCM solution.

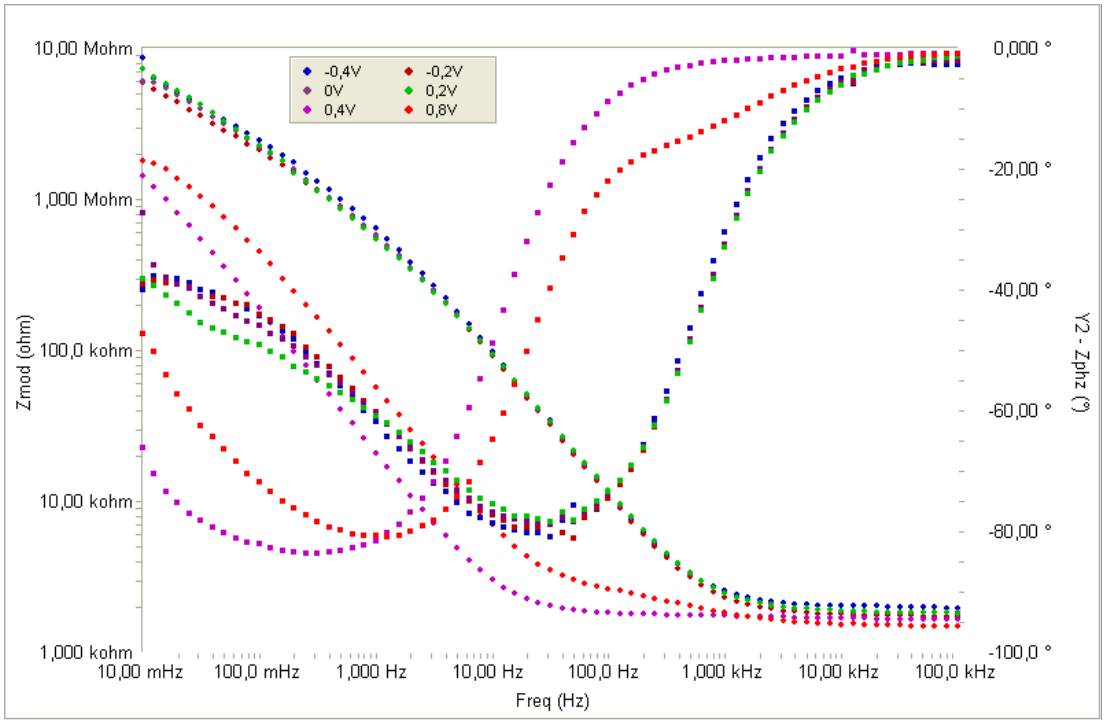

Figure 4.56. Z mod and Z phase plots at -0.4 V to 0,8V V for a P(NMePyEBTNMePy)film deposited at 100 mV/s, 2cycle in 0.1 M $TBAPF_6$/DCM solution

Resuts of the EIS measurements are given in Figure 4.55 as Nyquist and in Figure 4.56 as Bode plots at different potentials for P(NMePyEBTNMePy) film. Phase angle very close to -90^{o}. Impedance behavior of the film similar in the range of -0,4 V to 0,2 V.

Bode plots shown in Figure 4.56 can be divided into a high frequency component (bended at -45^{o}) and a low frequency component (near vertical) with the transition between the two regions. The resistive and capacitive impedances are equal at the transition i.e. -45^{o}.

The low frequency capacitance values from impedance spectroscopy were obtained from the slope of a plot of the imaginary component (Z_{IM}) of the impedance at low frequencies versus inverse of the reciprocal frequency (f) using following equation.

$$\mathbf{C_{LF} = (2\pi f Z_{im})^{-1}} \qquad \mathbf{(4.8)}$$

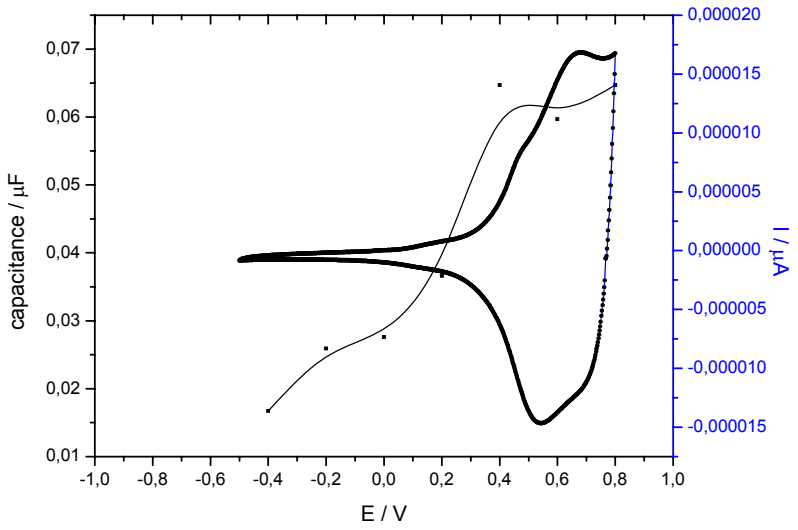

Figure 4.57. Variation of the low frequency capacitance values of the electrochemically polymerized P(NMePyEBTNMePy) film deposited at 100 mV/s, 2 cycle in 0.1 M $TBAPF_6$/DCM solution

The shape of the graph illustrated in Figure 4.57 shows good agreement with the corresponding CV of the polymer film in monomer free solution. As illustrated in Figure 4.57 P(NMePyEBTNMePy) does not show electroactivity in the rang of -0,4 to 0,4 V current starts to increase from this point. System starts to show capacitive behaviour starting from 0,4V. Than capacitve value drops as similar behaviour like CV.

4.5.2. Thickness effect of P(NMePyEBTNMePy); EIS Investigation

Figure 4.58 shows the Bode magnitude and the Bode phase angle and Figure 4.59 shows the Nyquist plot of P(NMePyEBTNMePy) film prepared by application of different scan numbers during the electropolymerization. P(NMePyEBTNMePy)films were prepared by depositing at 100 mV/s, 2, 3 and 4 cycles in 0.1 M $TBAClO_4$/DCM solution.

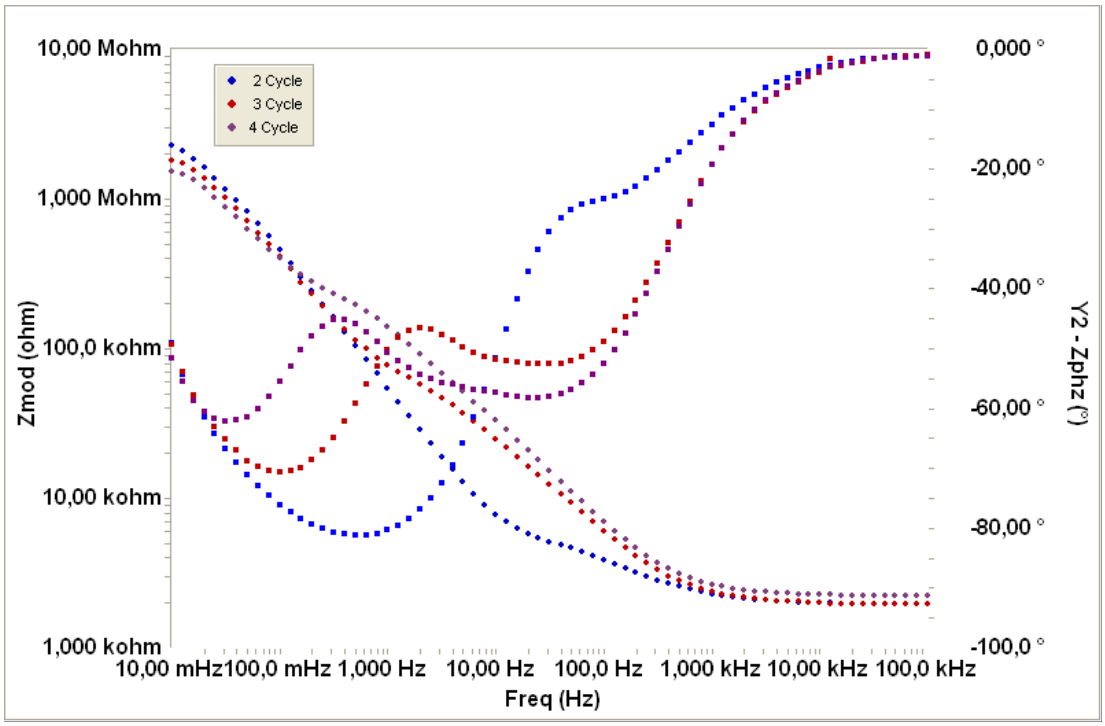

Figure 4.58. Z mod and Z phase plots at 0,6V for a P(NMePyEBTNMePy)film deposited at 100 mV/s, 2, 3 and 4 cycles in 0.1 M $TBAClO_4$/DCM solution

$C_{sp,}$ C_{dl} and phase angle values of a P(NMePyEBTNMePy)film deposited at 100 mV/s, 2, 3 and 4 cycle in 0.1 M $TBAClO_4$/DCM solution is given at Table 4.17.

Table 4.17. $C_{sp,}$ C_{dl} and phase angle values of a P(NMePyEBTNMePy)film deposited at 100 mV/s, 2, 3 and 4 cycle in 0.1 M $TBAClO_4$/DCM solution.

cycle	C_{sp}	C_{dl}	Phase angle
2	0,42	18,9	83,77
3	0,68	22,18	82,85
4	0,59	20,30	81,93

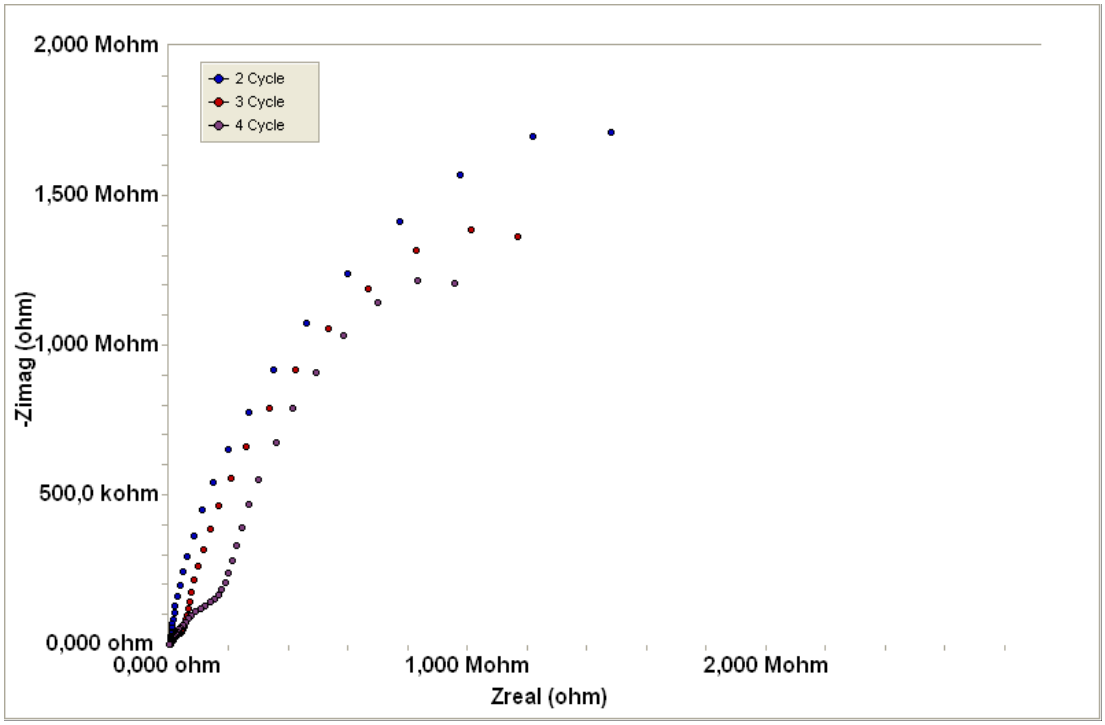

Figure 4.59. Nyquist plots at -0.4 V to 0,8V V for a P(NMePyEBTNMePy)film deposited at 100 mV/s, 2, 3 and 4 cycle in 0.1 M $TBAClO_4$/DCM solution.

From the values below, it could be said that, capacitive behaviour of P(NMePyEBTNMePy) films capacitive behaviour demostrates at 4 cycle polymerization. This result is also in a harmony with CV measurements which point outs that with increasing cycle number polymer films redox behaviour gets worsen.

Figure 4.60 shows the Bode magnitude and the Bode phase angle and Figure 4.61 shows the Nyquist plot of P(NMePyEBTNMePy) film prepared by application of different scan numbers during the electropolymerization. P(NMePyEBTNMePy)films were prepared by depositing at 100 mV/s, 2, 3, 4 and 8 cycles in 0.1 M $TBAPF_6$/DCM solution.

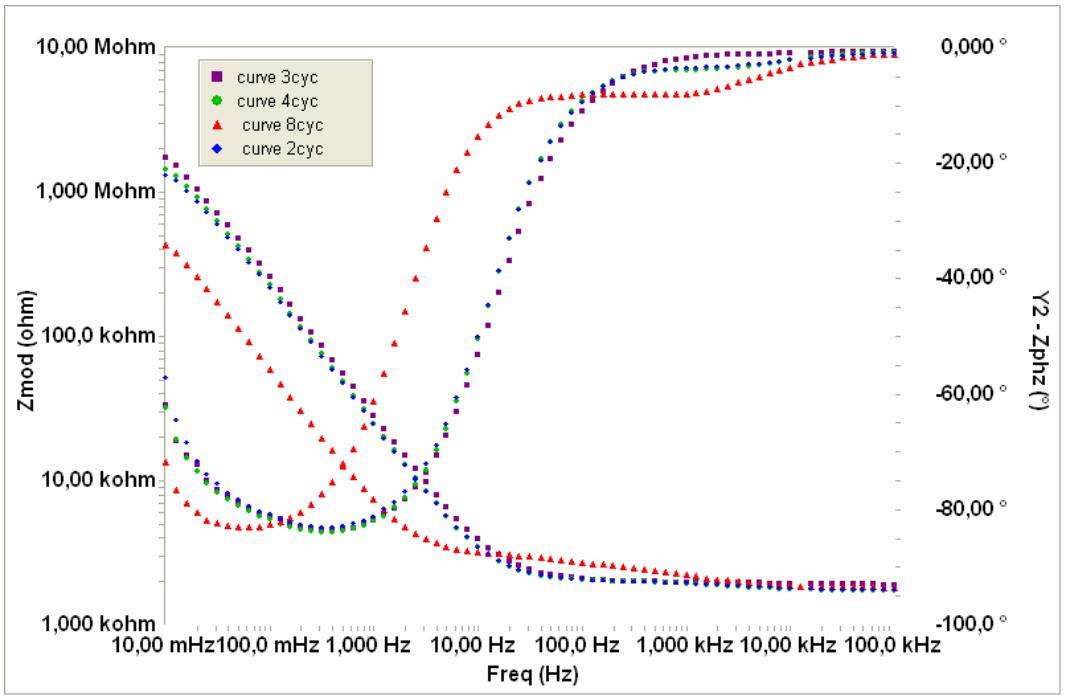

Figure 4.60. Z mod and Z phase plots at 0,6V for a P(NMePyEBTNMePy)film deposited at 100 mV/s, 2, 3,4 and 8 cycles in 0.1 M $TBAPF_6$/DCM solution

$C_{sp,}$ C_{dl} and phase angle values of a P(NMePyEBTNMePy)film deposited at 100 mV/s, 2, 3 and 4 cycle in 0.1 M $TBAPF_6$/DCM solution is given at Table 4.18.

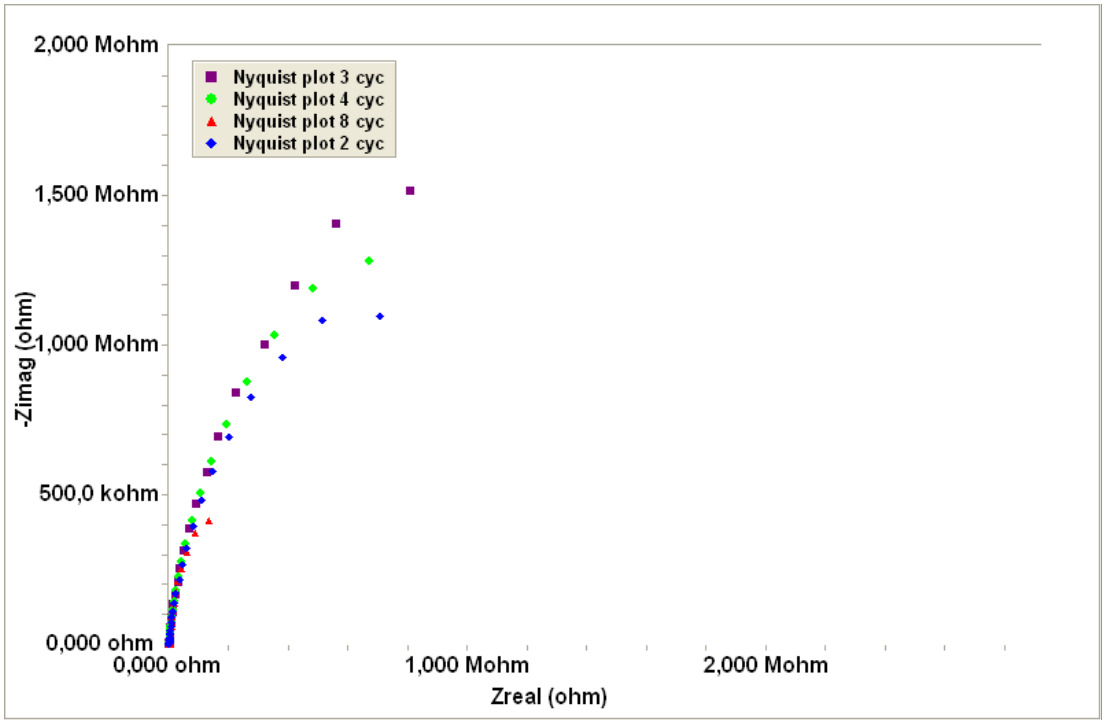

Figure 4.61. Nyquist plots at -0.4 V to 0,8V V for a P(NMePyEBTNMePy)film deposited at 100 mV/s, 2, 3, 4 and 8cycle in 0.1 M $TBAPF_6$/DCM solution.

From the results Figure 4.60, Figure 4.61 and Table 4.17. it is seen that with increasing cycle number capacitive behaviour demonstrates but redox behaviour gets

better which we know from the CV results. Also, from the Bode mod plot we discover that our polymer shows capacitive behaviour at low frequency values. With increasing cycle number capacitve region shifts lower frequency values.

Table 4.18. $C_{sp,}$ C_{dl} and phase angle values of a P(NMePyEBTNMePy)film deposited at 100 mV/s, 2, 3,4 and 8 cycle in 0.1 M $TBAPF_6$/DCM solution.

cycle	C_{sp}	C_{dl}	Phase angle
2	0,62	40,70	86
3	0,69	35,21	88
4	0,65	40,03	89
8	0,58	186	86

Figure 4.62 shows the Bode magnitude and the Bode phase angle and Figure 4.63 shows the Nyquist plot of P(NMePyEBTNMePy) film prepared by application of different times during the electropolymerization by CA. P(NMePyEBTNMePy)films were prepared by depositing at at 0,6 V , 5, 15 and 30 seconds in 0.1 M $TBAPF_6$/DCM solution.

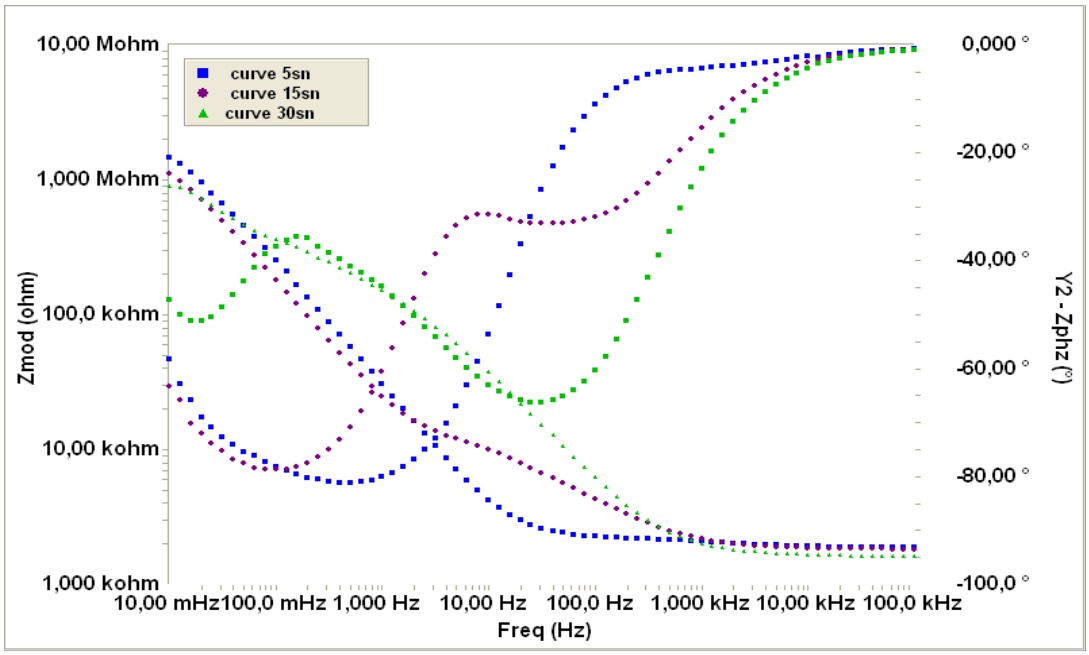

Figure 4.62. Z mod and Z phase plots at 0,6V for a P(NMePyEBTNMePy)film deposited at 0,6 V , 5, 15 and 30 seconds in 0.1 M $TBAPF_6$/DCM solution.

$C_{sp,}$ C_{dl} and phase angle values of a P(NMePyEBTNMePy)film deposited at 1,1V 5, 15 and 30 seconds in 0.1 M $TBAPF_6$/DCM solution is given at Table 4.18.

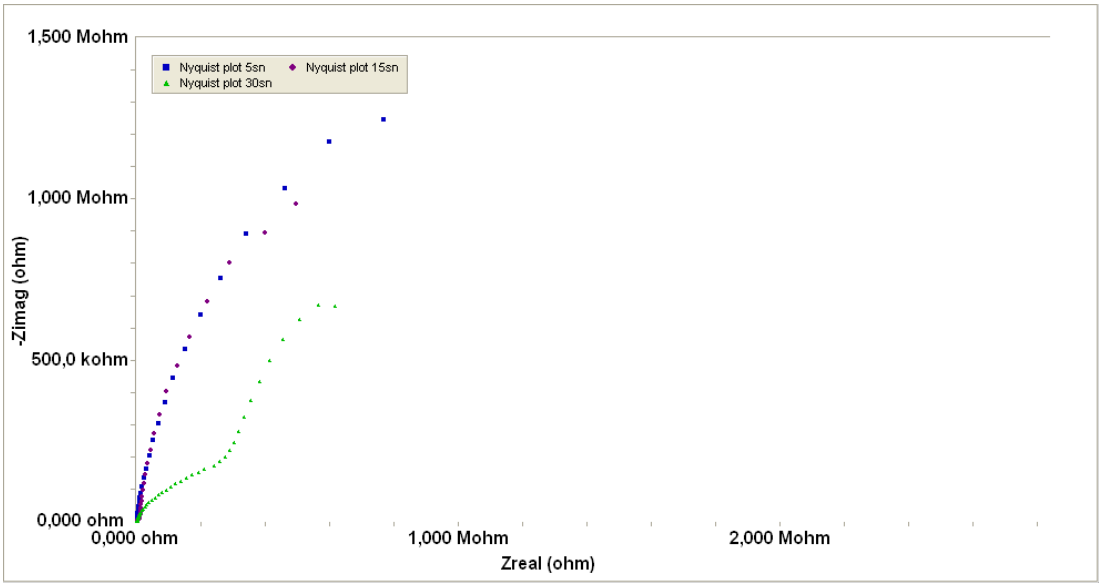

Figure 4.63. Nyquist plots at -0.4 V to 0,8V V for a P(NMePyEBTNMePy)film deposited at 0,6V, 5, 15 and 30 seconds in 0.1 M $TBAPF_6$/DCM solution.

From the results it is well seen that the polymer formed by appling potential for 30 minutes gets destroy that is also in a harmony eith CV results. C_{sp} values of 30 second polymerized film decreases which means capacitive behaviour decreases.

Table 4.19. $C_{sp,}$ C_{dl} and phase angle values of a P(NMePyEBTNMePy)film deposited at 1,1 V , 5, 15 and 30 seconds in 0.1 M $TBAPF_6$/DCM solution.

time	**C_{sp}**	**C_{dl}**	**Phase angle**
5	0,63	33	83
15	0,59	41	80
30	0,58	6,62	66

At low frequency values, P(NMePyEBTNMePy) films shows kinetic control behaviour while higher frequencies mass transport occurs. This behaviour is also general with other conditions polymer films.

Figure 4.64 shows the Bode magnitude and the Bode phase angle and Figure 4.65 shows the Nyquist plot of P(NMePyEBTNMePy) film prepared by application of different times during the electropolymerization by CA. P(NMePyEBTNMePy)films

were prepared by depositing at 1,1 V , 5, 15 and 30 seconds in 0.1 M $TBAClO_4$/DCM solution.

C_{sp}, C_{dl} and phase angle values of a P(NMePyEBTNMePy)film deposited at 1,1V 5, 15 and 30 seconds in 0.1 M $TBAClO_4$/DCM solution is given at Table 4.18.

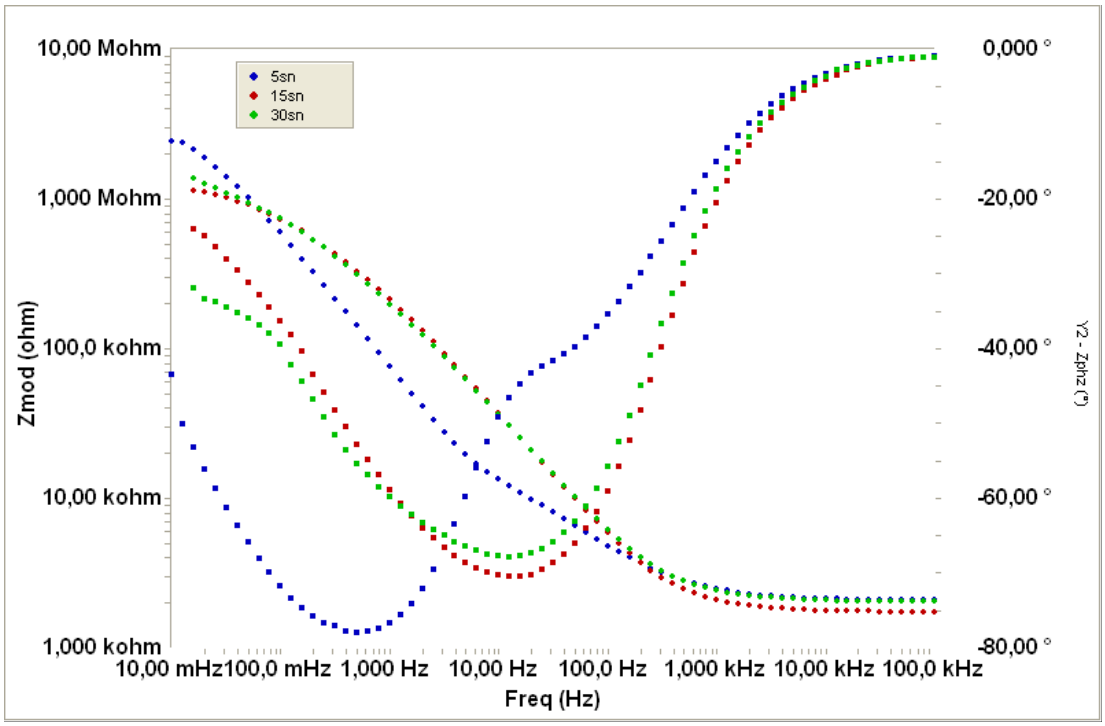

Figure 4.64. Z mod and Z phase plots at 0,6V for a P(NMePyEBTNMePy)film deposited at 1,1 V , 5, 15 and 30 seconds in 0.1 M $TBAClO_4$/DCM solution.

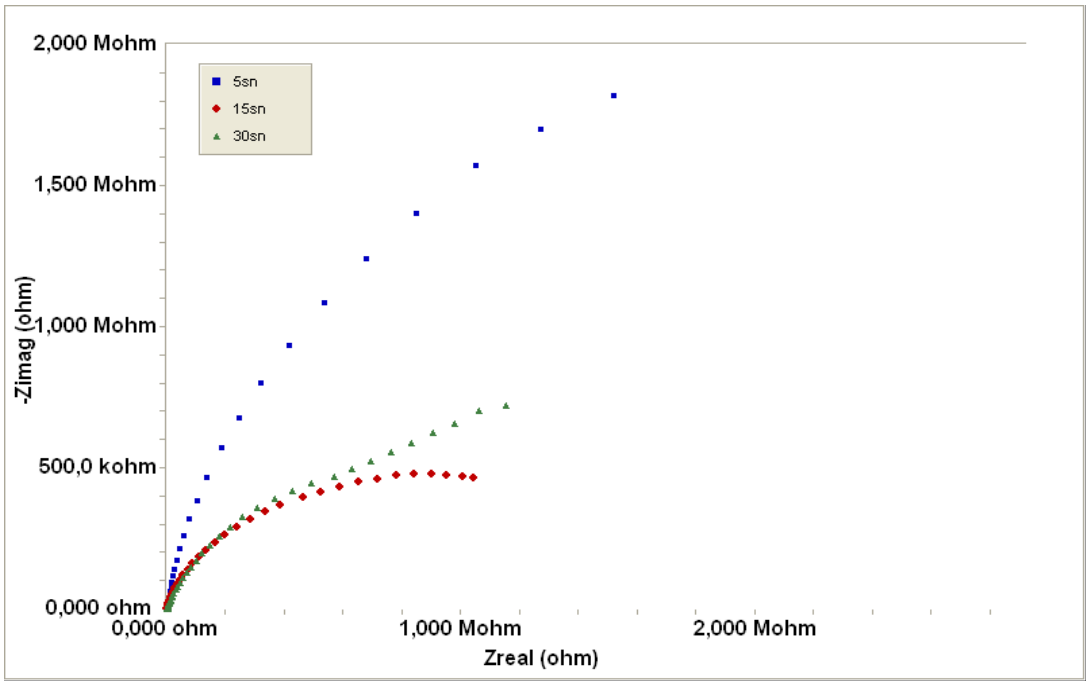

Figure 4.65. Nyquist plots at -0.4 V to 0,8V V for a P(NMePyEBTNMePy)film deposited at 1,1 V , 5, 15 and 30 seconds in 0.1 M $TBAClO_4$/DCM solution.

From the Nyquist plot seen in Figure 4.65 while time increases the film gets thicker,seen from semi circle behaviour. At low frequency values, thinner films shows good capacitive behaviour while as at high frequency values thicker films good capacitive behaviour.

Table 4.20. $C_{sp,}$ C_{dl} and phase angle values of a P(NMePyEBTNMePy)film deposited at 1,1 V , 5, 15 and 30 seconds in 0.1 M $TBAClO_4$/DCM solution.

Time	C_{sp}	C_{dl}	Phase angle
5	0,44	13,25	81
15	0,49	4,7	72
30	0,43	5	68

From EIS measurements it was found that thinner P(NMePyEBTNMePy) films show better capacitive value also covers with CV results. The polymer films are kinetic controlled at low freguency values and at hich frequency values diffusion controlled. Polymers show capacitive behaviour at low frequency region and also at 0,6V DC applied.

4.6. ATR-FTIR Characterization of P(NMePyEBTNMePy)

The FTIR-ATR spectra of Py and electrochemically synthesized PPy (galvanostically in 0,1M $TBAPF_6$/DCM) showed the corresponding spectra between 4000 and 650 cm^{-1}. (Figure 4.66).

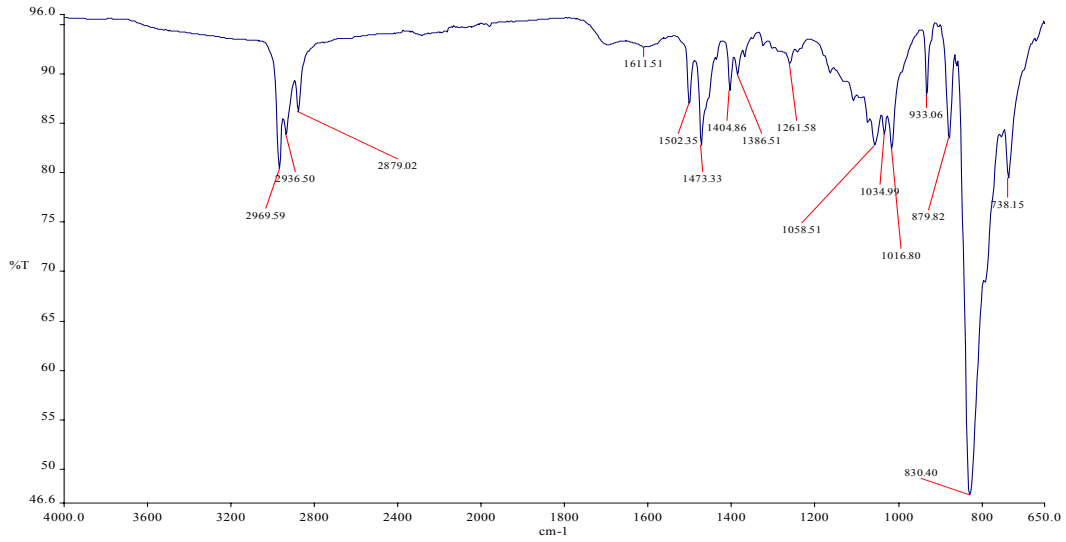

Figure 4.66. ATR-FTIR spectrum of P(NMePyEBTNMePy) doped wtih PF_6^- dopant ion.

The characteristic peaks of stretching vibration of Pyrrole ring are shown around 1638cm^{-1}, 1527cm^{-1} and 1471cm^{-1}. 3425 cm^{-1} on PPy and 1072, 1044 and 1011 peaks of Py are vanished on PPy which is because of the lack of out of plane vibration due to $2H^{+}$ loss during the polymerization mechanism. The peak around 2900 cm^{-1} is for ring C-H group. 832 cm^{-1} peak is due to the anion of $TBAPF_6$.1360- 1030cm^{-1} corresponds to C-N streching of N-methyl group.

4.7. Spectroelectrochemistry of P(NMePyEBTNMePy)

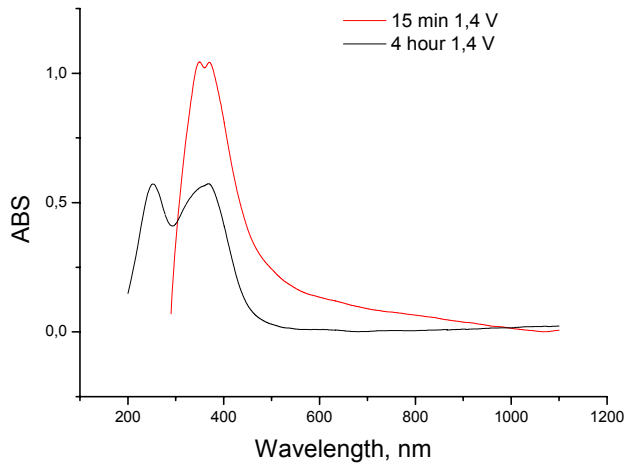

Figure 4.67. Spectroelectrochemistry of potentiostatically deposited P(NMePyEBTNMePy) on a ITO coated glass slide in in 0.1 M TBAPF6 in DCM. Doped to 1.1 V, for 15 minute and 4 hour.

Spectroelectrochemistry of P(NMePyEBTNMePy) was given in Figure 4.67 indicated that light navy-brown color in the oxide form at 1,1V. π to π^{*} transition was seen at 400 nm.

5. CONCLUSIONS

In this thesis, NMePyEBTNMePy comonomer was succesfully synthesis via Stille coupling reaction. NMePyEBTNMePy was characterize with H-NMR and ATR-FTIR spectroscopies. NMePyEBTNMePy comonomer was electropolymerize in different conditions with different methods. Comonomer had been polymerized in $TBAPF_6$/DCM and $TBAClO_4$/DCM with CV and CA methods. Obtained polymers redox behaviour was investigated with CV and also capacitive properties were determined with EIS. n-doping properties of comonomer had also studied.

Compared to N-MePy monomer NMePyEBTNMePy comonomer found to have higher oxidation values due to N atom at the thiazole ring of the comonomer. It ıs found that polymerization with a scan rate of 100mV/sn gives polymer films with better redox properties. Doping with PF_6^- ion gives polymer films more stable than the ones doped with ClO_4^-. Altough it was not possible to polymerize comonomer with 8 cycles with ClO_4^-, it was obtained with PF_6^-.

CA results show that thinner films shows better redox behaviour. So, it could be said that CV is a better method to get thickher polymer films. PF_6^- is a better ion for CQ method, ΔE and E_o decreases in PF_6^- dopant. But compaired with CV method PF_6^- is a better dopant in CV measurements. Altough 8 cycles were scaned and obtained a well behaved redox film it was not possible in CA measurements with 30 seconds. Dedoping is a advantage way to get thicker polymer films.

n-doping properties of P(NMePyEBTNMePy) was investigated seen that n-doping occurs in -1,047V also we calculated E_g of obtained polymer found 0,417 eV.

From EIS measurements it was found that thinner P(NMePyEBTNMePy) films show better capacitive value also covers with CV results. The polymer films are kinetic controlled at low freguency values and at hich frequency values diffusion controlled. Polymers show capacitive behaviour at low frequency region and also at 0,6V DC applied.

REFERENCES

[1] **Friend, R. H., Gymer, R. W., Holmes, A.B., Burroughes, J. H.; Marks, R.N., Taliani, C.; Bradley, D.D.C., Dos Santos, D. A., Bredas, J.L., Lolund, M., Salaneck, W.R.,** 1999, *Nature*, **397**, 121**.**

[2] (a) **Kraft, A.; Grimsdale, A. C.; Holmes, A. B.,** 1998, *Angew. Chem.,Int. Ed.*, ***37***, 402. (b) **Mitschke, U.; Ba¨uerle, P**., 2000, *J. Mater. Chem.*, **10**, 1471.

[3] **Yamamoto, T.,** 1999, *Bull. Chem. Soc. Jpn*., **72**, 621.

[4] (a) **Millard, I. S.,** 2000, *Synth. Met.*, *111-112*, 119. (b) **Inbasekaran, M.; Woo, E.; Wu, W.; Bernies, M.; Wujkowski, L.,** 2000, *Synth. Met. 111-112*, 397. (c) **Ng, S.-C.; Lu, H.-F.; Chan, H. S. O.; Fuji, A.; Laga, T.; Yoshino, K.,** 2000, *Adv. Mater.,* **12**, 1122. (d) **Agrawal, A. K.; Jenekhe, S. A.,** 1993, *Macromolecules*, **26**, 895. (e) **Agrawal, A. K.; Jenekhe, S. A.,** 1991, *Macromolecules*, **24**, 6806.

[5] (a) **Karikomi, M.; Kitamura, C.; Tanaka, S.; Yamashita**, 1995, Y. *J. Am. Chem. Soc.*, **117**, 6791. (b) **Zhang, Q. T.; Tour, J. M.,** 1998, *J. Am. Chem. Soc.*, **120**, 5355. (c) **Akoudad, A.; Roncali**, 1998, J. *Chem. Commun.*, 2081.

[6] **Rodriguez, J.; Grande, H.-J.; Otero, T. F.,** 1996, In *Handbook of Organic Conductive Molecules and Polymers*; Nalwa, H. S., Ed.; Wiley: New York,; Vol. 2, Chapter 10.

[7] (a) **Andrieux, C. P.; Hapiot, P.; Audebert, P.; Guyard, L.;Nguyen Dinh An, M.; Groenendaal, L.; Meijer. E. W**., 1997 *Chem. Mater.*, **9**, 723. (b) **Zotti, G.; Martina, S.; Wegner, G.;Schlu¨ ter; A.-D**., 1992, *Adv. Mater.*, **4**, 798.

[8] **Martina, S.; Schluter, A.,** 1992 *Macromolecules*, **25**, 3607.

[9] **Parakka, J. P.; Chacko, A. P.; Nikles, D. E.; Wang, P.; Hasegawa, S.; Maruyama, Y.; Metzger, R. M.; Cava, M. P**., 1996, *Macromolecules*, **29**, 1928.

[10] **Van Mullekom, H. A. M.; Vekemans, J. A. J. M.; Meijer, E. W.,** 1996, *Chem. Commun.*, 2163.

[11] **Stille, J. K**., 1986, *Angew. Chem., Int. Ed. Engl.*, **25**, 508.

[12] (a) **Bao, Z.; Chan, W.; Yu, L.,** 1993, *Chem. Mater.*, **5**, 2. (b) **Delnoye, D. A. P.; Sijbesma, R. P.; Vekemans, J. A. J. M.; Meijer, E. W.,** 1996, *J. Am. Chem. Soc.* **118**, 8717. (c) **Saadeh, H.; Goodson III, T.; Yu, L**., 1997, *Macromolecules*, **30**, 4608. (d) **Yao, Y.; Zhang, Q. T.; Tour, J. M.,** 1998, *Macromolecules*, **31**, 8600. (e) Y**ao, Y.; Lamba, J. J. S.; Tour, J. M.,** 1998, *J. Am. Chem. Soc.*, **120**, 2805. (f) **Lee, B.-L.; Yamamoto, T.,** 1999, *Macromolecules*, **32**, 1375. (g) **Tsuie, B.; Reddinger, J. L.;Sotzing, G. A.; Soloducho, J.; Katritzky, A. R.; Reynolds, J.R.,** 1999, *J. Mater. Chem.*, **9**, 2189. (h) **Devasagayaraj, A.; Tour, J. M.,** 1999, *Macromolecules*, **32**, 6425. (i) **Zhang, C. Y.; Tour, J. M.,** 1999, *J. Am. Chem. Soc.*, **121**, 8783.

[13] **Miyaura, N.; Suzuki, A.**, 1995, *Chem. Rev.*, **95**, 2457.

[14] **Kim, S.; Jackiw, J.; Robinson, E.; Schanze, K. S.; Reynolds, J. R.; Baur, J.; Rubner, M. F.; Boils, D.,** 1998, *Macromolecules*, **31**, 964.

[15] **Martina, S.; Enkelmann, V.; Wegner, G.; Schluter, A.** , 1992, *Synth. Met.*, **51**, 299.

[16] **Groenendaal, L.; Peerlings, H. W. I.; Van Dongen, J. L. J.; Havinga, E. E.; Vekemans, J. A. J. M.; Meijer, E. W.,** 1995, *Macromolecules*, **28**, 116.

[17] **Kijima, M.; Abe, S.; Shirakawa, H.,** 1999, *Synth. Met.*, **101**, 61.

[18] **Jones, R. A.; Karatza, M.; Voro, T. N.; Civeir, P. U.; Franck, A.; Ozturk, O.; Seaman, J. P.; Whitmore, A. P.; Williamson, D. J.,** 1996, *Tetrahedron*, **52**, 8707.

[19] **L. Gonzalez-Ronda, D.C. Martin, J.I. Nanos, J.K. Politis, M.D. Curtis**, 1999, *Macromolecules*, **32** 4558.

[20] **J.I. Nanos, J.W. Kampf, M.D. Curtis**, 1995, *Chem. Mater.*, **7** , 2232.

[21] **A.B. Koren, M.D. Curtis, J.W. Kampf**, 2000, *Chem. Mater*. **,12,** 1519.

[22] **T. Yamamoto, H. Suganuma, T. Maruyama, T. Inoue, Y. Muramatsu, M. Arai, D. Komarudin, N. Ooba, S. Tomaru, S. Sasaki, K. Kubota**, 1997, *Chem. Mater*., **9** ,1217.

[23] **T. Yamamoto, H. Suganuma, T. Maruyama, K. Kubota**, 1995, *Chem. Commun*. 1613.

[24] **T. Yamamoto, T. Maruyama, Z.H. Zhou, T. Ito, T. Fukuda, Y. Yoneda, F. Begum, T. Ikeda, S. Sasaki, H. Takezoe, A. Fukuda, K. Kubota**, 1994, *J. Am. Chem. Soc*. **116** 4832.

[25] **J.K. Politis, M.D. Curtis, L. Gonzalez, D.C. Martin, Y. He, J. Kanicki**, 1998, *Chem. Mater*., **10**, 1713.

[26] **J.K. Stille**, 1986, *Angew. Chem. Int. Ed*., **25**, 508.

[27] **Bard, A. J. and Faulkner, L. R.,** 2001. Electrochemical Methods : Fundamentals And Applications, John Wiley, New York.

[28] **Barsoukov, E. and Macdonald, J. R.,** 2005. Impedance spectroscopy : theory, experiment, and applications, Wiley-Interscience, Hoboken, N.J.

[29] **F. Goppelsroeder,** 1891, *Die Internationale Electrotechnische Ausstellung* **18,** 978; **19** 1891, 1047.

[30] **H. A. Pohl:** "Electronic Behavior of Organic Macromolecular Solids," **B. A. Bolto**: "Semiconducting Organic Polymers Containing Metal Groups," **D. D. Eley**: "Semiconducting Biological Polymers," in **J. E. Katon (ed.)**: *Organic Semiconducting Polymers,* Marcel Dekker, New York 1968.

[31] **W. A. Little**, 1964, Phys. Rev. **134,** A 1416.

[32] **H. Naarmann, F. Beck:** "Neuartige Polymerisate aus aromatischen und heterocyclischen Verbindungen und ihre elektrophysikalischen Eigenschaften," GDCh Meeting, Munich, Oct. 12, 1964. BASF, DE 1 178 529, 1964 (H. Naarmann, F. Beck, E. G. Kastning). BASF, DE 1 195 497, 1963 (H. Naarmann, F. Beck, E. G. Kastning). BASF, DE 1 092 137, 1964 (H. Naarmann, F. Beck, E. G. Kastning).

[33] **W. Slough** et al., 1969, in pp. 55, 118 – 163. **H. Naarmann,** *Angew. Chem. Int. Ed. Engl.* **8** 915. BASF, DE-OS 1 953 898, 1969 (H. Willersinn, H. Naarmann, K. Schneider).

[34] **R. Greene, G. B. Street, L. J. Süter**, 1975, *Phys. Rev. Lett*., **34,** 577.

[35] **A. J. Heeger** *et al.*, 1977, *J. Chem. Soc. Chem. Commun*., 578 – 580.

[36] **H. Shirakawa, S. Ikeda,** 1971, *Polym. J.* (Tokyo) **2**. **T. Ito, H. Shirakawa, S. Ikeda, J**., 1974, *Polym. Sci. Polym. Chem. Ed*. **12**, 11.

[37] **Skotheim, T. A., Elsenbaumer, R. L. and Reynolds, J. R.,** 1998. Handbook Of Conducting Polymers, M. Dekker, New York.

[38] **Lee, Y. S. and Kertesz, M.,** 1988. The Effect of Heteroatomic Substitutions on the Band-Gap of Polyacetylene and Polyparaphenylene Derivatives, *Journal of Chemical Physics,* **88,** 2609-2617.

[39] **Bredas, J. L., Cornil, K., Meyers, F. and Beljonne, D.,** 1998. Electronic Structure and Optical Response of Highly Conducting and Semiconducting Conjugated Polymers and Oligomers, *Handbook of conducting polymers,* xiii, 1097 p., Skotheim, T. A., Elsenbaumer, R. L. and Reynolds, J. R., M. Dekker, New York.

[40] **Peierls, R.,** 1955. In Quantum Theory Of Solids, Oxford Universtiy Press, Oxford.

[41] **Shimamura, K., Karasz, F. E., Hirsch, J. A. and Chien, J. C. W.,** 1981. Crystal-Structure of Trans-Polyacetylene, *Makromolekulare Chemie-Rapid Communications,* **2,** 473-480.

[42] **Bauerle, P., Segelbacher, U., Maier, A. and Mehring, M.,** 1993. Electronic-Structure of Monomeric and Dimeric Cation Radicals in End-Capped Oligothiophenes, *Journal of the American Chemical Society,* **115,** 10217-10223.

[43] **Hill, M. G., Penneau, J. F., Zinger, B., Mann, K. R. and Miller, L. L.,** 1992. Oligothiophene Cation Radicals - Pi-Dimers as Alternatives to Bipolarons in Oxidized Polythiophenes, *Chemistry of Materials,* **4,** 1106-1113.

[44] **Bolognesi, A., Catellani, M., Destri, S. and Porzio, W.,** 1987. Polythiazole - a New Semiconducting Polymer Having a Heteroatom in the Conduction Pathway, *Synthetic Metals,* **18,** 129-132.

[45] **Catellani, M., Destri, S., Porzio, W., Themans, B. and Bredas, J. L.,** 1988. Thiazole-Based Polymers - Synthesis, Characterization and Electronic-Structure, *Synthetic Metals,* **26,** 259-265.

[46] **Bredas, J. L.,** 1986. Electronic Structure of Highly Conducting Polymers, *Handbook of conducting polymers,* 559-567, Skotheim, T. A., M. Dekker, New York.

[47] **Dall'Olio, A., Dascola, Y., Varacco, V. and Bocchi, C. R.,** 1968. CRC Seances Acad. Sci. Ser. C, 466.

[48] **Kanazawa, K. K., Diaz, A. F., Geiss, R. H., Gill, W. D., Kwak, J. F., Logan, J. A., Rabolt, J. F. and Street, G. B.,** 1979. Organic Metals - Polypyrrole, a Stable Synthetic Metallic Polymer, *Journal of the Chemical Society-Chemical Communications,* 854-855.

[49] **Schnoller, M., Wersing, W. and Naarman, H.,** 1987. Intrinsically Conductive Organic Polymers as Electrode Material for Functional Ceramics in Electronics, *Makromolekulare Chemie-Macromolecular Symposia,* **8,** 83-95.

[50] **Patil, A. O., Ikenoue, Y., Wudl, F. and Heeger, A. J.,** 1987. Water-Soluble Conducting Polymers, *Journal of the American Chemical Society,* **109,** 1858-1859.

[51] **Bittihn, R., Ely, G. and Woeffler, F.,** 1987. Polypyrrole as an Electrode Material for Secondary Lithium Cells, *Makromolekulare Chemie-Macromolecular Symposia,* **8,** 51-59.

[52] **Friend, R. H., Gymer, R. W., Holmes, A. B., Burroughes, J. H., Marks, R. N., Taliani, C., Bradley, D. D. C., Dos Santos, D. A., Bredas, J. L., Logdlund, M. and Salaneck, W. R.,** 1999. Electroluminescence in conjugated polymers, *Nature,* **397,** 121-128.

[53] **Burroughes, J. H., Bradley, D. D. C., Brown, A. R., Marks, R. N., Mackay, K., Friend, R. H., Burns, P. L. and Holmes, A. B.,** 1990. Light-Emitting-Diodes Based on Conjugated Polymers, *Nature,* **347,** 539-541.

[54] **Roth, S.,** 1995. One-Dimensional Metals, Weinheim VCH,

[55] **Salaneck, W. R., Lundstrom, I. and Randby, B.,** 1993. Nobel Symposium in Chemistry: Conjugated Polymers and Related Materials, Oxford Sci, Oxford.

[56] **Berggren, M., Inganas, O., Gustafsson, G., Rasmusson, J., Andersson, M. R., Hjertberg, T. and Wennerstrom, O.,** 1994. Light-Emitting-Diodes with Variable Colors from Polymer Blends, *Nature,* **372,** 444-446.

[57] **Lyons, M. E. G.,** 1997. Advances in Chemical Physics, Polymeric Systems, John Wiley & Sons, New York.

[58] **Levi, M. D., Lopez, C., Vieil, E. and Vorotyntsev, M. A.,** 1997. Influence of ionic size on the mechanism of electrochemical doping of polypyrrole films studied by cyclic voltammetry, *Electrochimica Acta,* **42,** 757-769.

[59] **Andrieux, C. P., Audebert, P., Hapiot, P. and Saveant, J. M.,** 1991. Observation of Some Reactive Pyrrolic Radical-Cations by Use of Fast Voltammetry at Ultramicroelectrodes, *Synthetic Metals,* **43,** 2877-2880.

[60] **Park, S. M. and Yoo, J. S.,** 2003. Electrochemical impedance spectroscopy for better electrochemical measurements, *Analytical Chemistry,* **75,** 455A-461A.

[61] **Parsons, R.,** 1990. Electrical Double-Layer - Recent Experimental and Theoretical Developments, *Chemical Reviews,* **90,** 813-826.

[62] **Randles, J. E. B.,** 1948. A Cathode Ray Polarograph: Part II The Current Voltage Curves, *Transactions of the Faraday Society,* **44,** 327-338.

[63] **Singhal, P., Kawagoe, K. T., Christian, C. N. and Kuhr, W. G.,** 1997. Sinusoidal voltammetry for the analysis of carbohydrates at copper electrodes, *Analytical Chemistry,* **69,** 1662-1668.

[64] **Harrick, N. J.,** 1979. Internal Reflection Spectroscopy, Harrick Publications, New York.

[65] **H. Naarmann**, 1982, Synthese elektrisch leitfähiger Polymere, Angew. Makromol. Chem. **109/110** 295 – 338. **W. J. Feast**: "Synthesis of Conducting Polymers," in T. A. Skotheim (ed.) : Handbook of Conducting Polymers. Marcel Dekker, New York 1986, pp. 1 – 44. N. C. Billingham, P. D. Calvert: "Electrically Conducting Polymers," Adv. Polym. Sci. **80** (1989) 1 – 90.

[66] **H. W. Gibson:** "Substituted Polyacetylenes," in T. A. Skotheim (ed.): *Handbook of Conducting Polymers,* Marcel Dekker, New York 1986, pp. 405 –435.

[67] **H. Hopf, O. Kretschmer, H. Naarmann**, 1989, Adv. Mater. **1** no. 12, 445.

[68] **H. Naarmann**, 1990, *Adv. Mater.* **2** no. 8, 345 – 348. **W. R. Sorenson, T. W. Campbell**: *Präparative Methoden der Polymeren Chemie*, Verlag Chemie, Weinheim 1962, p. 167.

[69] **T. Yamanato, Y. Hayashi, A. Yamamoto,** 1978, *Bull. Chem. Soc. Jpn.,* **51,** 2091.

[70] **N. Miyaura, T. Yagani, A. Suzuki,** 1981, *Synth. Commun.* **11**, 513 – 519.

[71] **K. J. Stille,** 1972, *Makromol. Chem.,* **154**, 49.

[72] **M. Kanabe, M. Okawara,** 1968, *J. Polym. Sci. Polym. Chem. Ed*., **6,** 1058.

[73] **H. H. Edwards, W. J. Feast**, 1980, *Polymer* ,**21**, 595.

[74] **T. M. Swager, D. A. Dougherty, R. H. Grubbs,** 1989, *J. Am. Chem. Soc.*, **111,** 4413.

[75] **E. J. Ginsburg et al.,** 1990, "Conjugated Polymeric Materials," in J. L. Bredes, R. R. Chance (eds.): *NATO ASI Ser.* **182**, 65.

[76] A. W. Snow, 1981,Nature (London) **292** no. 40.

[77] **Tamao, K., Sumitani, K. and Kumada, M.,** 1972. Selective Carbon-Carbon Bond Formation by Cross-Coupling of Grignard-Reagents with Organic Halides - Catalysis by Nickel-Phosphine Complexes, *Journal of the American Chemical Society,* **94,** 4374-4376.

[78] **Kumada, M.,** 1980. Nickel and Palladium Complex Catalyzed Cross-Coupling Reactions of Organometallic Reagents with Organic Halides, *Pure and Applied Chemistry,* **52,** 669-679.

[79] **Corriu, J. P. and Masse, J. P.,** 1972. Activation of Grignard-Reagents by Transition-Metal Complexes - New and Simple Synthesis of Trans-Stilbenes and Polyphenyls, *Journal of the Chemical Society-Chemical Communications,* 144-146.

[80] **Tamura, M. and Kochi, J.,** 1971. Mechanism of Silver-Catalyzed Reaction of Grignard Reagents with Alkyl Halides, *Journal of the American Chemical Society,* **93,** 1483-1485.

[81] **Tamura, M. and Kochi, J.,** 1971. Alkylcopper(I) in Coupling of Grignard Reagents with Alkyl Halides, *Journal of the American Chemical Society,* **93,** 1485-1487.

[82] **Kochi, J. K.,** 1974. Electron-Transfer Mechanisms for Organometallic Intermediates in Catalytic Reactions, *Accounts of Chemical Research,* **7,** 351-360.

[83] **Murahash.Si, Tanba, Y., Yamamura, M. and Moritani, I.,** 1974. Reactions of Ortho-Carbon Sigma-Bonded Aromatics-Palladium Complexes with Alkyllithium - Selective Syntheses of Ortho-Alkyl Substituted Aromatic-Compounds, *Tetrahedron Letters,* **15***,* 3749-3752.

[84] **Negishi, E.-i.,** 1980. Organometallics in organic synthesis, Wiley, New York.

[85] **Negishi, E.-i.,** 2002. Handbook of organopalladium chemistry for organic synthesis, Wiley Interscience, New York.

[86] **Murahashi, S. I., Yamamura, M., Yanagisawa, K., Mita, N. and Kondo, K.,** 1979. Stereoselective Synthesis of Alkenes and Alkenyl Sulfides from Alkenyl Halides Using Palladium and Ruthenium Catalysts, *Journal of Organic Chemistry,* **44,** 2408-2417.

[87] **Kosugi, M., Hagiwara, I. and Migita, T.,** 1983. 1-Alkenylation on Alpha-Position of Ketone - Palladium-Catalyzed Reaction of Tin Enolates and 1-Bromo-1-Alkenes, *Chemistry Letters,* **12,** 839-840.

[88] **Kosugi, M., Shimizu, Y. and Migita, T.,** 1977. Alkylation, Arylation, and Vinylation of Acyl Chlorides by Means of Organotin Compounds in Presence of Catalytic Amounts of Tetrakis(Triphenylphosphine)Palladium(O), *Chemistry Letters***, 6***,* 1423-1424.

[89] **Stille, J. K.,** 1986. The Palladium-Catalyzed Cross-Coupling Reactions of Organotin Reagents with Organic Electrophiles, *Angewandte Chemie-International Edition in English,* **25,** 508-523.

[90] **Milstein, D. and Stille, J. K.,** 1979. Palladium-Catalyzed Coupling of Tetraorganotin Compounds with Aryl and Benzyl Halides - Synthetic Utility and Mechanism, *Journal of the American Chemical Society,* **101,** 4992-4998.

[91] **Jabri, N., Alexakis, A. and Normant, J. F.,** 1981. Vinyl-Copper Derivatives .13. Synthesis of Conjugated Dienes of Very High Stereoisomeric Purity, *Tetrahedron Letters,* **22,** 959-962.

[92] **Hatanaka, Y. and Hiyama, T.,** 1988. Cross-Coupling of Organosilanes with Organic Halides Mediated by Palladium Catalyst and Tris(Diethylamino)Sulfonium Difluorotrimethylsilicate, *Journal of Organic Chemistry,* **53,** 918-920.

[93] **Hatanaka, Y. and Hiyama, T.,** 1990. Stereochemistry of the Cross-Coupling Reaction of Chiral Alkylsilanes with Aryl Triflates - a Novel-Approach to Optically-Active Compounds, *Journal of the American Chemical Society,* **112,** 7793-7794.

[94] **Hatanaka, Y., Matsui, K. and Hiyama, T.,** 1989. A One-Pot Synthesis of Conjugated Dienynes by Palladium-Mediated 3 Component Cross-Coupling Reaction, *Tetrahedron Letters,* **30,** 2403-2406.

[95] **Kosugi, M., Shimizu, Y., Migita, T.**,1977, *Chem. Lett.*, 1423.

[96] **Kosugi, M., Shimizu, Y., Migita, T.,** 1977, *J. Organomet. Chem.,* **129**, C36.

[97] **Kosugi, M., Sasazawa, K., Shimizu, Y., Migita, T.**, 1977, *Chem. Lett.,* 301.

[98] **Milstein, D., Stille, J. K.,** 1978, *J. Am. Chem. Soc.*, **100**, 3636.

[99] **Beletskaya, I.P.**, 1983, *J. Organomet. Chem.*, **250**, 551.

[100] **Stille, J.K.**, 1986, *Angew. Chem., Int. Ed. Engl.,* **25**, 508.

[101] **Kumada, M.**, 1980, *Pure Appl. Chem*., **52**, 669.

[102] **Erdik, E.**, 1992, *Tetrahedron*, **48**, 9577.

[103] **Miyaura, N., Ishitama, T., Sasaki, H., Ishikawa, M., Satoh, M., Suzuki, A.J.**, 1989, *J.Am. Chem. Soc.*, **111**, 314.

[104] **Hatanaka, Y., Hiyama, T.**,1991, *Synlett*, 845.

[105] **Farina, V., Krishnan, B.**, 1991, *J. Am. Chem. Soc.,* **113**, 9585.

[106] **Liebeskind, L.S., Fengl, R.W.**, 1990, *J. Org. Chem*., **55**, 5359.

[107] **Mitchell, T.N.**, 1992, *Synthesis*, 803.

[108] **Farina, V., Roth, G.P.**, 1995, *Advantages in metal-organic chemistry*, Liebeskind, L.S. Ed., vol.5, JAI Pres, Greenwich, CT.

[109] **Stille, J.K.**, 1985, *The Chemistry of the metal-carbon bond*, Hartley, F.R., Patai S., Eds., Vol. 2, John Wiley, New York, 625.

[110] **Amatore, C., Azzabi, M., Jutand, A. J.**,1989, *Organomet. Chem.*, **363**, C41.

[111] **Fauvarque, J.F., Pflüger, F., Troupel, M.J.**,1981, *Organomet. Chem.*, **208**, 419.

[112] **Ugo, R., Pasini, A., Fusi, A., Cenini, S.**, 1972, *J.Am.Chem.Soc.*, **94**, 7364.

[113] **Milstein, D., Stille, J.K.**, 1979, *J.Am. Chem. Soc.*, **101**, 4992.

[114] **Amatore, C., Azzabi, M., Jutand, A.**, 1991, *J. Am.Chem. Soc.*, **113**, 1670.

[115] **Lau, K.S.Y., Wong,P.K., Stille, J.K.**, 1976, *J.Am.Chem. Soc.*, **98**, 5832.

[116] **Becker, Y., Stille, J.K.**, 1978, *J.Am.Chem.Soc.*, **100**, 838.

[117] **Kramer, A.V., Osborn, J.A.**, 1974, *J. Am. Chem. Soc.*, **96**, 7832.

[118] **Sheffy, F.K., Godschalx, J.P., Stille, J.K.**, 1984, *J. Am. Chem. Soc.*, **106**, 4833.

[119] **Kurosawa, H., Ogoshi, S., Kawasaki, Y., Murai, S., Miyoshi, M., Ikeda, I.**, 1990, *J.Am.Chem. Soc*., **112**, 2813.

[120] **Kurosawa, H., Kajimaru, H., Ogoshi, S., Yoneda, H., Miki, K., Kasai, N., Murai, S., Ikeda, I.,** 1992, *J.Am. Chem. Soc.*, **114**, 8417.

[121] **Labadie, J.W., Stille, J.K.**, 1983, *J.Am. Chem. Soc.*, **105**, 6129.

[122] **Scott, W.J., Stille, J.K.**, 1986, *J.Am.Chem.Soc.*, **108**, 3033.

[123] **Chen, Q.-Y, He, Y.-B.**, 1990, *Chin. J. Chem.*, 451.

[124] **Farina, V., Krishnan, B., Marshall, D.R., Roth, G.P.**, 1993, *J. Org. Chem.*, **58**, 5434.

[125] **Piers, E., Friesen, R.W., Keay, B.A.**, 1985, *J. Chem. Soc., Chem. Commun.*, 809.

[126] **Gronowitz, S., Messmer, A., Timari, G.**, 1992, *J. Heterocycl. Chem.*, **29**, 1049.

[127] **Farina, V., Kapadia, S., Krishnan, B., Wang., C., Liebeskind, L.**, 1994, *J. Org. Chem.*, **59**, 5905.

[128] **Milstein, D., Stille, J.K.**, 1979, *J.Am.Chem.Soc.*, **101**, 4981.

[129] **Godschalx, J., Stille, J.K.**, 1980, *Tetrahedron Lett.*, **21**, 2599.

[130] **Trost, B.M., Keinan, E.**, 1980, *Tetrahedron Lett.*, **21**, 2595.

[131] **Keinan, E., Roth, Z.**, 1983, *J. Org. Chem.*, **48**, 1769.

[132] **Goliaszewski, A., Schwartz**, 1985, *J. Organometallics*, **4**, 417.

[133] **Goliaszewski, A., Schwartz,** 1985, *J. Tetrahedron*, **41**, 5779.

[134] **Farina, V., Baker, S.R., Benigni, D.A., Hauck, S.I., Sapino, C., Jr.**, 1990, *J. Org. Chem.*, **55**, 5833.

[135] **Vedejs, E., Haight, A.R., Moss, W.O.**, 1992, *J.Am.Chem. Soc.*, **114**, 6556.

[136] **Brown, J.M., Pearson, M., Jastrzebski, J.T.B.H., van Koten, G.**, 1992, *J.Chem. Soc. Chem. Commun*, 1440.

[137] **Peet, W.G., Tam, W.J.,** 1983, *J. Chem.Soc.Chem.Commun.*, 853.

[138] **Kobayashi, Y., Kato, N., Shimazaki, T., Sato, F.**, 1988, *Tetrahedron Lett.*, **29**, 6297.

APPENDICES

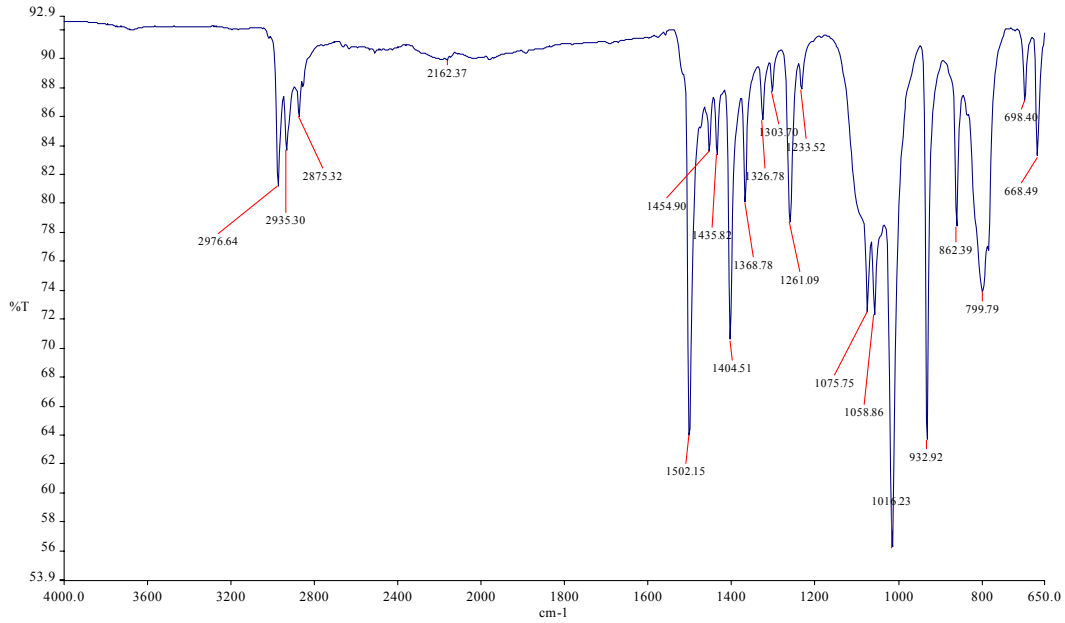

Appendix A.1. ATR-FTIR spectrum of bromoethylbithiazolebromo.

BIOGRAPHY

Şebnem Şaziye TAYYAR was born in Kadıköy/İstanbul in 1983. After finishing primary and secondary school in İstanbul, she obtained High School at Zonguldak Science High School. She started her B.Sc. at İstanbul Technical University Chemistry Department in 2002. She has graduated and started M.Sc.at İstanbul Technical University Polymer Science and Technology programin 2006.